The Hong Kong Polytechnic University

Department of Mechanical Engineering

A New Design of Rotational Hybrid Vibration Absorber for Global Structural Vibration Control

By

Tso, Man Ho

A thesis submitted in partial fulfillment of the requirements for the
Degree of Master of Philosophy

September 2009

CERTIFICATE OF ORIGINALITY

I hereby declare that this thesis is my own work and that, to the best of my knowledge and belief, it reproduces no material previously published or written, nor material that has been accepted for the award of any other degree or diploma, except where due acknowledgement has been made in the text.

_____(Signed)

_____(Name of student)

ABSTRACT

In this project, an analytical model of rotational hybrid vibration absorber (RHVA), which is coupled with a flexible structure, is derived for controller design and vibration suppression. Unlike the case of translational HVA, it is easier to tune the passive absorption frequency of the rotational HVA. A novel controller, which is applicable to either rotational HVA or translational HVA, is developed on the basis of the pole placement method. The proposed controller introduces active damping to a flexible structure and attenuates vibration of the entire structure. This controller, hereinafter, is called a global structural vibration controller.

The proposed rotational HVA and the global structural vibration controller was coupled to the end position of a cantilever beam for global structural vibration control in simulation tests, when random disturbance was applied at either a single point or a portion of the beam structure. Two indices, which are used to quantify the structural vibration motion, were calculated from the numerical test results. They include mean square motion which can be used to observe vibration motion at a single point, and spatial average mean square motion which can be used to observe average vibration motion of the beam structure. Simulation results demonstrate that the rotational HVA can mitigate more than 85% of mean square motion at the coupling point and more than 85% of spatial average mean square motion along the entire beam structure. This indicates that a rotational HVA can significantly suppress both point and entire beam structural vibration simultaneously.

Groundhook damper and translational HVA, which are conventional devices used for structural vibration control, were also coupled with the same cantilever beam at the end position for global structural vibration control in separated simulation tests. Numerical results show that a groundhook damper and a translational HVA can alleviate more than 83% and more than 79% of mean square motions at their respective coupling points, and can alleviate more than

85% and more than 80% of spatial average mean square motions along the entire beam structure respectively. This signifies that a rotational HVA could provide better vibration attenuation ability than a translational HVA in global structural vibration control and similar vibration attenuation performance as a groundhook damper.

Experimental rotational HVA and beam structure were fabricated to verify the proposed controller. The proposed analytical model of the rotational HVA and the global structural vibration controller were validated by the experimental results. Mean square motions and spatial average mean square motions were calculated from the experimental results and compared with those values calculated from the numerical results. It was found that experimental results are reasonably close to the numerical results.

This investigation provides better understanding on the performance and design of a rotational HVA and its active controller. Numerical results clearly demonstrate that a rotational HVA itself can be an effective device and is feasible as a better alternative device to a groundhook damper or a translational HVA for global structural vibration control of a cantilever structure.

PUBLICATIONS ARISING FROM THE THESIS

Conference Proceedings:

M.H. Tso, J. Yuan, W.O. Wong, Structural vibration control with hybrid vibration absorbers, *3rd International Conference on Integrity, Reliability and Failure*, Porto, Portugal, Paper no. S1120_A0335, 2009

ACKNOWLEDGEMENTS

It is a pleasure to express my gratitude to many who have help in this research project. I would like to thank Dr. J. Yuan and Dr. W. O. Wong, for their guidance, comment and constructive criticism throughout my research study.

I would also like to appreciate the financial support on the studentship and the conference from the Hong Kong Polytechnic University.

Finally, I wish to thank my parents and my wife for their love, support and encouragement in the last two years.

TABLE OF CONTENTS

LIST OF FIGURES

LIST OF TABLES

1 INTRODUCTION

1.1 Scope and Background

Vibration attenuation is a well-known and important problem for civil or mechanical engineers, because violent vibration can cause structure damage or machine failure and may even inflict severe damage on assets and lives of human being. Vibration control of structures and mechanical systems, therefore, becomes a significant research topic for vibration engineers and researchers to study. In the past, lots of approaches were developed to suppress the structural and mechanical vibration by different researchers and engineers. In the literature, skyhook/groundhook viscous damper and vibration absorber are two of the major devices used for vibration attenuation.

Typically, a groundhook viscous damper shown in Figure 1-1 is mounted between a vibrating body and a fixed boundary such as ground. The mounting base is used to provide a reaction force for the damper. With the help of the viscous damper, vibration energy of the vibrating body can be dissipated. Actually, the application of a damper is a simple and low cost approach for vibration mitigation, but its demand on the mounting base may cause it unfeasible to be installed for some structures such as cantilever beam. In real practice, tall building or wing of a plane can be considered as a cantilever beam structure. For a cantilever beam, violent vibration typically exists at the tip position of the beam structure. In these cases, the skyhook/groundhook damper cannot be coupled with the cantilever beam structure at its tip position since mounting base is not available.

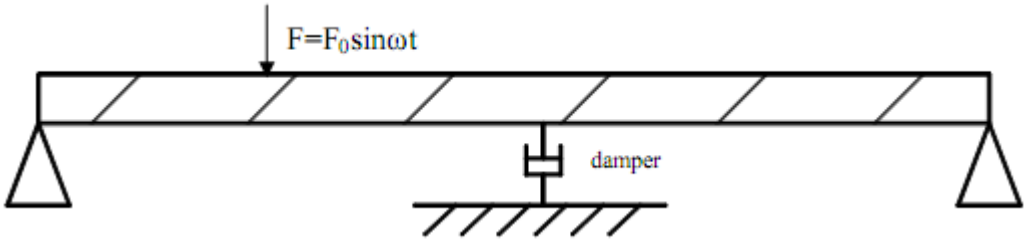

Figure 1-1 Schematic of a groundhook damper

In contrast, vibration absorber can avoid the requirement on the mounting base; and can be directly mounted on the vibrating body to achieve vibration alleviation. Vibration absorbers shown in Figure 1-2 mainly can be categorized into passive/dynamic vibration absorber (DVA), adaptive passive/dynamic vibration absorber (ADVA), active vibration absorber (AVA) and hybrid vibration absorber (HVA). Basically, DVA is composed of passive elements such as spring and damper. ADVA is an advanced design on the DVA in which the parameters of the passive elements can be automatically changed with time-variant disturbance. AVA is a pure active element. HVA consists of both passive and active elements and can be considered as an integration of DVA and AVA. Among the 4 types of vibration absorbers, hybrid vibration absorber is more advanced in its design and possesses the advantages of the other three types of absorbers. It can suppress vibration for a frequency band, introduce active damping into the structure-absorber coupled system and require lower power consumed actuator.

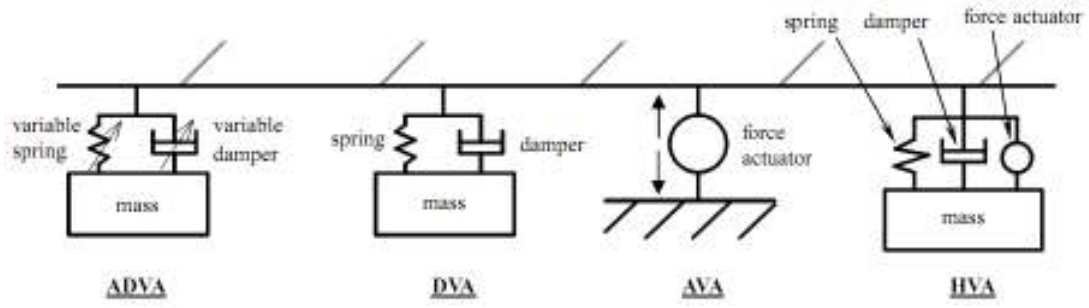

Figure 1-2 Schematic of DVA, ADVA, AVA and HVA

In some HVA designs, its passive counterpart should be tuned with respect to a target resonance before HVA can be installed in a vibrating structure. The tuning procedure actually is the same as the conventional passive vibration absorber (DVA). In the literature, Wong *et al.* (2007) proposed a DVA designed in rotational form. Comparing with the translational DVA, the rotational DVA is easier to tune its resonant frequency. Since the HVA can be either in translational or rotational form, one would like to see whether a rotational HVA can provide similar ability to suppress vibration as the translational HVA. If the answer is positive, then the

rotational HVA would be a better alternative because of the ease of tuning its resonant frequency.

On the other hand, control algorithms are necessary for generation of the control signal in an active HVA application. In the literature, there are lots of prior research works on the controller design and zero-pole placement method is one of the designs. Yuan (2001) indicated that applying zero-pole placement method into a closed-loop of a structure-absorber coupled system can simultaneously introduce an absorption band and enhance the damping effect of the system, and this advantage cannot be achieved by most of the controllers. In his work, he proposed a Proportional-Integral-Derivative (PID) controller, which can use a single acceleration feedback as the control signal, on the basis of the zero-pole placement method for local point structural vibration control. Recently, more and more research works [Jacquot (2003); Dayou (2006)] focus on global structural vibration control which aims at suppressing the vibration of entire beam structure instead of suppressing a point vibration. This is because vibration attenuated at a point may enhance vibration at ambient locations. Global structural vibration control, therefore, becomes significant to prevent vibration magnification at the structural ambient locations. Comparing with point vibration control, global structural vibration control is more complicated. However, the prior knowledge on point vibration control still can be helpful in the global structural vibration control problem. Typically, an active element can introduce active damping into the structure-absorber coupled system at the controlled point in point vibration control. Therefore, the feasibility of introducing active damping to the entire beam structure with the active element for global structural vibration control is still a worthy research question. In addition, it is of interest to design a global structural vibration controller on the basis of the zero-pole placement method to introduce absorption frequency and active damping simultaneously to the entire beam structure to achieve the global structural vibration control.

1.2 Research Objectives

From the background information, three research questions can be aroused. First, a skyhook/groundhook damper can be an effective method to dissipate vibration energy of the vibrating structure, but its demand on the mounting base causes it unfeasible to install in some cantilever beam structures such as tall building or wing of a plane. However, HVA can be directly mounted on a vibrating structure for structural vibration attenuation. Implementing a HVA to replace the application of a skyhook/groundhook damper for structural vibration control, therefore, can be a significant research question. Second, rotational passive vibration absorber (DVA) has the advantage on its ease of tuning. As rotational HVA is composed of similar passive counterpart as the DVA, rotational HVA may also possess the advantage on its ease of tuning than the translational HVA. It is, therefore, worth to investigate whether rotational HVA can provide similar vibration mitigation ability as the translational one and has the possibility as a better alternative design of HVA to solve the practical tuning difficulty. Third, local point vibration control may enhance the vibration amplitude of the structural ambient locations, global structural vibration control, however, can guarantee the vibration attenuation of entire structure. In view of structure protection, global structural vibration control can be more effective and reliable to protect the structure from damage. In prior research works, controller designed on the basis of zero-pole placement method has been demonstrated to provide an excellent vibration suppression performance to a flexible structure in point vibration control. With the prior knowledge in point vibration control, further study on controller designed with zero-pole placement method and developing it as a global structural vibration controller can be another important research question.

From the above three research questions, five objectives are established for this project:

1) Establish an analytical model for a rotational HVA which is coupled with a flexible structure.

2) Design a novel global structural vibration controller, which is applicable to either translational or rotational HVA, on the basis of pole placement method to introduce active damping and an absorption frequency to the entire flexible structure.
3) Evaluate whether a rotational HVA can be a better alternative design of HVA by measuring its local and global vibration suppression performance and comparing those values with a translational HVA numerically.
4) Evaluate whether a rotational HVA can be implemented to replace a groundhook damper, which is mounted between a vibrating structure and a fixed base, by measuring its local and global vibration suppression performance and comparing those values with the damper numerically.
5) Validate the established analytical model of the rotational HVA and the developed global structural vibration controller by comparing its local and global vibration suppression performance between experimental and numerical results.

To achieve the above five objectives, ten tasks should be performed:

1) Establish an analytical model on the basis of Euler-Bernoulli beam equation for the proposed rotational HVA (RHVA).
2) Develop a global structural vibration controller, which is applicable to either translational or rotational HVA, on the basis of pole placement method and Bezout equation to introduce active damping and an absorption frequency to the entire beam structure.
3) Model beam-rotational HVA coupled system, beam-translational HVA coupled system and beam-groundhook damper coupled system by commercial software "MatLAB" and conduct simulation tests.
4) Calculate the mean square motions, which can be used to observe the structural vibration amplitude at a single point, and the spatial average mean square motions, which can be used to observe the average vibration amplitude of the entire beam structure, to quantify the structural vibration amplitude from the simulation results for a rotational and a translational HVA separately, and

hence use these values to evaluate and compare the vibration suppression performance between a rotational HVA and a translational HVA.

5) Calculate the mean square motions and the spatial average mean square motions for a rotational HVA and a groundhook damper separately from the simulation results, and hence use these values to evaluate and compare the vibration suppression performance between the rotational HVA and the groundhook damper.
6) Design and fabricate a test rig which is composed of a beam and a rotational type HVA.
7) Conduct the experiment, collect data and analyze data.
8) Calculate the mean square motions and the spatial average mean square motions for the rotational HVA from the experimental results.
9) Conduct the simulation test for the beam-rotational HVA coupled system with real experimental parameters such as beam modal damping ratio, beam mass and absorber mass.
10) Calculate the mean square motions and the spatial average mean square motions for the rotational HVA from the numerically results, and use the values to compare with the experimental one.

1.3 Project Significance

This project has both academic value and practical significance to the industry if the project objectives can be achieved. An analytical model for the proposed rotational HVA, which is rarely found in the literature, is established. This model can be useful for further development on similar type of rotational HVA. A novel controller, which is applicable to either translational HVA or rotational HVA, is developed to introduce active damping and an absorption frequency to entire beam structure, and to achieve global structural vibration control. For global structural vibration control, the proposed rotational HVA is expected to have similar vibration suppression performance as the conventional translational HVA. Since it is easier to tune the passive absorption frequency of rotational HVA than the translational one, the

rotational HVA can be a better alternative design of HVA. The proposed rotational HVA is also able to replace a skyhook/groundhook damper, it thus can provide a better alternative way to solve the global structural vibration control problem in case skyhook/groundhook damper is not available to be installed.

1.4 Layout of Present Thesis

The thesis includes both numerical and experimental study reports presented in seven chapters.

Chapter 1 provides an overview of the scope and background of the present project. Research questions, project objectives, tasks and its significance are also presented.

Chapter 2 offers a complete literature review on skyhook/groundhook damper, the four kinds of vibration absorbers and active control algorithms. Summary of the literature review is reported in the end of this chapter. Idea on development of a new design of rotational HVA and a novel global structural vibration controller are inspired from the prior research works.

Chapter 3 presents the new design of the proposed rotational HVA, the structure of the conventional translational HVA and the limitation of skyhook/groundhook damper. The analytical model of the rotational HVA – beam coupled system under point and distributed disturbance is derived. The well-known analytical models of translational HVA – beam coupled system and groundhook damper – beam coupled system under point and distributed disturbance are also derived.

Chapter 4 proposes the idea on the global structural vibration controller design. Its design is on the basis of the pole placement method and the Bezout equation. Implementation method of the proposed controller on real application and stability of the proposed controller are discussed.

Chapter 5 reports the numerical results of the rotational HVA – beam coupled system, translational HVA – beam coupled system and groundhook damper – beam coupled system under point and distributed random disturbance. Calculation, comparison and discussion on some indices, which are used to quantify the structural vibration, are also presented for these systems.

Chapter 6 describes the experimental configuration and experimental methodology. Experimental results are reported. Indices, which are used to quantify the structural vibration, are calculated with the experimental results and compared with the simulation results.

Chapter 7 concludes all the important findings in this investigation. Suggestions on future works on this project are also discussed.

2 LITERATURE REVIEW

Vibration is an important dynamic problem in the engineering world. Violent vibration can damage structures, buildings and machines. It can also introduce acoustic problems such as noise and hence cause discomfort to human-being when vibration propagates from an operating machine to its thin case. Isolating or attenuating vibration from its source, therefore, is a significant engineering problem for engineers. In the literature, skyhook/groundhook damper and vibration absorber are two possible devices used for isolation or attenuation of vibration. For the vibration absorbers, there are mainly four kinds of absorbers including passive/dynamic vibration absorber (DVA), adaptive passive/dynamic vibration absorber (ADVA), active vibration absorber (AVA) and hybrid vibration absorber (HVA).

2.1 Review of Skyhook/Groundhook Damper

Viscous damper is a well known device used for structural vibration control [Main and Krenk (2005); Mansoori and Moghadam (2009); Occhiuzzi (2009)]. It is a cheap, low cost and effective device. One of the special and ideal cases for the application of viscous damper is a skyhook/groundhook damper [Jacquot (2000); Engelen *et al.* (2007)]. Skyhook/groundhook viscous damper shown in Figure 2-1 is a translational viscous damper which is mounted between a vibrating structure and a fixed mounting base. The word “skyhook” or “groundhook” means the damper is hooked at an inertial reference point such as wall or ground which can provide absolute zero displacement and velocity to the damper. Generally, skyhook/groundhook damper can provide better vibration suppression performance to the vibrating structure since the mounting base provides reaction force to the damper. However, it is difficult to offer a mounting base to the skyhook/groundhook damper in some of the cases like cantilever beam. For example, wing of a plane or a building structure can be considered as a cantilever beam. Normally, violent vibration exists at the tip position

of the vertical cantilever beam. Coupling the skyhook damper to its tip position can effectively attenuate the vibration of the entire beam structure, but it is impossible to install the damper since mounting base is not available in this case. To overcome this limitation, it is, therefore, necessary to seek an alternative device to replace the skyhook/groundhook damper in which the replaced device should provide similar or better vibration mitigation performance as the skyhook/groundhook damper. In this project, it is found that a rotational hybrid vibration absorber (RHVA) can provide similar vibration attenuation performance as the skyhook/groundhook damper. Moreover, RHVA can avoid the demand on a mounting base since it can be directly mounted on the tip position of a cantilever beam. The details of the RHVA on its structure and its vibration suppression performance are discussed in later chapters.

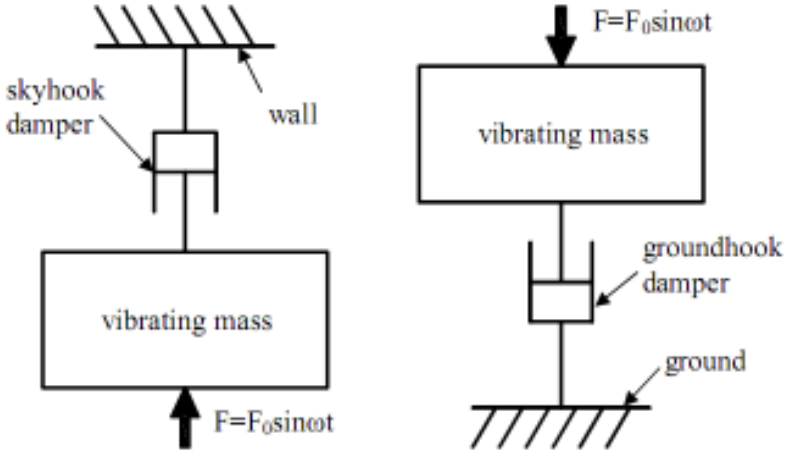

Figure 2-1 Schematic of a skyhook and a groundhook viscous dampers

2.2 Review of Passive/Dynamic Vibration Absorber (DVA)

Passive/dynamic vibration absorber (DVA), which was invented for almost a century [Hermann (1909)], is a well-known device used to cease vibration of a vibrating system under harmonic excitation and to protect the vibrating system from vibration. DVA shown in Figure 2-2 is a translational DVA (TDVA) and has translational DOF. It is basically composed of an auxiliary mass which is mounted to a vibrating system by spring and damping devices. After proper tuning, it can be

used to absorb vibration energy from the vibrating source of a primary structure [Hunt (1979); Inman (1994)] or to isolate vibration from the primary structure [von Flotow *et al.* (1994)]. Optimum tuning theories for conventional DVA tuning were initially proposed by Den Hartog (1956) and Snowdon (1968).

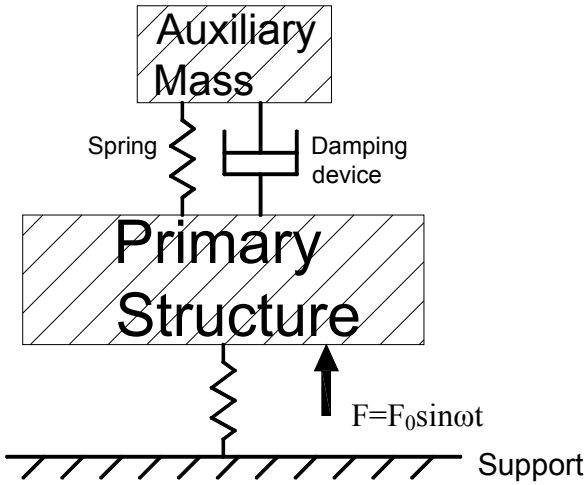

Figure 2-2 Schematic of a translational dynamic vibration absorber

Although DVA can reduce vibration of a primary system, DVA application still accompanies with a number of restrictions. DVA can effectively suppress vibration amplitude at the pre-tuned resonant frequency but not function well at other resonant frequencies. If DVA coupling position is in a nodal position of a structure, coupled DVA may not be able to absorb vibrating energy from the primary structure [Tang (2004)]. As structural resonant frequencies and disturbance frequency may vary under different ambient conditions or time passing, a pre-tuned DVA may provide unexpected performance to the structure due to mistuning of parameters. The worst case could be enhancement of vibration level to the primary structure at certain frequencies [Sun *et al.* (1995)]. Another detrimental effect of using DVA is elicitation of one extra resonant peak in the primary frequency spectrum. As DVA with single degree of freedom (DOF) is coupled with the primary structure, the DOF of the integrated system is increased by one. One extra resonant peak, therefore, is elicited in the integrated system after mounting with DVA [Korenev and Reznikov (1993)].

Making DVA more flexible to be used in real applications, different kinds of prior research works have been done. Researchers tried to modify the design of a conventional DVA [Hagood and von Flotow (1991); Igusa and Xu (1994); Wu (1998); Jang and Choi (2007); Wong and Cheung (2008)] for better vibration alleviation. Some researchers found a set of optimal parameters including damping ratio, tuning ratio and coupling position for one or multiple DVA(s) aiming at vibration mitigation of a vibrating system over a frequency band [Warburton (1982); Kwanami and Seto (1984); Chiba and Sugimoto (2003); Jacquot (2003); Dayou (2006); Lee *et al.* (2006); Li and Zhu (2006); Taniguchi *et al.* (2008); Bai and Grigoriadis (2009); Cheung and Wong (2009)].

Apart from the discussed translational DVA, there is another design of DVA which has rotational DOF called rotational DVA (RDVA). In real practice, vibrating system may have more than one DOF, so its motion can basically be modeled by translational and rotational motions in one dimensional consideration. RDVA, therefore, can be used to absorb the rotational vibration of the primary vibrating system. The fundamental design of RDVA could be a pendulum-like absorber as shown in Figure 2-3.

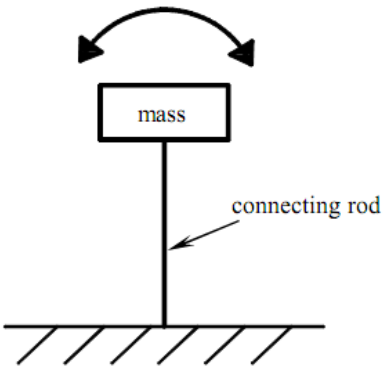

Figure 2-3 Schematic of a pendulum-like rotational dynamic vibration absorber

Some prior research works have been studied on implementing a pendulum absorber for vibration suppression of a primary system [Cartmell and Lawson (1994); Ertas *et al.* (2000); Vyas and Bajaj (2001); Cicek and Ertas (2002); Cuvalci *et al.* (2002)]. Researchers found that non-linearity exists in the pendulum-structure coupled system if the pendulum absorber is under violent vibration. The non-linear effect

causes instability of the coupled structure, and induces bifurcation and chaos problems [Haxton and Barr (1972); Mustafa and Ertas (1995); Warminski and Kecik (2009)]. Although non-linearity problems exist in the pendulum absorber application, this can be avoided if the motion of pendulum absorber is small. Linear assumption, therefore, still can be used for the pendulum absorber. Webster and Semke (2005) designed and analyzed an effective RDVA for the use in space borne remote sensing with linear assumption. The presented RDVA demonstrated performance improvement over nearly the entire anticipated operational range. Recently, researchers attempted to design new kind of DVA by combining two kinds of DVA(s) including TDVA and RDVA as one for further vibration alleviation. Cha and Zhou (2006) presented an idea of imposing points with zero displacements and zero slopes at any location of interest along a linear structure which is under harmonic excitations. Their study showed that nodes can be introduced at any location of interest on a beam by using a combined type of absorber. Wong *et al.* (2007) proposed using the combined type absorber for vibration isolation of a beam which is under point or distributed harmonic disturbance. They proved a segment of beam with zero amplitude can be obtained if the combined type absorber is attached at a suitable location on the beam. Most researchers, up to now, have focused on the design and the working performance of the TDVA, however, very few research reports can be found on the design and the working performance of the RDVA in the literature. On the basis of the RDVA presented by Wong *et al.* (2007), a pure rotational DVA is much easier to fabricate, tune and implement into a vibrating system than the conventional translational one.

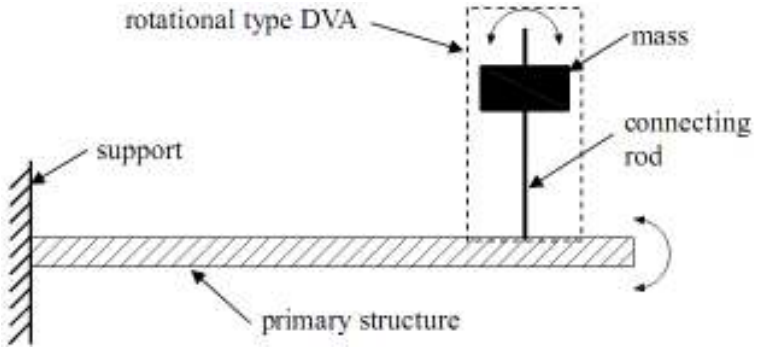

Figure 2-4 Schematic of a rotational dynamic vibration absorber

The presented RDVA shown in Figure 2-4 is simply composed of a beam and a mass. Its mass is attached onto the connecting beam of the RDVA. This design allows easy RDVA tuning by changing the mass position along the connecting beam vertically. As the RDVA can provide a tunable moment arm for the mass, inertial moment can be easily changed. Comparing with the conventional TDVA, its tuning should be accompanied with replacement of spring or mass. RDVA, therefore, can provide greater tuning flexibility. With the advantages of simply fabrication, easy tuning and effective attenuation of vibration, further research works on RDVA studies and designs for vibration suppression is necessary in the future.

2.3 Review of Adaptive Passive/Dynamic Vibration Absorber (ADVA)

Structural resonant frequencies or disturbance frequencies may vary under different ambient conditions or time passing, attenuated performance of an accurately pre-tuned DVA, therefore, may degrade and hence even evoke vibration enhancement to the primary vibrating structure. To overcome the restriction of DVA on accurate tuning, an adaptive technique is used to dynamically modify the passive characteristics such as stiffness or damping of the DVA. This kind of modified DVA is called adaptive passive/dynamic vibration absorber (ADVA) [Sun *et al.* (1995)]. ADVA can effectively alleviate vibration level of a primary vibrating structure under parametric exciting such as operating machine with varying rotating speed or structure under wind induced vibration. A number of prior research works have been done on different adaptive design including spring stiffness variation [Fujino *et al.* (1993); Ryan *et al.* (1994); Buhr *et al.* (1997); Nagarajaiah and Varadarajan (2005); Williams *et al.* (2005); Deng *et al.* (2006); Sun *et al.* (2008)], piezoelectric-based device stiffness variation [Davis and Lesieutre (2000); Niederberger *et al.* (2004)] and damping variation [Hrovat *et al.* (1983); Anusonti-Inthra and Gandhi (2004)]. As control signal is required to vary the dynamic parameters of the ADVA, active control scheme is vital for generation of control signal. Active control scheme could be fuzzy logic controller [Lai and Wang (1996); Kidner and Brennan (2002)], fuzzy-PD controller [Rustighi *et al.* (2005)], hierarchical fuzzy logic controller [Lin

(2007)] and fuzzy-genetic algorithm controller [Kim and Roschke (2006)]. Although ADVA can effectively suppress vibration for structure under parametric excitation, restrictions are still bounded by its design. von Flotow *et al.* (1994) indicated three kinds of delays including logic delay, actuation delay and dynamic delay that may affect the performance of ADVA and restrict its application to slowly-varying disturbance frequencies. Morgan and Wang (2002) also noted ADVA is not suitable to be used for multiple frequencies or broadband excitation since its design is difficult to achieve fast and accurate tuning.

2.4 Review of Active Vibration Absorber (AVA)

Apart from the discussed DVA and ADVA, active vibration absorber (AVA) is the third kind of vibration absorber. It is mainly composed of a controller and active components. With the help of the active component, AVA can provide a counter-counting force or moment to the vibrating structure and hence achieve the goal of zero vibration to the primary structure [Williams *et al.* (2002)]. AVA shown in Figure 2-5 is different from the conventional DVA, it can be treated as a virtual DVA which is composed of virtual spring-damper-mass system. It is a special type of dynamic compensator which possesses a second order dynamic equation in the same form of that of a physical DVA. In the closed-loop form, it is equivalent to a composite system in which the physical primary structure and the virtual structure are connected through virtual springs, dashpots and acceleration dampers. The dynamic parameters of the virtual absorber can hence be tuned by different active control schemes [Bruner *et al.* (1992); Xu (1993); Lee Glauser *et al.* (1995)].

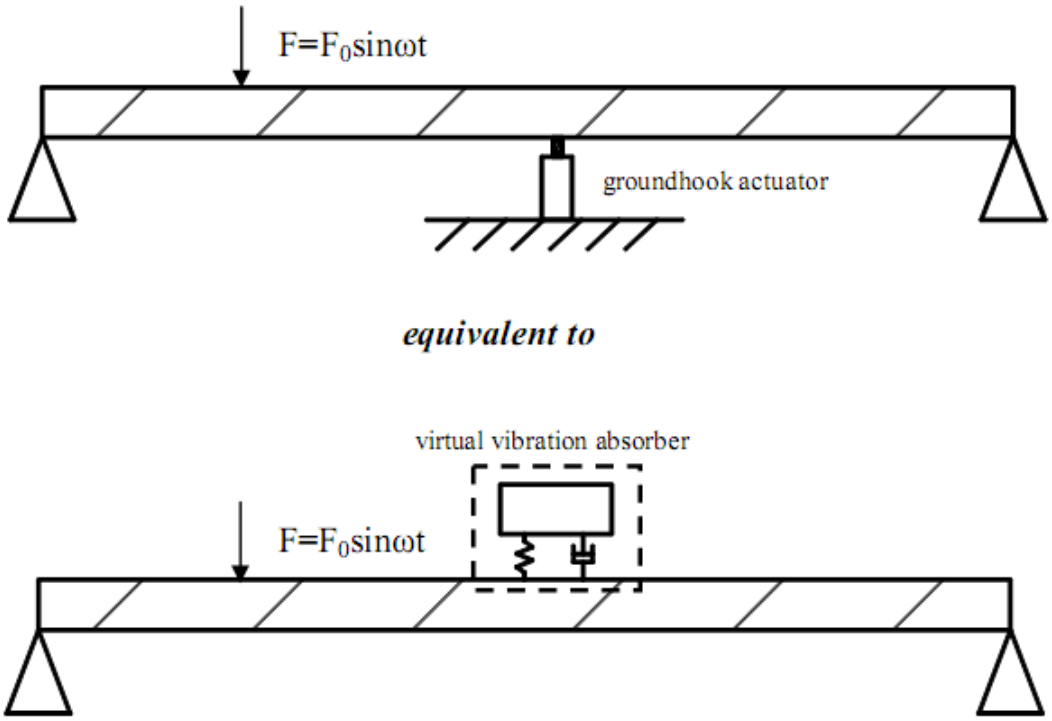

Figure 2-5 Schematic of an active vibration absorber

Since the controller is critically important to control signal synthesis for the AVA, a number of research efforts have been done on the controller design in the past including linear quadratic optimal based controller [Balas (1978); Gupta (1980); Chung *et al.* (1989); Sievers and Von Flotow (1989); Lee Glauser *et al.* (1995)], Fuzzy-PD controller [Lin *et al.* (2007)] and Fuzzy-Genetic Algorithm controller [Pourzeynali *et al.* (2007)]. Studies of implementing AVA into real applications for vibration control have also been done including vibration control of flexible space structures [Kaplow and Velman (1978); Wie and Gonzalez (1990)], beam structures [Chung *et al.* (1989); Wu *et al.* (2007)], vehicle seat [Wu and Chen (2004)] and system damping enhancement [Rockwell (1965); Lindquist and Yakubovich (1997); Bhatta and Sinha (2003)].

With the help of active elements, robustness of AVA to changes in excitation frequencies can be improved. Vibration attenuation over a frequency band can be achieved [Xu (1993); Williams *et al.* (2002)]. Active damping can also be introduced into multi-resonant structures [Rockwell (1965)]. Although AVA can be an effective approach used for vibration mitigation, restrictions on implementation

of AVA into real applications still exist. As all counter efforts used for vibration suppression are generated by the actuator, its power should be sufficiently large in case of implementing AVA for large structural vibration control. The power consumption and actuator size, therefore, may be very large [von Flotow *et al.* (1994); Franchek *et al.* (1996); Wu *et al.* (2007)]. Another restriction is that mounting sometimes necessary for the skyhook/groundhook type actuator to generate its reaction force in AVA implementation [Rockwell (1965); Balas (1978); Wu and Chen (2004) Wu and Shao (2007)], this kind of design sometimes may not be practical in real structural application. Reliability and maintenance problems are also important considerations for AVA implementation. As the suppression performance of AVA relies on the actuator and its controller, failure of either component may cause malfunction of the entire vibrating control system. Comparing with DVA or ADVA which are fully or partially dependent on the passive components, AVA, however, may have lower reliability.

2.5 Review of Hybrid Vibration Absorber (HVA)

To achieve the goal of structural vibration control for random disturbance with lower power consumed actuator, an advanced design of vibration absorber called hybrid vibration absorber (HVA) is proposed. A typical translational HVA (THVA) shown in Figure 2-6 basically is an integration of a DVA and a force actuator [Sun *et al.* (2007)]. Reaction mass is supported by an active element which is parallel to resilient elements including spring and damper. Comparing with DVA and AVA, HVA seems possessing their advantages. In fact, HVA can cover a wider band frequency for vibration suppression and have higher control authority in case of comparing with DVA [Sun *et al.* (1995); Burdisso and Heilmann (1998)]. As passive spring is integrated in the HVA, it can help to share part of the counter-disturbance effort and the power requirement of the actuator can hence be much minimized [Wu *et al.* (2007)]. With the help of reaction mass and resilient elements, passive counterpart of the HVA can act as a DVA. In view of structural vibration protection,

HVA can be considered as a fail-safe device since it can perform as a DVA to continuously suppress structural vibration in case of active elements failure happened [Sun *et al.* (1995)]. In real practice, designers take the advantage of the characteristic of HVA which is composed of passive elements and active element. They design the HVA to work into two modes including active mode and passive mode. Active mode is used to control relatively small vibration of the primary structure while passive mode is used to control strong and violent vibration [Sun *et al.* (1995)]. Moreover, inertial actuator of HVA does not require mounting base to provide its reaction force, it can be directly installed in a vibrating structure [Benassi and Elliott (2004)]. This makes HVA more practical to implement into real application.

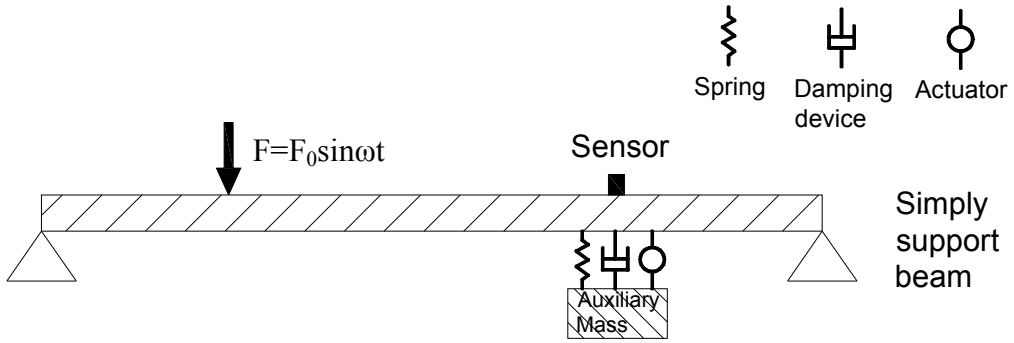

Figure 2-6 Schematic of a translational hybrid vibration absorber

In the past, different kinds of actuator designs have been studied in previous research works. Most of these actuators are designed in translational form. These designs include dual mass HVA [Burdisso and Heilmann (1998); Du *et al.* (2005)], voice-coil type electromagnetic actuator [Yasuda *et al.* (1996); Nagem *et al.* (1997); Ikai *et al.* (2000); Chen *et al.* (2005)], electro-hydraulic actuator [Zhang and Alleyne (2003)] and hybrid piezoelectric absorber [Tang and Wang (2001); Morgan and Wang (2002)]. In real practice, researchers have implemented HVA(s) into real application including vibration control for bridges [Patten *et al.* (1996)], buildings [Chang and Soong (1980); Lee Glauser *et al.* (1995); Nonami *et al.* (1996)] and vehicles [Hirata *et al.* (1995); Huang and Lin (2003)]. Up to now, lots of researchers have focused on the development of translational-type HVA. Very few researchers,

however, focused on the development of rotational HVA (RHVA). Since HVA is composed of both active and passive elements, pre-tuning of its passive counter part is necessary in some kinds of absorber design [Yasuda *et al.* (1996); Yuan (2000)]. Its tuning process basically is the same as the DVA tuning. In the review of DVA, advantage of rotation type DVA on its ease of tuning has been presented. It is, therefore, of interest to investigate whether a rotational HVA can also possess the same advantages as the pure rotational DVA, whether a rotational HVA can provide similar vibration suppression ability as the conventional translational HVA and hence can be a better alternative design of HVA.

Since the active element is integrated into the HVA, control algorithm is required to generate control signal for the actuator. There are basically two types of control schemes including modal control scheme and simple control scheme in the literature. HVA(s) controlled by modal control scheme and simple control scheme, hereinafter, are called modal hybrid vibration absorber (modal HVA) and simple hybrid vibration absorber (simple HVA) respectively [Yuan (2001)].

In modal control scheme, modal states of the primary structure are used as a reference in the control process. The modal states basically cannot be measured directly and should be recovered from its feedback measurements via modal filter. This, therefore, requires a large amount of sensors for the feedback measurements [Balas (1978)]. In addition to modal state feedback, modal control scheme is highly dependent on the exact mode functions of the primary structure in order to recover the modal states. In practice, it is very difficult for us to obtain the exact mode functions of the primary structure. Incorrect or inaccurate modal functions may lead to modal error and unsatisfactory control performance [Yuan (2001)]. Apart from the dependence of the exact mode functions and modal state feedback, modal control scheme needs on-line computation for the modal states recovery and hence leads to slower control performance [Yuan (2001)]. In the past, controllers designed on the basis of the modal control scheme have been studied by different researchers [Chang and Soong (1980); Nonami *et al.* (1994); Hirata *et al.* (1995); Yasuda *et al.* (1996); Lee Glauser *et al.* (1997); Adachi *et al.* (2004)].

Comparing with modal control scheme, simple control scheme does not need to recover the modal states of the primary structure in the control process. It can directly process and use the sensor feedback signals for vibration control. With the help of simple control scheme, the amount of feedback sensors can be significantly minimized. Moreover, simple control scheme can save the on-line computation and avoid modal error since exact mode functions of the primary structure are unnecessary to recover the modal states [Yuan (2001)]. In the literature, a number of simple control schemes have been studied in the prior research works. They include delayed resonator [Olgac and Holm Hansen (1994)], PD controller [Elmali *et al.* (2000)], PID controller [Yuan (2000); Benassi and Elliott (2004)], feedforward controller [Burdisso and Heilmann (1998)], band-pass scheme [Filipovic and Schröder (1998)], neural network controller [Ma and Sinha (1996)], hierarchical fuzzy controller [Jalili (2000)], virtual passive devices [Wu *et al.* (2007)], active resonator [Filipovic and Schröder (1999)] and adaptive active resonator [Sun *et al.* (2007)]. Among those of the simple control schemes, Yuan (2001) indicated that most of the simple control algorithms can only assign closed-loop poles but lack the ability to assign closed-loop zeros and poles simultaneously to a structure-absorber coupled system. In fact, zeros and poles play important roles in a linear vibrating system. It can affect the frequency response of the system such as zeros can introduce absorption band and poles can attenuate resonance peaks. In his work, he presented using a PID controller, which is designed on the basis of the zero-pole placement method, with a HVA to assign closed-loop zeros and poles to a beam-absorber coupled system. This approach successfully attenuates resonant peaks of multi-modes and introduces an absorption frequency at the HVA coupling location for point vibration control. On the other hand, there are rare studies working on the controller designed with zero-pole placement method in the prior research works. Since zero-pole placement method has been clearly demonstrated its effectiveness on vibration mitigation of a vibrating system, further research works on controller design with zero-pole placement method are significantly important.

Recently, more and more research works [Dayou and Brennan (2003); Jacquot (2003)] focus on global structural vibration control which aims at suppressing the

vibration of an entire beam structure instead of suppressing a point vibration. This is because vibration attenuated at a point may enhance vibration at ambient locations. Global structural vibration control, therefore, becomes significant to prevent vibration magnification at the structural ambient locations. Comparing with point vibration control, global structural vibration control is more complicated. However, the prior knowledge on point vibration control still can be useful on the global structural vibration control problem. Typically, active element can introduce active damping to the structure-absorber coupled system at the controlled point for point vibration control [Rockwell (1965); Bhatta and Sinha (2003)]. Therefore, the feasibility of introducing active damping to the entire beam structure with the active element for global structural vibration control is still a worth research question. In addition, it is of interest to design a global structural vibration controller with the zero-pole placement method to introduce absorption frequency and active damping simultaneously to the entire beam structure to achieve global structural vibration control.

2.6 Summary of Literature Review

Generally, skyhook/groundhook damper can be used for structural vibration control since it is an effective device used to dissipate vibration energy of a vibrating structure. However, its demand on the mounting base causes it unfeasible to install in some structures such as tall building or wing of a plane. On the other hand, HVA can be directly mounted on a vibrating structure for structural vibration attenuation and avoid the necessity of the mounting base. Implementing a HVA to replace the application of a skyhook/groundhook damper for structural vibration control, therefore, can be a significant research question.

In addition, rotational passive vibration absorber (DVA) is easier to tune its absorption frequency when comparing with the translational one. As rotational HVA is composed of similar passive counter part as the DVA, rotational HVA may also possess the advantage on its ease of tuning. Therefore, it is worth to investigate

whether rotational HVA can provide similar vibration mitigation ability as the translational one and has the possibility as a better alternative design of HVA.

Moreover, local point vibration control may enhance vibration amplitude of the structural ambient locations, global structural vibration control, however, can guarantee the vibration attenuation of the entire structure. In view of structure protection, global structural vibration control can be more effective and reliable to protect the structure from damage. In prior research works, controller designed on the basis of zero-pole placement method has been demonstrated to provide an excellent vibration suppression performance to a flexible structure in point vibration control. With the prior knowledge in point vibration control, further study on developing a global structural vibration controller with zero-pole placement method can be another important research question.

3 MATHEMATICAL MODELS

In this chapter, the structure of a conventional translational hybrid vibration absorber (THVA), a new design of rotational hybrid vibration absorber (RHVA) and the limitations of a skyhook/groundhook damper are discussed. Analytical model of the RHVA, which is coupled with a beam structure, is derived when random disturbance is acting on a point or a portion of beam span; whereas this analytical model is rarely found in the literature. Well-known analytical models of a THVA and a groundhook damper, which are separately coupled with a beam structure, are also derived for further comparison with the RHVA on their vibration attenuation performance. Those analytical models are finally derived into their closed-loop transfer function for further controller design.

3.1 Conventional Design of a Translational Hybrid Vibration Absorber (THVA)

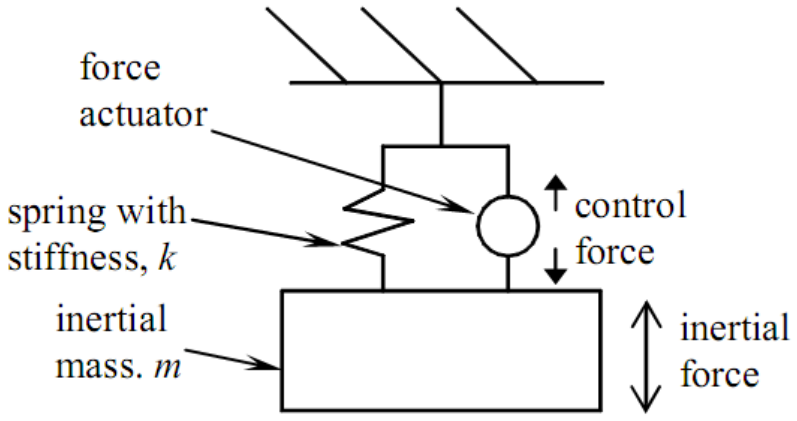

Figure 3-1 Structure of a translational hybrid vibration absorber

Conventional translational hybrid vibration absorber (THVA) shown in Figure 3-1 is basically composed of a linear spring, a linear damper, an inertial mass and a force actuator. The inertial mass is supported by the passive elements and the force actuator, which is in parallel with the passive elements. Typical force actuator can be

voice-coil electromagnetic actuator or electro-hydraulic actuator. Unlike the pure passive sprung-mass resonator, HVA typically can be used to achieve vibration mitigation within a frequency band since active element is integrated. In some HVA applications, its passive part can be tuned with respect to a disturbance frequency for vibration absorption. The absorption frequency f_p of its passive counterpart in rad/s can be simply tuned with equation (3-1) where k and m are the stiffness and mass of the passive elements.

$$f_p = \sqrt{\frac{k}{m}} \tag{3-1}$$

3.2 Mathematical Model of a Translational Hybrid Vibration Absorber (THVA) – Beam Coupled System

Mathematical model of a THVA, which is coupled with a beam, is derived for the cases of applying disturbance at a point and a portion of the beam structure separately. The models are finally derived to their closed-loop transfer functions for further controller design.

3.2.1 Point Disturbance

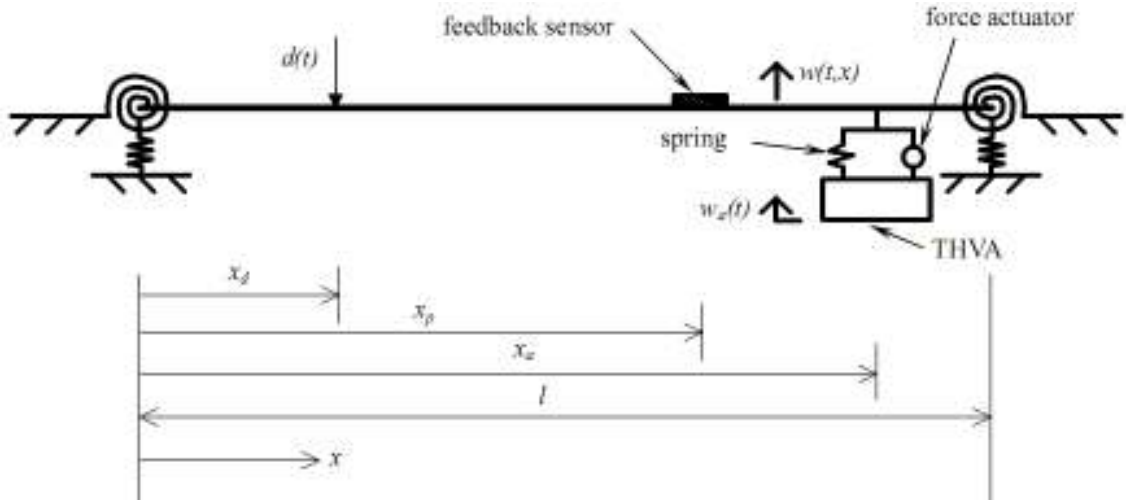

Figure 3-2 Point disturbance on a THVA-beam structure

A THVA shown in Figure 3-2 is coupled with a beam. The THVA consists of a sprung-mass as the passive part and an actuator as the active part. The beam is connected by two pairs of rotational and translational springs with different stiffness at its end points. Different types of boundary conditions can, therefore, be modeled via varying the stiffness of the springs. The beam has length l and its linear displacement is denoted as $w(t,x)$ while linear displacement of the THVA is denoted as $w_a(t)$. A disturbance $d(t)$ acts at point x_d and the THVA couples with the beam at point x_a. The beam is assumed to satisfy the Euler-Bernoulli hypothesis. The system dynamics are described by the following equations:

$$\rho\ddot{w}(t,x) + EIw''''(t,x) = d(t)\delta(x-x_d) + F_a\delta(x-x_a), \qquad 0 < x < l \tag{3-2}$$

$$F_a = \bar{v}_a[\dot{w}_a(t) - \dot{w}(t,x_a)] + \bar{k}_a[w_a(t) - w(t,x_a)] + F_{act} \tag{3-3}$$

$$m_a\ddot{w}_a(t) = -F_a \tag{3-4}$$

Equation (3-2) is the dynamic equation of the beam in terms of its translational motions where ρ is the mass density per length; E is the Young's modulus; I is the moment of inertia of the cross section of the beam; $\ddot{w}(t,x)$ is the second derivative of the linear displacement of the beam with respective to time, $w''''(t,x)$ is the fourth derivative of the linear displacement of the beam with respective to x and $\delta(x-x_a)$ is the Dirac delta function. Equation (3-3) models the coupling force F_a with its active part F_{act} generated by the actuator. $\dot{w}(t,x_a)$ is the first derivative of the linear displacement of the beam at point x_a with respect to time and $\dot{w}_a(t)$ is the first derivative of the linear displacement of the THVA with respect to time. Parameters $\bar{v}_a$ and $\bar{k}_a$ represent the damping coefficient and the stiffness of the translational passive part. The damping effect is assumed coming from the spring friction and as proportional damping. Equation (3-4) is a Newton's equation where m_a is the mass of the translational passive part and $\ddot{w}_a(t)$ is the second derivative of the linear displacement of the THVA with respect to time.

From the above formulation, the total linear displacement of the coupled system is represented by a vector $W^T = [w(t,x), w_a(t)]$. In general, it is difficult to solve a coupled system which consists of lumped-parameter system and distributed-parameter system. An easier alternative is to focus on the linear displacement of the beam $w(t,x)$ and decompose it into modal space through inner products. Separation of variables method is applicable to transform the spatial-temporal beam linear displacement $w(t,x)$ to an infinite series with its separated spatial and temporal terms.

$$w(t,x) = \sum_{i=1}^{\infty} \varphi_i(x) q_i(t) \tag{3-5}$$

where $\varphi_i(x)$ and $q_i(t)$ are the i^{th} mode eigen-function of translational motion and the i^{th} modal coordinate respectively.

The inner products are volume integrals over the beam structure with its i^{th} mode eigen-function of translational motion $\varphi_i(x)$.

$$q_i(t) = \int_{x=0}^{l} \varphi_i(x) w(t,x) dx = \frac{EI}{\rho \omega_i^2} \int_{x=0}^{l} \varphi_i(x) w''''(t,x) dx, \quad i = 1,2,3... \tag{3-6}$$

$$\ddot{q}_i(t) = \int_{x=0}^{l} \varphi_i(x) \ddot{w}(t,x) dx, \qquad i = 1,2,3... \tag{3-7}$$

$$\int_{x=0}^{l} \varphi_i(x) \varphi_j(x) dx = \begin{cases} 1 & i = j \quad i,j = 1,2,3\ldots \\ 0 & i \neq j \quad i,j = 1,2,3\ldots \end{cases} \tag{3-8}$$

In equations (3-6) and (3-7), $q_i(t)$ and $\ddot{q}_i(t)$ represent the i^{th} modal coordinate and the secondary derivative of the i^{th} modal coordinate with respect to time respectively; while ω_i denotes the natural frequency of the beam at the i^{th} mode. Using equations (3-6) and (3-7), equation (3-2) can be transformed to

$$\ddot{q}_i(t) + \omega_i^2 q_i(t) = d(t) \int_0^l \varphi_i(x) \delta(x - x_d) dx + F_a \int_0^l \varphi_i(x) \delta(x - x_a) dx, \qquad i = 1,2,3...$$

$$= \varphi_i(x_d) d + \varphi_i(x_a) F_a \tag{3-9}$$

where $d = d(t)$, $\varphi_i(x_d) = \int_0^l \varphi_i(x) \delta(x - x_d) dx$ and $\varphi_i(x_a) = \int_0^l \varphi_i(x) \delta(x - x_a) dx$

Applying Laplace transformation to equations (3-9), (3-3), (3-4) and (3-5) a set of dynamic equations can be derived and written as

$$q_i(s) = \frac{\varphi_i(x_d)d + \varphi_i(x_a)F_a}{s^2 + \omega_i^2}, \qquad i = 1,2,3... \tag{3-10}$$

$$F_a = (s\bar{v}_a + \bar{k}_a)[w_a(s) - w(s,x_a)] + F_{act} \tag{3-11}$$

$$s^2 m_a w_a(s) = -F_a \tag{3-12}$$

$$w(s,x) = \sum_{i=1}^{\infty} \varphi_i(x) q_i(s) \tag{3-13}$$

Using equations (3-10) and (3-13), linear displacement of the beam can be expressed as spatial-temporal equations.

$$w(s,x_p) = \sum_{i=1}^{\infty} \varphi_i(x_p) q_i(s) \approx \sum_{i=1}^{m} \varphi_i(x_p) \left[\frac{\varphi_i(x_d)d + \varphi_i(x_a)F_a}{s^2 + \omega_i^2} \right], \tag{3-14}$$

where x_p is the feedback sensor location and m is the truncated number of modes. Equation (3-14) can be written in vector-matrix form.

$$\begin{aligned} w_p = w(s,x_p) &\approx [\varphi_1(x_p) \cdots \varphi_m(x_p)] \begin{bmatrix} \frac{1}{s^2+\omega_1^2} & 0 & 0 \\ 0 & \ddots & 0 \\ 0 & 0 & \frac{1}{s^2+\omega_m^2} \end{bmatrix} \left\{ \begin{bmatrix} \varphi_1(x_d) \\ \vdots \\ \varphi_m(x_d) \end{bmatrix} d + \begin{bmatrix} \varphi_1(x_a) \\ \vdots \\ \varphi_m(x_a) \end{bmatrix} F_a \right\} \\ &\approx (\varphi_p)^T diag\left[\frac{1}{s^2+\omega^2} \right] (\varphi_d d + \varphi_a F_a), \end{aligned} \tag{3-15}$$

where $(\varphi_p)^T = [\varphi_1(x_p) \cdots \varphi_m(x_p)]$, $(\varphi_d)^T = [\varphi_1(x_d) \cdots \varphi_m(x_d)]$,

$(\varphi_a)^T = [\varphi_1(x_a) \cdots \varphi_m(x_a)]$, and

$$diag\left[\frac{1}{s^2+\omega^2}\right]=\begin{bmatrix}\frac{1}{s^2+\omega_1^{\ 2}} & 0 & 0\\ 0 & \ddots & 0\\ 0 & 0 & \frac{1}{s^2+\omega_m^{\ 2}}\end{bmatrix}.$$

Equation (3-15) can be further derived into the following transfer function form.

$$\begin{aligned} w_p &= (\varphi_p)^T diag\left[\frac{1}{s^2+\omega^2}\right](\varphi_d d)+(\varphi_p)^T diag\left[\frac{1}{s^2+\omega^2}\right](\varphi_a F_a)\\ &= \overline{H}_d(s)d+H_f(s)F_a=\frac{1}{A_p(s)}\{\overline{B}_d(s)d+B_f(s)F_a\}, \end{aligned} \tag{3-16}$$

where $\overline{H}_d(s)=(\varphi_p)^T diag\left[\frac{1}{s^2+\omega^2}\right]\varphi_d$; $H_f(s)=(\varphi_p)^T diag\left[\frac{1}{s^2+\omega^2}\right]\varphi_a$;

In equation (3-16), $A_p(s)=\prod_{i=1}^{m}(s^2+\omega_i^{\ 2})$ is the common denominator; $\overline{B}_d(s)$ is the numerator of $\overline{H}_d(s)$ and $B_f(s)$ is the numerator of $H_f(s)$.

Once the feedback sensor collocates with the THVA, one may substitute equations (3-12) into equations (3-11) and obtain

$$F_a=(s\overline{v}_a+\overline{k}_a)[-\frac{F_a}{s^2m_a}-w_p]+F_{act} \tag{3-17}$$

where F_{act} is the active force and may be synthesized by

$$F_{act}=-\overline{G}(s)w_p, \tag{3-18}$$

where $\overline{G}(s)$ is the controller transfer function of the THVA and to be discussed in the next chapter.

A substitution of equation (3-18) into equation (3-17) leads to

$$F_a = -\frac{s^2}{\overline{K}(s)}\left[s\bar{v}_a + \bar{k}_a + \overline{G}(s)\right]w_p, \tag{3-19}$$

where $\overline{K}(s) = s^2 + s\frac{\bar{v}_a}{m_a} + \frac{\bar{k}_a}{m_a}$

One may substitute equation (3-19) into equation (3-16) and obtain the closed-loop transfer function.

$$\frac{w_p}{d} = \frac{\overline{K}(s)\overline{B}_d(s)}{\overline{Q}(s) + s^2 B_f(s)\overline{G}(s)}, \tag{3-20}$$

where $\overline{Q}(s) = A_p(s)\overline{K}(s) + s^2 B_f(s)(s\bar{v}_a + \bar{k}_a)$

In real practice, coefficients of $\overline{Q}(s)$, $\overline{B}_d(s)$ and $s^2 B_f(s)$ can be obtained via offline system identification. Equation (3-20), therefore, can be expressed in its discrete-time form written as

$$\frac{w_p}{d} = \frac{\overline{K}(z)\overline{B}_d(z)}{\overline{Q}(z) + B_f(z)\overline{G}(z)}, \tag{3-21}$$

Equation (3-21) is the closed-loop transfer function of the THVA-beam coupled system when arbitrary disturbance is acting on a point of the beam structure. A global structural vibration controller is developed on the basis of the transfer function and introduced in the next chapter.

3.2.2 Distributed Disturbance

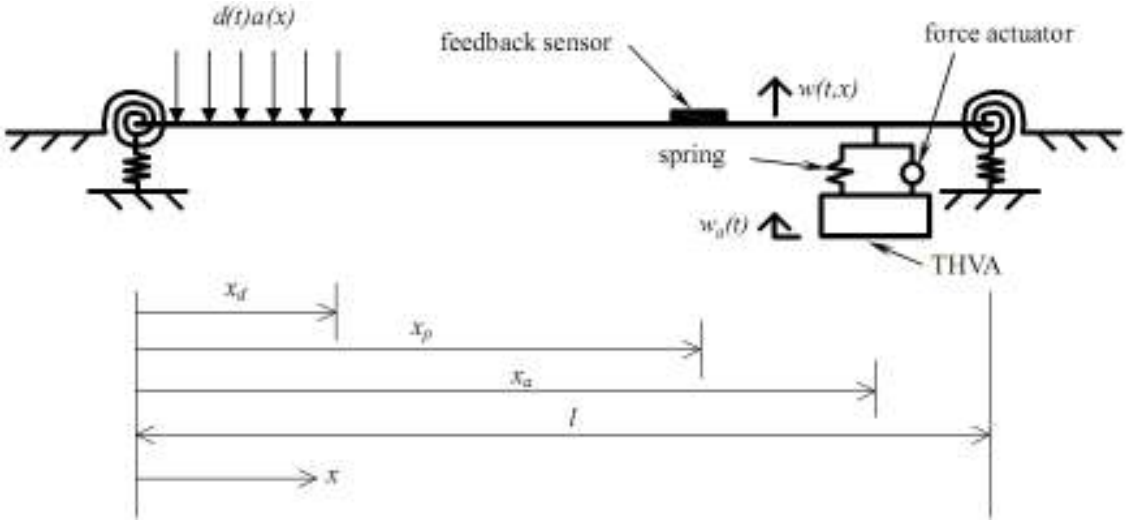

Figure 3-3 Distributed disturbance on a THVA-beam structure

The same THVA is coupled with the same beam at point x_a and shown in Figure 3-3. The beam detail has been described in the section 3.2.1 for Figure 3-2. A distributed disturbance modeled by $d(t)a(x)$ acts on a portion of the beam span from its mounting position to point x_d. $d(t)$ is a temporal function and $a(x)$ is a spatial function bounded everywhere except at a finite number of points (a possible example is $a(x)=\begin{cases}1 & 0<x<x_d\\ 0 & x_d<x<l\end{cases}$). The system dynamics are described by the following equations:

$$\rho\ddot{w}(t,x)+EIw''''(t,x)=d(t)a(x)+F_a\delta(x-x_a),\quad 0<x<l, \tag{3-22}$$

$$F_a=\bar{v}_a[\dot{w}_a(t)-\dot{w}(t,x_a)]+\bar{k}_a[w_a(t)-w(t,x_a)]+F_{act} \tag{3-3}$$

$$m_a\ddot{w}_a(t)=-F_a \tag{3-4}$$

Equation (3-22) is the dynamic equation of the beam in terms of its translational motions. All beam parameters have the same meaning as described in the section 3.2.1 for Figure 3-2. Since the THVA coupling detail is the same as the one shown in Figure 3-2, equations (3-3) and (3-4) are used to model the THVA coupling

force F_a. The prior presented equations are shown here for convenient reading purpose only.

Linear displacement of the beam $w(t,x)$ is decomposed into modal space via inner products. The inner products are volume integrals over the beam structure with its i^{th} mode eigen-function of translational motion $\varphi_i(x)$.

Using equations (3-6) and (3-7), equation (3-22) can be transformed to

$$\ddot{q}_i(t) + \omega_i^2 q_i(t) = d(t)\int_0^l \varphi_i(x)a(x)dx + F_a\int_0^l \varphi_i(x)\delta(x-x_a)dx\,, \qquad i = 1,2,3...$$

$$= \alpha_i d + \varphi_i(x_a)F_a \tag{3-23}$$

where $d = d(t)$, $\alpha_i = \int_0^l \varphi_i(x)a(x)dx$ and $\varphi_i(x_a) = \int_0^l \varphi_i(x)\delta(x-x_a)dx$

Applying Laplace transformation to equation (3-23), the dynamic equation of the beam can be derived and written as

$$q_i(s) = \frac{\alpha_i d + \varphi_i(x_a)F_a}{s^2 + \omega_i^2}\,, \qquad i = 1,2,3... \tag{3-24}$$

Using equations (3-24) and (3-13), linear displacement of the beam can be expressed as spatial-temporal equations.

$$w(s,x_p) = \sum_{i=1}^{\infty}\varphi_i(x_p)q_i(s) \approx \sum_{i=1}^{m}\varphi_i(x_p)\left[\frac{\alpha_i d + \varphi_i(x_a)F_a}{s^2 + \omega_i^2}\right], \tag{3-25}$$

where x_p is the feedback sensor location and m is the truncated number of modes. Equation (3-25) can be written in vector-matrix form.

$$w_p = w(s,x_p) \approx [\varphi_1(x_p)\cdots\varphi_m(x_p)]\begin{bmatrix} \frac{1}{s^2+\omega_1^2} & 0 & 0 \\ 0 & \ddots & 0 \\ 0 & 0 & \frac{1}{s^2+\omega_m^2} \end{bmatrix}\left\{\begin{bmatrix}\alpha_1 \\ \vdots \\ \alpha_m\end{bmatrix} d + \begin{bmatrix}\varphi_1(x_a) \\ \vdots \\ \varphi_m(x_a)\end{bmatrix} F_a\right\}$$

$$\approx (\varphi_p)^T \, diag\left[\frac{1}{s^2+\omega^2}\right](\alpha d + \varphi_a F_a), \tag{3-26}$$

where $(\varphi_p)^T = [\varphi_1(x_p)\cdots\varphi_m(x_p)]$, $(\alpha)^T = [\alpha_1\cdots\alpha_m]$,

$(\varphi_a)^T = [\varphi_1(x_a)\cdots\varphi_m(x_a)]$, and

$$diag\left[\frac{1}{s^2+\omega^2}\right] = \begin{bmatrix} \frac{1}{s^2+\omega_1^2} & 0 & 0 \\ 0 & \ddots & 0 \\ 0 & 0 & \frac{1}{s^2+\omega_m^2} \end{bmatrix}.$$

Equation (3-26) can be further derived into the following transfer function form.

$$w_p = (\varphi_p)^T \, diag\left[\frac{1}{s^2+\omega^2}\right](\alpha d) + (\varphi_p)^T \, diag\left[\frac{1}{s^2+\omega^2}\right](\varphi_a F_a)$$

$$= \hat{\bar{H}}_d(s)d + H_f(s)F_a = \frac{1}{A_p(s)}\{\hat{\bar{B}}_d(s)d + B_f(s)F_a\}, \tag{3-27}$$

where $\hat{\bar{H}}_d(s) = (\varphi_p)^T \, diag\left[\frac{1}{s^2+\omega^2}\right]\alpha$; $H_f(s) = (\varphi_p)^T \, diag\left[\frac{1}{s^2+\omega^2}\right]\varphi_a$;

In equation (3-27), $A_p(s) = \prod_{i=1}^{m}(s^2+\omega_i^{\,2})$ is the common denominator; $\hat{\bar{B}}_d(s)$ is the numerator of $\hat{\bar{H}}_d(s)$ and $B_f(s)$ is the numerator of $H_f(s)$.

Once the feedback sensor collocates with the THVA, one may substitute equation (3-19) into equation (3-27) and obtain the closed-loop transfer function.

$$\frac{w_p}{d} = \frac{\overline{K}(s)\hat{\overline{B}}_d(s)}{\overline{Q}(s) + s^2 B_f(s)\overline{G}(s)}, \tag{3-28}$$

where $\overline{K}(s) = s^2 + s\frac{\overline{v}_a}{m_a} + \frac{\overline{k}_a}{m_a}$ and $\overline{Q}(s) = A_p(s)\overline{K}(s) + s^2 B_f(s)(s\overline{v}_a + \overline{k}_a)$

In real practice, coefficients of $\overline{Q}(s)$, $\hat{\overline{B}}_d(s)$ and $s^2 B_f(s)$ can be obtained via offline system identification. Equation (3-28), therefore, can be expressed in its discrete-time form written as

$$\frac{w_p}{d} = \frac{\overline{K}(z)\hat{\overline{B}}_d(z)}{\overline{Q}(z) + B_f(z)\overline{G}(z)}, \tag{3-29}$$

Equation (3-29) is the closed-loop transfer function of the THVA-beam coupled system when random disturbance is acting on a portion of the beam span. In fact, equation (3-29) is very similar to equation (3-21), which is the closed-loop transfer function of the THVA-beam coupled system when the disturbance is applied at a point of the beam structure. The major difference between the two transfer functions is at their closed-loop numerators. The closed-loop numerator in equation (3-21) is composed of $\overline{K}(z)\overline{B}_d(z)$ and the one in equation (3-29) is composed of $\overline{K}(z)\hat{\overline{B}}_d(z)$. The numerators clearly demonstrated $\overline{B}_d(z)$ and $\hat{\overline{B}}_d(z)$ are basically related to the position of the disturbance. This signifies that the disturbance location can only affect the closed-loop numerator instead of the closed-loop denominator. Therefore, the stability of the closed-loop system is not affected by the disturbance. This characteristic is briefly discussed in the chapter 4.

3.3 New Design of a Rotational Hybrid Vibration Absorber (RHVA)

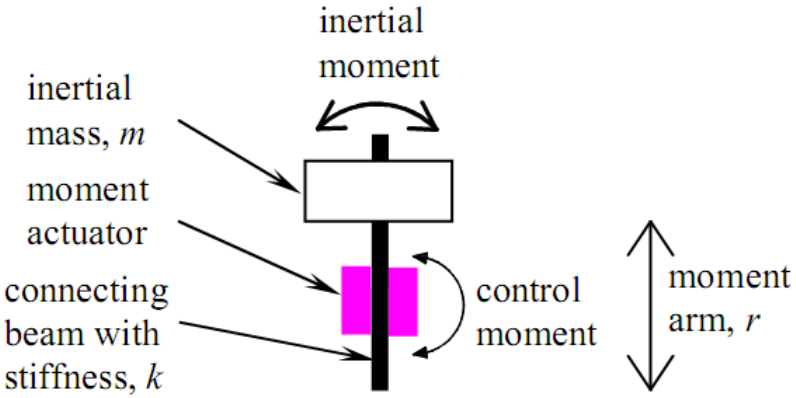

Figure 3-4 Structure of a rotational hybrid vibration absorber

A new design of a rotational hybrid vibration absorber (RHVA) is proposed and shown in Figure 3-4. It simply consists of an inertial mass, a connecting beam and a moment actuator. The inertial mass is mounted on the connecting beam and can be slid along the beam vertically. The moment actuator can be small motor or piezoelectric actuator. In this project, a pair of piezoelectric actuators is used and attached to both sides of the connecting beam near the root position of the beam. The actuators are used to provide an active moment for the RHVA in the control process. Similar to the translational hybrid vibration absorber (THVA), the passive absorption frequency f_p of the RHVA in rad/s can be tuned with its passive parameters in the following equation.

$$f_p = \sqrt{\frac{k}{J}} = \sqrt{\frac{k}{mr^2}} \tag{3-30}$$

where parameters k and J are the effective rotational stiffness of the connecting beam and second moment of inertia of the inertial mass respectively. m and r are the mass value and moment arm of the inertial mass.

Unlike the THVA, it is easier to tune the passive absorption frequency f_p of the RHVA by changing the moment arm r of its inertia mass. This can be achieved in the proposed design via sliding the inertial mass along the connecting beam vertically. The proposed RHVA can also avoid bulky linear actuators such as voice-coil electromagnetic actuator or electro-hydraulic actuator used in the THVA.

3.4 Mathematical Model of a Rotational Hybrid Vibration Absorber (RHVA) – Beam Coupled System

Mathematical model of a RHVA, which is coupled with a beam structure, is derived for the cases of applying disturbance at a point and a portion of the beam structure separately. The models are finally derived to their closed-loop transfer functions for further controller design.

3.4.1 Point Disturbance

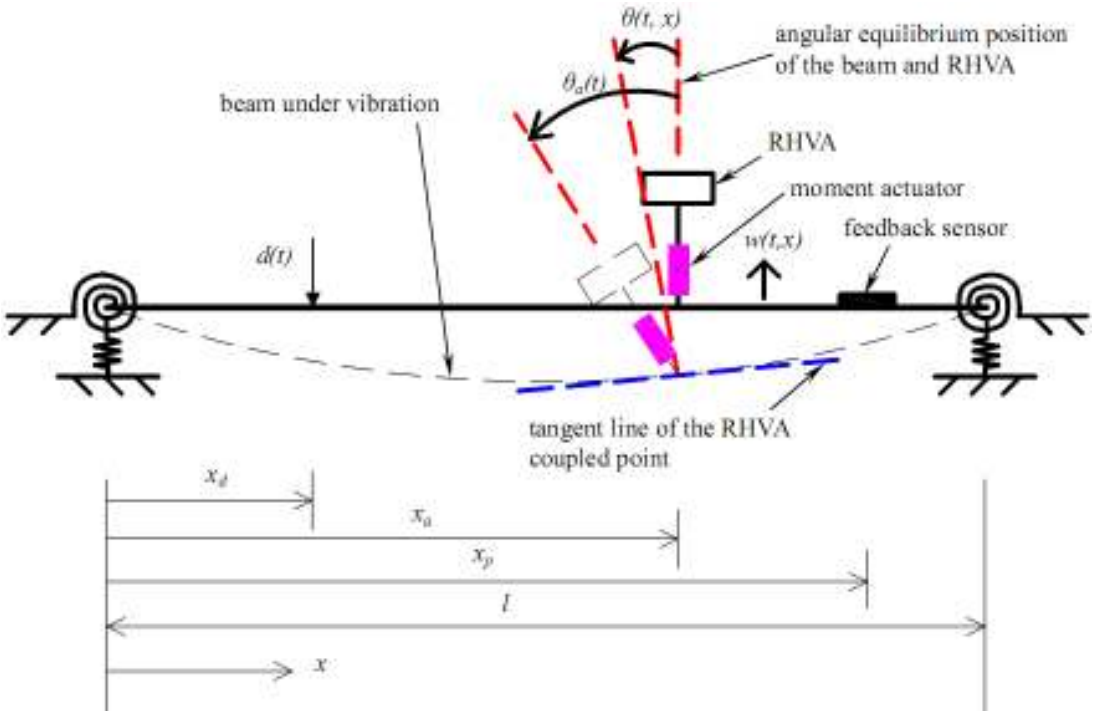

Figure 3-5 Point disturbance on a RHVA-beam structure

The proposed RHVA is coupled with a beam and shown in Figure 3-5. The structure of the beam is the same as the one described in the section 3.2.1 for Figure 3-2. The beam has length l and its linear displacement is denoted as $w(t,x)$; the angular displacement of the beam is denoted as $\theta(t,x)=\frac{\partial}{\partial x}w(t,x)$; while angular displacement of the RHVA is denoted as $\theta_a(t)$. A disturbance $d(t)$ acts at point x_d and the RHVA couples with the beam at point x_a. The beam is assumed to satisfy the

Euler-Bernoulli hypothesis. The system dynamics are described by the following equations:

$$\rho\ddot{w}(t,x) + EIw''''(t,x) = d(t)\delta(x - x_d) + \frac{\partial[M_a\delta(x - x_a)]}{\partial x}, \qquad 0 < x < l, \tag{3-31}$$

$$M_a = v_a[\dot{\theta}_a(t) - \dot{\theta}(t,x_a)] + k_a[\theta_a(t) - \theta(t,x_a)] + M_{act} \tag{3-32}$$

$$J_a\ddot{\theta}_a(t) = -M_a \tag{3-33}$$

Equation (3-31) is the dynamic equation of the beam in terms of its translational motions. It is modified from Cheung and Wong (2008). Where ρ is the mass density per length; E is the Young's modulus; I is the moment of inertia of the cross section of the beam; $\ddot{w}(t,x)$ is the second derivative of the linear displacement of the beam with respective to time, $w''''(t,x)$ is the fourth derivative of the linear displacement of the beam with respective to x and $\delta(x - x_a)$ is the Dirac delta function. Equation (3-32) models the coupling moment M_a with its active part M_{act} generated by the actuators. $\theta(t,x_a)$ is the angular displacement of the beam at point x_a and $\dot{\theta}(t,x_a)$ is its first derivative with respect to time; while $\theta_a(t)$ is the angular displacement of the RHVA and $\dot{\theta}_a(t)$ is its first derivative with respect to time. Parameters v_a and k_a represent the damping coefficient and the stiffness of the rotational passive part. The damping effect is assumed coming from the connecting beam friction and as proportional damping. Equation (3-33) is a Newton's equation where J_a is the second moment of inertia of the rotational passive part and $\ddot{\theta}_a(t)$ is the second derivative of the angular displacement of the RHVA with respect to time. From the above formulation, the total angular displacement of the coupled system is represented by a vector $\Theta^T = [\theta(t,x), \theta_a(t)]$. In general, it is difficult to solve a coupled system which consists of lumped-parameter system and distributed-parameter system. An easier alternative is to focus on the angular displacement of the beam $\theta(t,x)$ by decomposing the linear displacement of the beam $w(t,x)$ into modal space through inner products. Separation of variables

method is applicable to transform the spatial-temporal beam angular displacement $\theta(t,x)$ to an infinite series with its separated spatial and temporal terms.

$$\theta(t,x) = \sum_{i=1}^{\infty} \varphi_i'(x) q_i(t) \tag{3-34}$$

where $\varphi_i'(x)$ and $q_i(t)$ are the i^{th} mode eigen-function of angular motion and the i^{th} modal coordinate respectively.

The inner products are volume integrals over the beam structure with its i^{th} mode eigen-function of linear motion $\varphi_i(x)$.

$$q_i(t) = \int_{x=0}^{l} \varphi_i(x) w(t,x) dx = \frac{EI}{\rho \omega_i^2} \int_{x=0}^{l} \varphi_i(x) w''''(t,x) dx, \quad i = 1,2,3... \tag{3-6}$$

$$\ddot{q}_i(t) = \int_{x=0}^{l} \varphi_i(x) \ddot{w}(t,x) dx, \qquad i = 1,2,3... \tag{3-7}$$

$$\int_{x=0}^{l} \varphi_i(x) \varphi_j(x) dx = \begin{cases} 1 & i = j \;\; i,j = 1,2,3\ldots \\ 0 & i \neq j \;\; i,j = 1,2,3\ldots \end{cases} \tag{3-8}$$

Equations (3-6) to (3-8) are presented in the section 3.2.1 and shown here for convenient reading purpose only. In equations (3-6) and (3-7), $q_i(t)$ and $\ddot{q}_i(t)$ represent the i^{th} modal coordinate and the secondary derivative of the i^{th} modal coordinate with respect to time respectively; while ω_i denotes the natural frequency of the beam at the i^{th} mode. Using equations (3-6) and (3-7), equation (3-31) can be transformed to

$$\ddot{q}_i(t) + \omega_i^2 q_i(t) = d(t) \int_0^l \varphi_i(x) \delta(x - x_d) dx + M_a \int_0^l \varphi_i(x) \frac{\partial[\delta(x - x_a)]}{\partial x} dx, \qquad i = 1,2,3...$$

$$= \varphi_i(x_d) d - \varphi_i'(x_a) M_a \tag{3-35}$$

where $d = d(t)$, $\varphi_i(x_d) = \int_0^l \varphi_i(x) \delta(x - x_d) dx$, $-\varphi_i'(x_a) = \int_0^l \varphi_i(x) \frac{\partial[\delta(x - x_a)]}{\partial x} dx$

(http://mathworld.wolfram.com/DeltaFunction.html)

Applying Laplace transformation to equations (3-35), (3-32), (3-33) and (3-34), a set of dynamic equations can be derived and written as

$$q_i(s) = \frac{\varphi_i(x_d)d - \varphi_i'(x_a)M_a}{s^2 + \omega_i^2}, \qquad i = 1,2,3... \qquad (3\text{-}36)$$

$$M_a = (sv_a + k_a)[\theta_a(s) - \theta(s,x_a)] + M_{act} \qquad (3\text{-}37)$$

$$s^2 J_a \theta_a(s) = -M_a \qquad (3\text{-}38)$$

$$\theta(s,x) = \sum_{i=1}^{\infty} \varphi_i'(x) q_i(s) \qquad (3\text{-}39)$$

Using equations (3-36) and (3-39), angular displacement of the beam can be expressed as spatial-temporal equations.

$$\theta(s,x_p) = \sum_{i=1}^{\infty} \varphi_i'(x_p) q_i(s) \approx \sum_{i=1}^{m} \varphi_i'(x_p) \left[\frac{\varphi_i(x_d)d - \varphi_i'(x_a)M_a}{s^2 + \omega_i^2} \right] \qquad (3\text{-}40)$$

where x_p is the feedback sensor location and m is the truncated number of modes. Equation (3-40) can be written in vector-matrix form.

$$\theta_p = \theta(s,x_p) \approx [\varphi_1'(x_p) \cdots \varphi_m'(x_p)] \begin{bmatrix} \frac{1}{s^2+\omega_1^2} & 0 & 0 \\ 0 & \ddots & 0 \\ 0 & 0 & \frac{1}{s^2+\omega_m^2} \end{bmatrix} \left\{ \begin{bmatrix} \varphi_1(x_d) \\ \vdots \\ \varphi_m(x_d) \end{bmatrix} d - \begin{bmatrix} \varphi_1'(x_a) \\ \vdots \\ \varphi_m'(x_a) \end{bmatrix} M_a \right\}$$

$$\approx (\varphi_p')^T \, diag\left[\frac{1}{s^2 + \omega^2} \right] (\varphi_d d - \varphi_a' M_a) \qquad (3\text{-}41)$$

where $(\varphi_p')^T = [\varphi_1'(x_p) \cdots \varphi_m'(x_p)]$, $(\varphi_d)^T = [\varphi_1(x_d) \cdots \varphi_m(x_d)]$,

$(\varphi_a')^T = [\varphi_1'(x_a) \cdots \varphi_m'(x_a)]$, and

$$diag\left[\frac{1}{s^2 + \omega^2} \right] = \begin{bmatrix} \frac{1}{s^2+\omega_1^2} & 0 & 0 \\ 0 & \ddots & 0 \\ 0 & 0 & \frac{1}{s^2+\omega_m^2} \end{bmatrix}.$$

Equation (3-41) can be further derived into the following transfer function form.

$$\theta_p = (\varphi_p')^T \, diag\left[\frac{1}{s^2+\omega^2}\right](\varphi_d d) - (\varphi_p')^T \, diag\left[\frac{1}{s^2+\omega^2}\right](\varphi_a' M_a)$$

$$= H_d(s)d + H_m(s)M_a = \frac{1}{A_p(s)}\{B_d(s)d + B_m(s)M_a\} \tag{3-42}$$

where $H_d(s) = (\varphi_p')^T \, diag\left[\frac{1}{s^2+\omega^2}\right]\varphi_d$; $H_m(s) = -(\varphi_p')^T \, diag\left[\frac{1}{s^2+\omega^2}\right]\varphi_a'$.

In equation (3-42), $A_p(s) = \prod_{i=1}^{m}(s^2+\omega_i^2)$ is the common denominator; $B_d(s)$ is the numerator of $H_d(s)$ and $B_m(s)$ is the numerator of $H_m(s)$.

Once the feedback sensor collocates with the RHVA, one may substitute equation (3-38) into equation (3-37) and obtain

$$M_a = (sv_a + k_a)[-\frac{M_a}{s^2 J_a} - \theta_p] + M_{act} \tag{3-43}$$

where M_{act} is the active moment and may be synthesized by

$$M_{act} = -G(s)\theta_p \tag{3-44}$$

where $G(s)$ is the controller transfer function for the RHVA and will be discussed in the next chapter.

A substitution of equation (3-44) into equation (3-43) leads to

$$M_a = -\frac{s^2}{K(s)}[sv_a + k_a + G(s)]\theta_p \tag{3-45}$$

where $K(s) = s^2 + s\frac{v_a}{J_a} + \frac{k_a}{J_a}$

One may substitute equation (3-45) into equation (3-42) and obtain the closed-loop transfer function.

$$\frac{\theta_p}{d} = \frac{K(s)B_d(s)}{Q(s) + s^2 B_m(s)G(s)}, \tag{3-46}$$

where $Q(s) = A_p(s)K(s) + s^2 B_m(s)(sv_a + k_a)$

In real practice, coefficients of $Q(s)$, $B_d(s)$ and $s^2 B_m(s)$ can be obtained via offline system identification. Equation (3-46), therefore, can be expressed in its discrete-time form written as

$$\frac{\theta_p}{d} = \frac{K(z)B_d(z)}{Q(z) + B_m(z)G(z)}, \tag{3-47}$$

Equation (3-47) is the closed-loop transfer function of the RHVA-beam coupled system when random disturbance is acting on a point of the beam structure. A global structural vibration controller is developed on the basis of the transfer function and discussed in the next chapter.

3.4.2 Distributed Disturbance

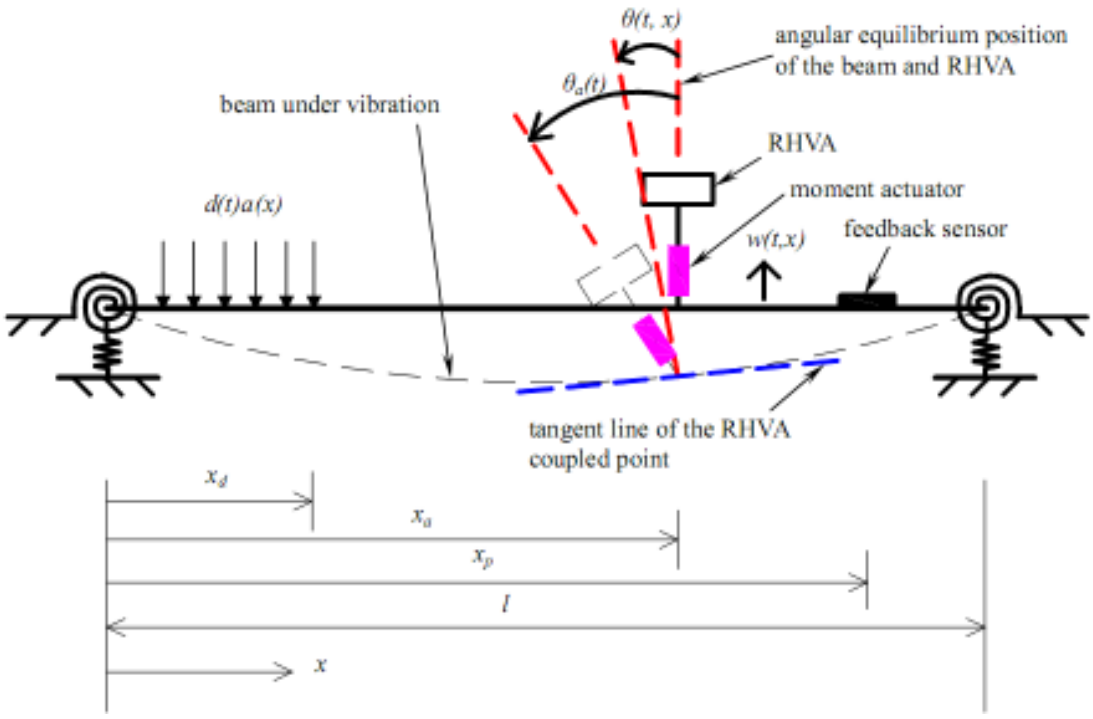

Figure 3-6 Distributed disturbance on a RHVA-beam structure

The same RHVA is coupled with the same beam at point x_a and shown in Figure 3-6. The beam detail has been described in the section 3.4.1 for Figure 3-5. A distributed disturbance modeled by $d(t)a(x)$ acts on a portion of the beam span from its mounting position to point x_d. $d(t)$ is a temporal function; $a(x)$ is a spatial function bounded everywhere except at a finite number of points (a possible example is $a(x)=\begin{cases}1 & 0<x<x_d\\ 0 & x_d<x<l\end{cases}$). The system dynamics are described by the following equations:

$$\rho\ddot{w}(t,x)+EIw''''(t,x)=d(t)a(x)+\frac{\partial[M_a\delta(x-x_a)]}{\partial x},\qquad 0<x<l, \tag{3-48}$$

$$M_a=v_a[\dot{\theta}_a(t)-\dot{\theta}(t,x_a)]+k_a[\theta_a(t)-\theta(t,x_a)]+M_{act} \tag{3-32}$$

$$J_a\ddot{\theta}_a(t)=-M_a \tag{3-33}$$

Equation (3-48) is the dynamic equation of the beam in terms of its translational motions. It is modified from Cheung and Wong (2008). All beam parameters have the same meaning as described in the section 3.4.1 for Figure 3-5. Since the RHVA coupling detail is the same as the one shown in Figure 3-5, equations (3-32) and (3-33) are used to model the RHVA coupling moment M_a. The prior presented equations shown here are for convenient reading purpose only.

Angular displacement of the beam $\theta(t,x)$ can be obtained by decomposing the linear displacement of the beam $w(t,x)$ into modal space via inner products. The inner products are volume integrals over the beam structure with its i^{th} mode eigen-function of linear motion $\varphi_i(x)$.

Using equations (3-6) and (3-7), equation (3-48) can be transformed to

$$\ddot{q}_i(t)+\omega_i^2 q_i(t)=d(t)\int_0^l \varphi_i(x)a(x)dx+M_a\int_0^l \varphi_i(x)\frac{\partial[\delta(x-x_a)]}{\partial x}dx, \qquad i=1,2,3...$$
$$=\beta_i d-\varphi_i'(x_a)M_a \tag{3-49}$$

where $d=d(t)$, $\beta_i=\int_0^l \varphi_i(x)a(x)dx$ and $-\varphi_i'(x_a)=\int_0^l \varphi_i(x)\frac{\partial[\delta(x-x_a)]}{\partial x}dx$

Applying Laplace transformation to equation (3-49), the dynamic equation of the beam can be derived and written as

$$q_i(s)=\frac{\beta_i d-\varphi_i'(x_a)M_a}{s^2+\omega_i^2} \qquad i=1,2,3... \tag{3-50}$$

Using equations (3-50) and (3-39), angular displacement of the beam can be expressed as spatial-temporal equations.

$$\theta(s,x_p)=\sum_{i=1}^{\infty}\varphi_i'(x_p)q_i(s)\approx\sum_{i=1}^{m}\varphi_i'(x_p)\left[\frac{\beta_i d-\varphi_i'(x_a)M_a}{s^2+\omega_i^2}\right], \tag{3-51}$$

where x_p is the feedback sensor location and m is the truncated number of modes. Equation (3-51) can be written in vector-matrix form.

$$\theta_p = \theta(s, x_p) \approx [\varphi_1'(x_p) \cdots \varphi_m'(x_p)] \begin{bmatrix} \frac{1}{s^2+\omega_1^2} & 0 & 0 \\ 0 & \ddots & 0 \\ 0 & 0 & \frac{1}{s^2+\omega_m^2} \end{bmatrix} \left\{ \begin{bmatrix} \beta_1 \\ \vdots \\ \beta_m \end{bmatrix} d - \begin{bmatrix} \varphi_1'(x_a) \\ \vdots \\ \varphi_m'(x_a) \end{bmatrix} M_a \right\}$$

$$\approx (\varphi_p')^T \, diag\left[\frac{1}{s^2+\omega^2}\right](\beta d - \varphi_a' M_a) \tag{3-52}$$

where $(\varphi_p')^T = [\varphi_1'(x_p) \cdots \varphi_m'(x_p)]$, $(\beta)^T = [\beta_1 \cdots \beta_m]$,

$(\varphi_a')^T = [\varphi_1'(x_a) \cdots \varphi_m'(x_a)]$, and

$$diag\left[\frac{1}{s^2+\omega^2}\right] = \begin{bmatrix} \frac{1}{s^2+\omega_1^2} & 0 & 0 \\ 0 & \ddots & 0 \\ 0 & 0 & \frac{1}{s^2+\omega_m^2} \end{bmatrix}.$$

Equation (3-52) can be further derived into the following transfer function form.

$$\theta_p = (\varphi_p')^T \, diag\left[\frac{1}{s^2+\omega^2}\right](\beta d) - (\varphi_p')^T \, diag\left[\frac{1}{s^2+\omega^2}\right](\varphi_a' M_a)$$

$$= \hat{H}_d(s) d + H_m(s) M_a = \frac{1}{A_p(s)} \left\{ \hat{B}_d(s) d + B_m(s) M_a \right\} \tag{3-53}$$

where $\hat{H}_d(s) = (\varphi_p')^T \, diag\left[\frac{1}{s^2+\omega^2}\right]\beta$; $H_m(s) = -(\varphi_p')^T \, diag\left[\frac{1}{s^2+\omega^2}\right]\varphi_a'$.

In equation (3-53), $A_p(s) = \prod_{i=1}^{m}(s^2+\omega_i^2)$ is the common denominator; $\hat{B}_d(s)$ is the numerator of $\hat{H}_d(s)$ and $B_m(s)$ is the numerator of $H_m(s)$.

Once the feedback sensor collocates with the RHVA, one may substitute equation (3-45) into equation (3-53) and obtain the closed-loop transfer function.

$$\frac{\theta_p}{d} = \frac{K(s)\hat{B}_d(s)}{Q(s) + s^2 B_m(s)G(s)}, \tag{3-54}$$

where $K(s) = s^2 + s\frac{v_a}{J_a} + \frac{k_a}{J_a}$ and $Q(s) = A_p(s)K(s) + s^2 B_m(s)(sv_a + k_a)$

In real practice, coefficients of $Q(s)$, $\hat{B}_d(s)$ and $s^2 B_m(s)$ can be obtained via offline system identification. Equation (3-54), therefore, can be expressed in its discrete-time form written as

$$\frac{\theta_p}{d} = \frac{K(z)\hat{B}_d(z)}{Q(z) + B_m(z)G(z)}, \tag{3-55}$$

Equation (3-55) is the closed-loop transfer function of the RHVA-beam coupled system when random disturbance is acting on a portion of the beam span.

3.5 Limitation of a Skyhook/Groundhook Damper

Skyhook/groundhook damper is a damper which is mounted between a vibrating body and a fixed base such as wall or ground. It is a conventional and effective device used for structural vibration control. The mounting base is useful to provide a reaction force for the skyhook/groundhook damper but it may not always be available for the damper installation. RHVA could be a better alternative to be used for structural vibration control in case installation of a skyhook/groundhook damper is restricted. Mathematical model of a translational groundhook damper is derived in this section. The model to be used in further simulation tests can evaluate the vibration suppression performance of a groundhook damper and compare with a RHVA.

3.6 Mathematical Model of a Groundhook Damper – Beam Coupled System

Mathematical model of a groundhook damper, which is mounted between a beam and a fixed base, is derived for the cases of applying disturbance at a point and a portion of the beam span separately.

3.6.1 Point Disturbance

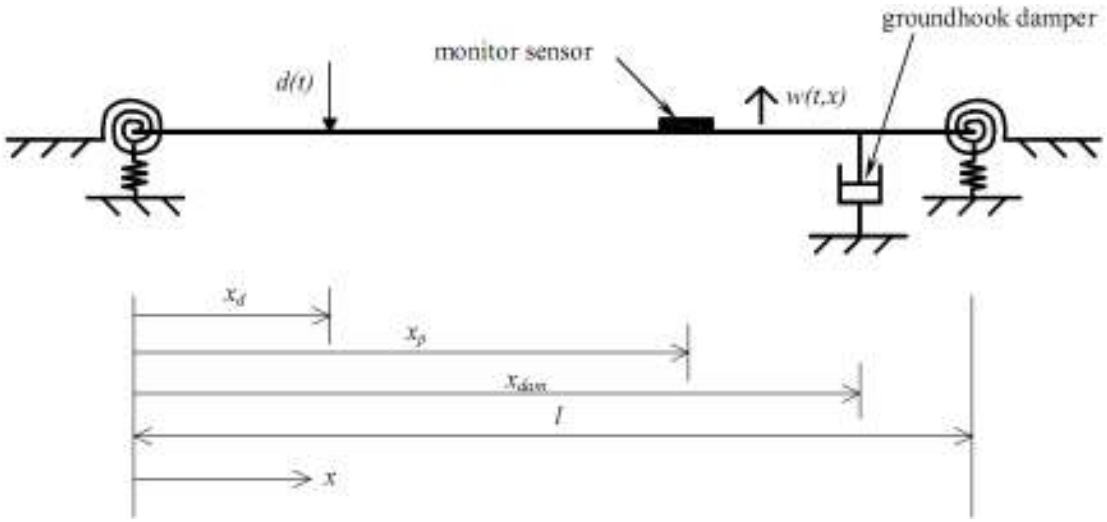

Figure 3-7 Point disturbance on a groundhook damper-beam structure

A groundhook damper is coupled with a beam and shown in Figure 3-7. The structure and detail of the beam are the same as the one described in the section 3.2.1 for Figure 3-2. The beam has length l and its linear displacement is denoted as $w(t,x)$. A disturbance $d(t)$ acts at point x_d and the groundhook damper couples with the beam at point x_{dam}. The beam is assumed to satisfy the Euler-Bernoulli hypothesis. The system dynamics are described by the following equations:

$$\rho\ddot{w}(t,x) + EIw''''(t,x) = d(t)\delta(x - x_d) + F_{dam}\delta(x - x_{dam}) \qquad 0 < x < l, \qquad (3\text{-}56)$$

$$F_{dam} = -\bar{v}_{dam}[\dot{w}(t,x_{dam})] \qquad (3\text{-}57)$$

Equation (3-56) is the dynamic equation of the beam in terms of its translational motions where ρ is the mass density per length; E is the Young's modulus; I is the moment of inertia of the cross section of the beam; $\ddot{w}(t,x)$ is the second derivative

of the linear displacement of the beam with respective to time, $w''''(t,x)$ is the fourth derivative of the linear displacement of the beam with respective to x and $\delta(x-x_{dam})$ is the Dirac delta function. Equation (3-57) models the coupling force F_{dam}. $\dot{w}(t,x_{dam})$ is the first derivative of the linear displacement of the beam at point x_{dam} with respect to time. Parameter $\bar{v}_{dam}$ represents the damping coefficient of the groundhook damper.

Linear displacement of the beam $w(t,x)$ is decomposed into modal space via inner products. The inner products are volume integrals over the beam structure with its i^{th} mode eigen-function of translational motion $\varphi_i(x)$.

Using equations (3-6) and (3-7), equation (3-56) can be transformed to

$$\ddot{q}_i(t)+\omega_i^2 q_i(t)=d(t)\int_0^l \varphi_i(x)\delta(x-x_d)dx+F_{dam}\int_0^l \varphi_i(x)\delta(x-x_{dam})dx,\quad i=1,2,3...$$
$$=\varphi_i(x_d)d+\varphi_i(x_{dam})F_{dam} \qquad (3\text{-}58)$$

where $d=d(t)$, $\varphi_i(x_d)=\int_0^l \varphi_i(x)\delta(x-x_d)dx$ and $\varphi_i(x_{dam})=\int_0^l \varphi_i(x)\delta(x-x_{dam})dx$

Applying Laplace transformation to equations (3-58) and (3-57), a set of dynamic equations of the beam can be derived and written as

$$q_i(s)=\frac{\varphi_i(x_d)d+\varphi_i(x_{dam})F_{dam}}{s^2+\omega_i^2}, \qquad i=1,2,3... \qquad (3\text{-}59)$$

$$F_{dam}=-s\bar{v}_{dam}[w(s,x_{dam})] \qquad (3\text{-}60)$$

Using equations (3-59) and (3-13), linear displacement of the beam can be expressed as spatial-temporal equations.

$$w(s,x_p)=\sum_{i=1}^{\infty}\varphi_i(x_p)q_i(s)\approx\sum_{i=1}^{m}\varphi_i(x_p)\left[\frac{\varphi_i(x_d)d+\varphi_i(x_{dam})F_{dam}}{s^2+\omega_i^2}\right] \qquad (3\text{-}61)$$

where x_p is the monitor sensor location and m is the truncated number of modes. Equation (3-61) can be written in vector-matrix form.

$$w_p = w(s, x_p) \approx [\varphi_1(x_p) \cdots \varphi_m(x_p)] \begin{bmatrix} \frac{1}{s^2+\omega_1^2} & 0 & 0 \\ 0 & \ddots & 0 \\ 0 & 0 & \frac{1}{s^2+\omega_m^2} \end{bmatrix} \left\{ \begin{bmatrix} \varphi_1(x_d) \\ \vdots \\ \varphi_m(x_d) \end{bmatrix} d + \begin{bmatrix} \varphi_1(x_{dam}) \\ \vdots \\ \varphi_m(x_{dam}) \end{bmatrix} F_{dam} \right\}$$

$$\approx (\varphi_p)^T \, diag\left[\frac{1}{s^2+\omega^2}\right](\varphi_d d + \varphi_{dam} F_{dam}), \tag{3-62}$$

where $(\varphi_p)^T = [\varphi_1(x_p) \cdots \varphi_m(x_p)]$, $(\varphi_d)^T = [\varphi_1(x_d) \cdots \varphi_m(x_d)]$,

$(\varphi_{dam})^T = [\varphi_1(x_{dam}) \cdots \varphi_m(x_{dam})]$, and

$$diag\left[\frac{1}{s^2+\omega^2}\right] = \begin{bmatrix} \frac{1}{s^2+\omega_1^2} & 0 & 0 \\ 0 & \ddots & 0 \\ 0 & 0 & \frac{1}{s^2+\omega_m^2} \end{bmatrix}.$$

Equation (3-62) can be further derived into the following transfer function form.

$$w_p = (\varphi_p)^T \, diag\left[\frac{1}{s^2+\omega^2}\right](\varphi_d d) + (\varphi_p)^T \, diag\left[\frac{1}{s^2+\omega^2}\right](\varphi_{dam} F_{dam})$$

$$= \overline{H}_d(s) d + H_{dam}(s) F_{dam} = \frac{1}{A_p(s)} \{\overline{B}_d(s) d + B_{dam}(s) F_{dam}\}, \tag{3-63}$$

where $\overline{H}_d(s) = (\varphi_p)^T \, diag\left[\frac{1}{s^2+\omega^2}\right]\varphi_d$; $H_{dam}(s) = (\varphi_p)^T \, diag\left[\frac{1}{s^2+\omega^2}\right]\varphi_{dam}$;

In equation (3-63), $A_p(s) = \prod_{i=1}^{m}(s^2+\omega_i^2)$ is the common denominator; $\overline{B}_d(s)$ is the numerator of $\overline{H}_d(s)$ and $B_{dam}(s)$ is the numerator of $H_{dam}(s)$.

Once the monitor sensor collocates with the groundhook damper, one may substitute equation (3-60) into equation (3-63) and obtain the closed-loop transfer function.

$$\frac{w_p}{d} = \frac{\overline{B}_d(s)}{A_p(s) + sB_{dam}(s)\overline{v}_{dam}} \tag{3-64}$$

In real practice, coefficients of $A_p(s)$, $\overline{B}_d(s)$ and $sB_{dam}(s)$ can be obtained via offline system identification. Equation (3-64), therefore, can be expressed in its discrete-time form written as

$$\frac{w_p}{d} = \frac{\overline{B}_d(z)}{A_p(z) + B_{dam}(z)\overline{v}_{dam}} \tag{3-65}$$

Equation (3-65) is the closed-loop transfer function of the groundhook damper-beam coupled system when random disturbance is applied on a point of the beam structure.

3.6.2 Distributed Disturbance

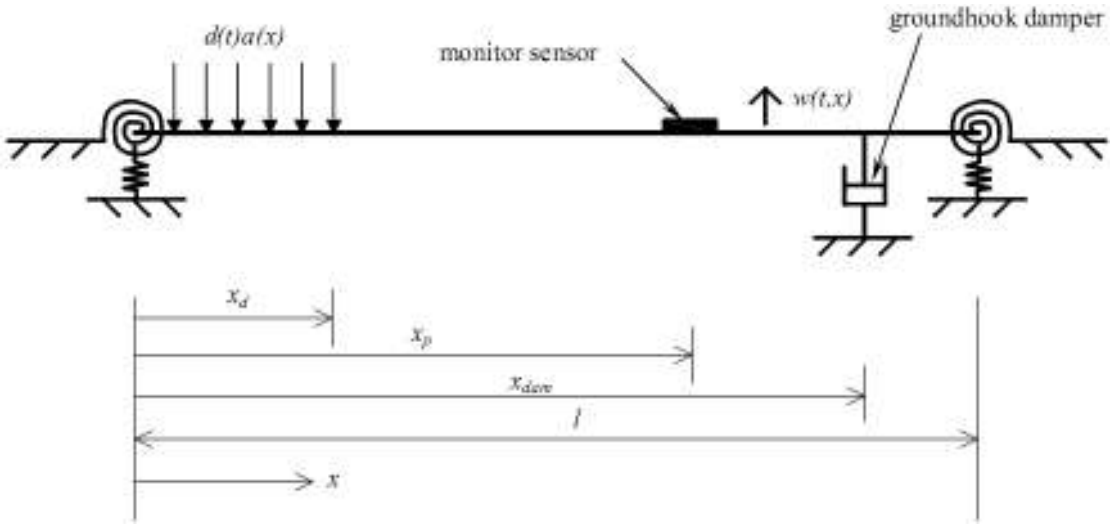

Figure 3-8 Distributed disturbance on a groundhook damper-beam structure

The same groundhook damper is coupled with the same beam at point x_{dam} and shown in Figure 3-8. The beam detail has been described in the section 3.6.1 for Figure 3-7. A distributed disturbance modeled by $d(t)a(x)$ acts on a portion of the beam span from its mounting position to point x_d. $d(t)$ is a temporal function and

$a(x)$ is a spatial function bounded everywhere except at a finite number of points (a possible example is $a(x)=\begin{cases}1 & 0<x<x_d\\ 0 & x_d<x<l\end{cases}$). The system dynamics are described by the following equations:

$$\rho\ddot{w}(t,x)+EIw''''(t,x)=d(t)a(x)+F_{dam}\delta(x-x_{dam}),\qquad 0<x<l, \tag{3-66}$$

$$F_{dam}=-\bar{v}_{dam}[\dot{w}(t,x_{dam})] \tag{3-57}$$

Equation (3-66) is the dynamic equation of the beam in terms of its translational motions. All beam parameters have the same meaning as described in the section 3.6.1 for Figure 3-7. Since the groundhook damper coupling detail is the same as the one shown in Figure 3-7, equation (3-57) is used to model the groundhook damper coupling force F_{dam}. The prior presented equation shown here is for convenient reading purpose only.

Linear displacement of the beam $w(t,x)$ is decomposed into modal space via inner products. The inner products are volume integrals over the beam structure with its i^{th} mode eigen-function of translational motion $\varphi_i(x)$.

Using equations (3-6) and (3-7), equation (3-66) can be transformed to

$$\ddot{q}_i(t)+\omega_i^2 q_i(t)=d(t)\int_0^l\varphi_i(x)a(x)dx+F_{dam}\int_0^l\varphi_i(x)\delta(x-x_{dam})dx,\qquad i=1,2,3...$$
$$=\alpha_i d+\varphi_i(x_{dam})F_{dam} \tag{3-67}$$

where $d=d(t)$, $\alpha_i=\int_0^l\varphi_i(x)a(x)dx$ and $\varphi_i(x_{dam})=\int_0^l\varphi_i(x)\delta(x-x_{dam})dx$

Applying Laplace transformation to equation (3-67), a dynamic equation of the beam can be derived and written as

$$q_i(s)=\frac{\alpha_i d+\varphi_i(x_{dam})F_{dam}}{s^2+\omega_i^2},\qquad i=1,2,3... \tag{3-68}$$

Using equations (3-68) and (3-13), linear displacement of the beam can be expressed as spatial-temporal equations.

$$w(s,x_p)=\sum_{i=1}^{\infty}\varphi_i(x_p)q_i(s)\approx\sum_{i=1}^{m}\varphi_i(x_p)\left[\frac{\alpha_i d+\varphi_i(x_{dam})F_{dam}}{s^2+\omega_i^2}\right], \tag{3-69}$$

where x_p is the monitor sensor location and m is the truncated number of modes. Equation (3-69) can be written in vector-matrix form.

$$w_p=w(s,x_p)\approx[\varphi_1(x_p)\cdots\varphi_m(x_p)]\begin{bmatrix}\frac{1}{s^2+\omega_1^2} & 0 & 0\\ 0 & \ddots & 0\\ 0 & 0 & \frac{1}{s^2+\omega_m^2}\end{bmatrix}\left\{\begin{bmatrix}\alpha_1\\ \vdots\\ \alpha_m\end{bmatrix}d+\begin{bmatrix}\varphi_1(x_{dam})\\ \vdots\\ \varphi_m(x_{dam})\end{bmatrix}F_{dam}\right\}$$

$$\approx(\varphi_p)^T diag\left[\frac{1}{s^2+\omega^2}\right](\alpha d+\varphi_{dam}F_{dam}) \tag{3-70}$$

where $(\varphi_p)^T=[\varphi_1(x_p)\cdots\varphi_m(x_p)]$, $(\alpha)^T=[\alpha_1\cdots\alpha_m]$,

$(\varphi_{dam})^T=[\varphi_1(x_{dam})\cdots\varphi_m(x_{dam})]$, and

$$diag\left[\frac{1}{s^2+\omega^2}\right]=\begin{bmatrix}\frac{1}{s^2+\omega_1^2} & 0 & 0\\ 0 & \ddots & 0\\ 0 & 0 & \frac{1}{s^2+\omega_m^2}\end{bmatrix}.$$

Equation (3-70) can be further derived into the following transfer function form.

$$w_p=(\varphi_p)^T diag\left[\frac{1}{s^2+\omega^2}\right](\alpha d)+(\varphi_p)^T diag\left[\frac{1}{s^2+\omega^2}\right](\varphi_{dam}F_{dam})$$

$$=\hat{\hat{H}}_d(s)d+H_{dam}(s)F_{dam}=\frac{1}{A_p(s)}\{\hat{\hat{B}}_d(s)d+B_{dam}(s)F_{dam}\}, \tag{3-71}$$

where $\hat{\hat{H}}_d(s)=(\varphi_p)^T diag\left[\frac{1}{s^2+\omega^2}\right]\alpha$; $H_{dam}(s)=(\varphi_p)^T diag\left[\frac{1}{s^2+\omega^2}\right]\varphi_{dam}$;

In equation (3-71), $A_p(s)=\prod_{i=1}^{m}(s^2+\omega_i^2)$ is the common denominator; $\hat{\hat{B}}_d(s)$ is the numerator of $\hat{\hat{H}}_d(s)$ and $B_{dam}(s)$ is the numerator of $H_{dam}(s)$.

Once the monitor sensor collocates with the groundhook damper, one may substitute equation (3-60) into equation (3-71) and obtain the closed-loop transfer function.

$$\frac{w_p}{d} = \frac{\hat{\bar{B}}_d(s)}{A_p(s) + sB_{dam}(s)\bar{v}_{dam}} \tag{3-72}$$

In real practice, coefficients of $A_p(s)$, $\hat{\bar{B}}_d(s)$ and $sB_{dam}(s)$ can be obtained via offline system identification. Equation (3-72), therefore, can be expressed in its discrete-time form written as

$$\frac{w_p}{d} = \frac{\hat{\bar{B}}_d(z)}{A_p(z) + B_{dam}(z)\bar{v}_{dam}} \tag{3-73}$$

Equation (3-73) is the closed-loop transfer function of the groundhook damper-beam coupled system when random disturbance is acting on a portion of the beam span.

3.7 Summary

In this chapter, structures of a conventional translational hybrid vibration absorber (THVA) and a new design of rotational hybrid vibration absorber (RHVA) are discussed. The limitation of implementing a skyhook/groundhook damper for structural vibration control is discussed. Analytical models for a THVA, a RHVA and a groundhook damper, which are separately coupled with a beam structure, are derived when random disturbance are applied on a point or a portion of the beam span. Those analytical models are finally derived into their closed-loop form for further controller design and analysis on their vibration suppression performance.

4 DESIGN OF GLOBAL STRUCTURAL VIBRATION CONTROLLER

In this chapter, a global vibration controller is designed with the pole-placement method. The controller can introduce active damping to an entire structure for global vibration control, and is applicable to either RHVA or THVA device. The closed-loop transfer function of the RHVA-beam coupled system, derived in the chapter 3, is used as a tool for the controller design. A novel approach is presented to select closed-loop poles, and Bezout equation is employed to calculate the controller parameters. Implementation technique of the proposed controller on a real HVA-beam coupled system is also discussed. Stability problem of the proposed controller is presented thereafter.

4.1 Design of a Global Structural Vibration Controller

The proposed global vibration controller is applicable to both RHVA and THVA devices. The controller design procedure is basically the same for either RHVA or THVA device. Since locations and forms of disturbance have no effects on the design procedure, the random disturbance on a point of a beam, which is coupled with a RHVA, is used as an example for demonstration of the controller design. The controller design is based on the closed-loop transfer function.

Equation (3-50) is the closed-loop transfer function of the aforementioned case in its discrete-time form. It has been derived in the chapter 3 as

$$\frac{\theta_p}{d} = \frac{K(z)B_d(z)}{Q(z) + B_m(z)G(z)}. \qquad (3\text{-}50)$$

In the closed-loop denominator, $G(z)$ is the controller transfer function. It may be designed as a rational function

$$G(z) = \frac{P(z)}{U(z)} \tag{4-1}$$

where $P(z) = \sum_{i=0}^{2m+1} p_i z^{-i}$, $U(s) = 1 + \sum_{i=1}^{2m+1} u_i z^{-i}$, with m being the order of the open-loop system. After substituting into equation (3-50), one can obtain

$$\frac{\theta_p}{d} = \frac{U(z)K(z)B_d(z)}{U(z)Q(z) + B_m(z)P(z)} \tag{4-2}$$

Equation (4-2) is the new closed-loop transfer function of the coupled system in which the proposed controller is integrated. It clearly shows that $K(z)$ is part of the closed-loop numerator. Actually $K(z)$ is directly related to the passive counterpart of the HVA. In equation (3-48), it can be found that $K(s) = s^2 + s\frac{v_a}{J_a} + \frac{k_a}{J_a}$ in its continuous-time form. That means passive counter part of the HVA can introduce tunable zeros into the closed-loop system with a proper set of passive parameters. A tunable absorption frequency, therefore, can be introduced into the frequency response of a structure.

Now the focus is on the closed-loop denominator. In general, the resonance of a structure is basically related to its closed-loop poles. Placing the closed-loop poles to suitable positions, therefore, can significantly suppress the resonant peaks of the structure. In general, stable closed-loop poles should be placed within a unit circle for discrete-time control system. One way to do this is to damp down open-loop poles and zeros. This is equivalent to introduce active damping to the structure. In equation (4-2), components of controller transfer functions, $P(z)$ and $U(z)$, become parts in the closed-loop denominator. With the help of Bezout equation, components $P(z)$ and $U(z)$ can be selected to place closed-loop poles to the desired positions. The closed-loop denominator of equation (4-2), hence, is used to construct a Bezout equation via

$$U(z)Q(z)+B_m(z)P(z)=T(z), \tag{4-3}$$

where $T(z)=1+\sum_{i=1}^{4m+3}t_i z^{-i}$ is a prototype polynomial that introduces $4m+3$ tunable poles to the closed-loop system. Roots of *T(z)* can be obtained via reciprocating or damping down the open-loop poles and zeros, which are the roots of the $Q(z)$ and $B_m(z)$. If $Rt_i=a+j\times b$ is one of the roots of $Q(z)$ and $B_m(z)$, one may obtain the damped roots with the following equation.

$$Rt_i'=\frac{1}{Rt_i}\times\alpha, \qquad |Rt_i|>1, \tag{4-4a}$$

$$Rt_i'=Rt_i\times\alpha, \qquad |Rt_i|<1, \tag{4-4b}$$

where $0<\alpha<1$. The closer α to zero, the stronger active damping is introduced to the root. The prototype polynomial *T(z)* is constructed by

$$T(z)=\prod_{i=1}^{4m+3}(z-Rt_i'). \tag{4-5}$$

The Bezout equation can be solved in the following matrix equation:

$$\begin{pmatrix}
1 & 0 & \cdots & \cdots & 0 & 0 & 0 & \cdots & \cdots & 0\\
q_1 & 1 & \ddots & \ddots & \vdots & b_1 & 0 & \ddots & \ddots & \vdots\\
q_2 & q_1 & \ddots & \ddots & 0 & b_2 & b_1 & \ddots & \ddots & \vdots\\
\vdots & q_2 & \ddots & \ddots & 0 & \vdots & b_2 & \ddots & \ddots & 0\\
\vdots & \vdots & \ddots & \ddots & 1 & \vdots & \vdots & \ddots & \ddots & 0\\
q_{2m+1} & \vdots & \ddots & \ddots & q_1 & b_{2m+1} & \vdots & \ddots & \ddots & b_1\\
q_{2m+2} & q_{2m+1} & \ddots & \ddots & q_2 & b_{2m+2} & b_{2m+1} & \ddots & \ddots & b_2\\
0 & q_{2m+2} & \ddots & \ddots & \vdots & 0 & b_{2m+2} & \ddots & \ddots & \vdots\\
\vdots & 0 & \ddots & \ddots & \vdots & \vdots & 0 & \ddots & \ddots & \vdots\\
\vdots & \vdots & \ddots & \ddots & q_{2m+1} & \vdots & \vdots & \ddots & \ddots & b_{2m+1}\\
0 & 0 & \cdots & \cdots & q_{2m+2} & 0 & 0 & \cdots & \cdots & b_{2m+2}
\end{pmatrix}
\begin{pmatrix}
1\\ u_1\\ \vdots\\ u_{2m}\\ u_{2m+1}\\ p_0\\ p_1\\ \vdots\\ p_{2m}\\ p_{2m+1}
\end{pmatrix}=
\begin{pmatrix}
1\\ t_1\\ \vdots\\ \vdots\\ \vdots\\ \vdots\\ \vdots\\ \vdots\\ \vdots\\ t_{4m+2}\\ t_{4m+3}
\end{pmatrix} \tag{4-6}$$

where $Q(z) = 1 + \sum_{i=1}^{2m+2} q_i z^{-i}$ and $B_m(z) = \sum_{i=1}^{2m+2} b_i z^{-i}$ are available via offline system identification in real implementations. Coefficients of $U(z)$ and $P(z)$ can be calculated with equation (4-6) for the construction of controller transfer function $G(z)$.

4.2 Implementation of the Proposed Controller on Real Application with Off-line System Identification Method

In section 4.1, it is clear that the controller design depends on roots of $Q(z)$ and $B_m(z)$. Typically, stability of the closed-loop control system mainly depends on the accuracy of these roots. In real practice, one popular approach to obtain the accurate roots is via offline system identification. Offline system identification can identify an open-loop transfer function between the actuator and the monitor sensor. It utilizes a large amount of system input signals u_k and feedback signals y_k to construct the finite difference equation and finally identifies its open-loop transfer function. The finite difference equation is

$$y_k = -\sum_{i=1}^{n} c_i y_{k-i} + \sum_{i=0}^{n} d_i u_{k-i} \tag{4-7}$$

where c_i, d_i are the coefficients of the open-loop transfer function and *n* is the order of the system. Applying z-transformation to equation (4-7), one may obtain

$$\frac{Y(z)}{U(z)} = \frac{\sum_{i=0}^{n} d_i z^{-i}}{1 + \sum_{i=1}^{n} c_i z^{-i}} = G_o(z) \tag{4-8}$$

where $G_o(z)$ is the open-loop transfer function between the actuator and the feedback sensor. In real practice, equation (4-7) can be expressed in the following matrix form.

$$\begin{bmatrix} y_k \\ y_{k-1} \\ y_{k-2} \\ y_{k-3} \\ \vdots \\ y_2 \\ y_1 \end{bmatrix} = \begin{bmatrix} y_{k-1} & y_{k-2} & \cdots & y_{k-n} & u_k & u_{k-1} & \cdots & u_{k-n} \\ y_{k-2} & y_{k-3} & \iddots & \vdots & u_{k-1} & u_{k-2} & \iddots & \vdots \\ y_{k-3} & y_{k-4} & \iddots & y_1 & u_{k-2} & u_{k-3} & \iddots & u_1 \\ \vdots & \vdots & \iddots & \vdots & \vdots & \vdots & \iddots & \vdots \\ y_2 & y_1 & \iddots & \vdots & \vdots & u_2 & \iddots & \vdots \\ y_1 & \vdots & \iddots & \vdots & u_2 & u_1 & \iddots & \vdots \\ 0 & 0 & \cdots & 0 & u_1 & 0 & \cdots & 0 \end{bmatrix} \begin{bmatrix} -c_1 \\ -c_2 \\ \vdots \\ -c_n \\ d_0 \\ d_1 \\ \vdots \\ d_n \end{bmatrix} + \begin{bmatrix} \tau_k \\ \tau_{k-1} \\ \tau_{k-2} \\ \vdots \\ \vdots \\ \tau_2 \\ \tau_1 \end{bmatrix} \tag{4-9}$$

where $y = \begin{bmatrix} y_k & y_{k-1} & y_{k-2} & \cdots & \cdots & y_2 & y_1 \end{bmatrix}^T$,

$\tau = \begin{bmatrix} \tau_k & \tau_{k-1} & \tau_{k-2} & \cdots & \cdots & \tau_2 & \tau_1 \end{bmatrix}^T$,

$\chi = \begin{bmatrix} -c_1 & -c_2 & \cdots & -c_n & d_0 & d_1 & \cdots & d_n \end{bmatrix}^T$

and $V = \begin{bmatrix} y_{k-1} & y_{k-2} & \cdots & y_{k-n} & u_k & u_{k-1} & \cdots & u_{k-n} \\ y_{k-2} & y_{k-3} & \iddots & \vdots & u_{k-1} & u_{k-2} & \iddots & \vdots \\ y_{k-3} & y_{k-4} & \iddots & y_1 & u_{k-2} & u_{k-3} & \iddots & u_1 \\ \vdots & \vdots & \iddots & \vdots & \vdots & \vdots & \iddots & \vdots \\ y_2 & y_1 & \iddots & \vdots & \vdots & u_2 & \iddots & \vdots \\ y_1 & \vdots & \iddots & \vdots & u_2 & u_1 & \iddots & \vdots \\ 0 & 0 & \cdots & 0 & u_1 & 0 & \cdots & 0 \end{bmatrix}$

Equation (4-9) can be simplified as

$$y = V\chi + \tau \tag{4-10}$$

where χ is composed of the coefficients c_i and d_i, and τ is the identification residue. If coefficients c_i and d_i are very close to their real values, the identification residue becomes very small and $\tau^T\tau \approx 0$. Coefficients c_i and d_i of the open-loop transfer function can, therefore, be identified by solving the following matrix equation in case the rank of V is $2n+1$.

$$\chi = \left[V^T V\right]^{-1} V^T y \tag{4-11}$$

In real practice, the accuracy of coefficients c_i and d_i depends on the system order *n*. If accurate system order is used to identify the open-loop transfer function, the residue error τ can be minimized and the accuracy of the coefficients can be

increased. To roughly evaluate the system order *n*, a feasibility function *J* is used and shown below.

$$J = (y - V\chi)^T (y - V\chi) \tag{4-12}$$

This function measures the error of the identified coefficients and is used to check the "fitness" of the identified transfer function. In general, the value of the feasibility function *J* decreases as system order *n* increases. However, the reduction of *J* ceases to be significant when *n* becomes greater than the true system order. Therefore, the real system order can be roughly evaluated by this principle.

In the RHVA-beam coupled system, $Q(z)$ and $B_m(z)$ are the open-loop transfer functions in the discrete-time form. Hereinafter the focus is how to identify the open-loop transfer functions from a real RHVA-beam coupled system via offline system identification. One may start at the continuous-time form of the open-loop transfer function. The open-loop transfer function between the RHVA actuator and its collocated feedback sensor in s-domain can be obtained from equations (3-45) and (3-46). They have been derived in the chapter 3 and shown here again.

$$\theta_p = \frac{1}{A_p(s)}\{B_d(s)d + B_m(s)M_a\} \tag{3-45}$$

$$M_a = (sv_a + k_a)[-\frac{M_a}{s^2 J_a} - \theta_p] + M_{act} \tag{3-46}$$

Equation (3-46) can be expanded as

$$M_a = -\left[\frac{s^2(sv_a + k_a)}{K(s)}\right]\theta_p + \frac{s^2 M_{act}}{K(s)} \tag{4-13}$$

where $K(s) = s^2 + s\frac{v_a}{J_a} + \frac{k_a}{J_a}$

Substituting equation (4-13) into equation (3-45), one obtains

$$\theta_p = \frac{1}{Q(s)}\left[K(s)B_d(s)d + s^2 B_m(s)M_{act}\right] \tag{4-14}$$

where $Q(s) = A_p(s)K(s) + s^2 B_m(s)(sv_a + k_a)$

Expressing equation (4-14) to its block diagram form, one may obtain

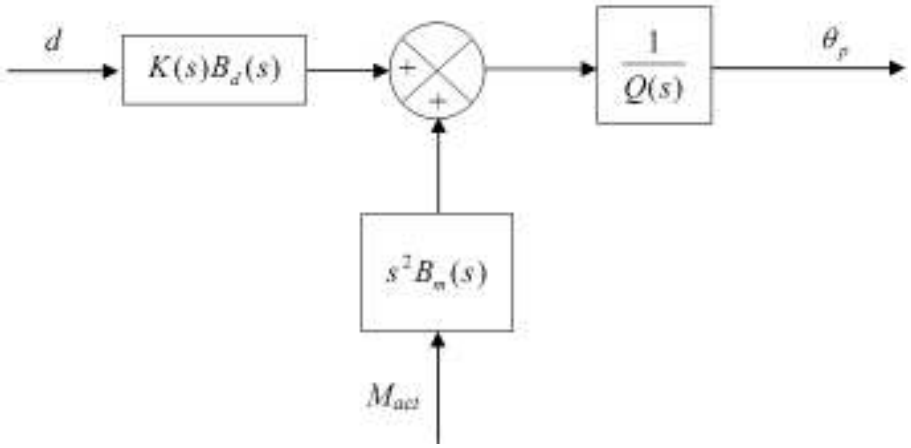

Figure 4-1 Block diagram of actuator, disturbance and feedback in RHVA-beam system

If disturbance is not applied on the beam, equation (4-14) can be simplified to

$$\theta_p = \frac{s^2 B_m(s)}{Q(s)} M_{act} \tag{4-15}$$

and its block diagram can be expressed as

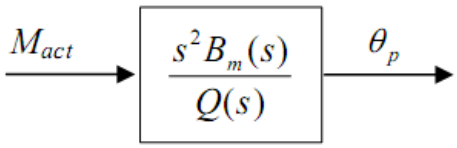

Figure 4-2 Continuous-time open-loop transfer function from actuator to feedback sensor in RHVA-beam system

In general, it is difficult to obtain the accurate transfer functions of a system in an analog approach. A better alternative is to identify them via offline system identification method in discrete-time domain. As described in the beginning of this section, offline system identification can identify an open-loop transfer function from a large amount of system input and feedback signals with the finite difference equation. In reality, this can be achieved by applying a random noise to the active control element of the coupled RHVA and recording both the noise and feedback signals. The identified open-loop transfer function, therefore, can be expressed as

$$\theta_p = \frac{B_m(z)}{Q(z)} M_{act} \tag{4-16}$$

and shown as the following block diagram.

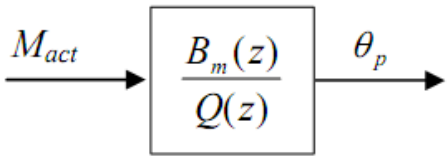

Figure 4-3 Discrete-time open-loop transfer function from actuator to feedback sensor in RHVA-beam system

After solving equation (4-11) with the measured data, coefficients of $Q(z)$ and $B_m(z)$ can be identified from the real RHVA-beam coupled system. Controller can be further designed with the roots of the identified transfer functions $Q(z)$ and $B_m(z)$.

4.3 Stability of the Closed-Loop Control System

In general, stability of a closed-loop control system mainly depends on its closed-loop denominator. In a discrete-time control system, stable closed-loop poles should be placed within a unit circle. With the help of equations (4-4a) and (4-4b), the prototype polynomial $T(z)$) can assign stable closed-loop poles to the closed-loop system. However, instability still can arise from the closed-loop denominator, because a stable closed-loop can be guaranteed only if accurate open-loop transfer functions can be obtained. In real practice, the accuracy of open-loop transfer functions can be affected by different factors including, but not limited to, plant dynamics, sensor dynamics, actuator dynamics, filter dynamics and amplifier dynamics. However, lots of controller designs may only concern with the plant dynamics and neglect the remaining. In fact, neglecting some of the dynamics may cause instability of the closed-loop control system.

The actuator and sensor dynamics, for example, may be considered as a transfer-function $M_{act}=G_{sd}(z)u$, where u is the actuation signal. Integrating it into equation (4-16), one may obtain

$$\theta_p = \frac{B_m(z)G_{sd}(z)}{Q(z)}u = \frac{\widetilde{B}_m(z)}{Q(z)}u \tag{4-17}$$

where $\widetilde{B}_m(z) = B_m(z)G_{sd}(z)$ and its block-diagram can be expressed as

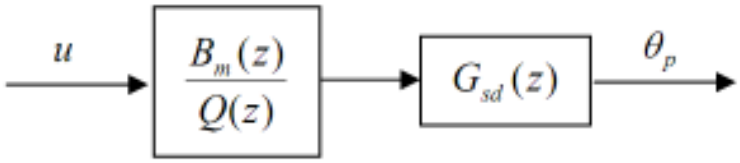

Figure 4-4 Open-loop transfer function from actuation signal u to feedback signal θ_p in RHVA-beam system with actuator/sensor dynamics

Via offline system identification, all dynamic effects can be identified and integrated into an open-loop transfer function $\frac{\widetilde{B}_m(z)}{Q(z)}$. This open-loop transfer function can provide more accurate roots to the proposed prototype polynomial and is closer to the real system dynamics. Therefore, stable closed-loop poles can be guaranteed to assign to the closed-loop system with the prototype polynomial and hence to prevent instability of the system arising from neglect of partial system dynamics. This advantage makes the proposed controller different from many popular controllers.

On the other hand, disturbance may be another factor to cause instability of a closed-loop control system. Disturbance actually is an uncertainty in real practice. The direction, acting position and form of the disturbance cannot be expected, stability problem arisen from the disturbance, therefore, should be addressed. However, the related stability problem has been briefly discussed in the end of section 3.2.2. Referring to equations (3-21) and (3-29), they are the closed-loop transfer functions for a THVA-beam coupled system when the disturbance is acting at a point and a portion of the beam span respectively. They have been derived in the chapter 3 and shown here again.

$$\frac{w_p}{d} = \frac{\overline{K}(z)\overline{B}_d(z)}{\overline{Q}(z) + B_f(z)\overline{G}(z)}, \tag{3-21}$$

$$\frac{w_p}{d} = \frac{\overline{K}(z)\hat{\overline{B}}_d(z)}{\overline{Q}(z) + B_f(z)\overline{G}(z)}, \tag{3-29}$$

The major difference between the two transfer functions is at their closed-loop numerators. The closed-loop numerator in equation (3-21) is composed of $\overline{K}(z)\overline{B}_d(z)$ and the one in equation (3-29) is composed of $\overline{K}(z)\hat{\overline{B}}_d(z)$. The numerators clearly demonstrated $\overline{B}_d(z)$ and $\hat{\overline{B}}_d(z)$ are basically related to the position of the disturbance. In fact, $\overline{B}_d(z)$ and $\hat{\overline{B}}_d(z)$ are the open-loop transfer functions between the disturbance and the feedback sensor. They may vary with different positions and forms of disturbance. Since $\overline{B}_d(z)$ and $\hat{\overline{B}}_d(z)$ can only affect their respective closed-loop numerator instead of their respective closed-loop denominator, the stability of the closed-loop system is not affected by the disturbance.

4.2 Summary

In this chapter, a global structural vibration controller is designed on the basis of the pole-placement method. This controller can introduce active damping to an entire structure for global vibration control, and is applicable to either RHVA or THVA device. The closed-loop transfer function of the RHVA-beam coupled system is used as an example for controller design. A novel approach is presented to assign stable closed-loop poles to the closed-loop control system on the basis of its open-loop transfer function. Bezout equation is employed to calculate the controller parameters. On the other hand, passive parameters of the HVA is presented on its ability to assign closed-loop zeros to the closed-loop system. Offline system identification is discussed on how to identify an open-loop transfer function, which integrates with the system dynamics, from a real HVA-beam coupled system. Stability problems of the closed-loop control system related to the accurate identification of system dynamics and the disturbance are also discussed.

5 NUMERICAL SIMULATIONS

In this chapter, three indices including mean square motion, spatial average motion and spatial average mean square motion [Jacquot (2003)] are introduced to quantify a point vibration motion, average vibration motion of an entire beam for a single frequency and a frequency band respectively. State-space models which were used to conduct the simulation tests are presented on their construction. A RHVA, a THVA and a groundhook damper have been separately applied to control a vibrating cantilever beam in simulation tests. Numerical results obtained from the simulation tests are presented. The introduced indices are calculated from the simulation results for each of the control devices. The percentages of reduction on these indices are used as references to evaluate the control performance for the RHVA, THVA and groundhook damper on their attenuation abilities of local and global vibration motions of a cantilever beam. Discussions and conclusions are finally presented on the basis of the calculated indices.

5.1 Measuring Indices for Vibration Motions

Mean square motion, spatial average motion and spatial average mean square motion are introduced in this section. They are used to observe the structural vibration amplitude at a single point, the average vibration amplitude of the entire beam structure at a single frequency and a frequency band respectively. Percentages of reduction on the mean square motion and the spatial average mean square motion can be used as references to evaluate the respective suppression performance of vibration motions at a point and on the entire beam structure for a device.

5.1.1 Mean Square Motion

Mean square motion is used to observe the structural vibration amplitude at a single point. It can be expressed in terms of translational and rotational motions to observe

the respective linear and angular vibration amplitudes of the beam structure at a point. They are denoted as $\sigma_w^2(x_m)$ and $\sigma_\theta^2(x_m)$ respectively where x_m is the monitor sensor location. Let $|w(e^{-j\omega}, x_m)|^2$ and $|\theta(e^{-j\omega}, x_m)|^2$ be power spectrum densities (PSDs) of their respective linear displacement $w(t, x_m)$ and angular displacement $\theta(t, x_m)$. The translational mean square motion $\sigma_w^2(x_m)$ and rotational mean square motion $\sigma_\theta^2(x_m)$ are obtained with the following equations in discrete-time simulation tests.

$$\sigma_w^2(x_m) = \frac{1}{2\pi}\int_{-\pi}^{\pi} |w(e^{-j\omega}, x_m)|^2 d\omega \approx \frac{1}{2\pi}\sum_{k=1}^{N} |w(e^{-j\omega_k}, x_m)|^2 \Delta\omega, \tag{5-1}$$

$$\sigma_\theta^2(x_m) = \frac{1}{2\pi}\int_{-\pi}^{\pi} |\theta(e^{-j\omega}, x_m)|^2 d\omega \approx \frac{1}{2\pi}\sum_{k=1}^{N} |\theta(e^{-j\omega_k}, x_m)|^2 \Delta\omega, \tag{5-2}$$

where $|w(e^{-j\omega_k}, x_m)|^2$ and $|\theta(e^{-j\omega_k}, x_m)|^2$ are the respective PSDs of $w(t, x_m)$ and $\theta(t, x_m)$ at the *k*th discrete frequency; *N* is the number of discrete frequency; $\Delta\omega$ is the frequency interval.

5.1.2 Percentage of Reduction on Point Vibration Motion

Respective percentage of reduction on the translational mean square motion $LR_w(x_m)$ and the rotational mean square motion $LR_\theta(x_m)$ is used as reference to evaluate the suppression performance of translational and rotational vibration motions of a beam structure at a point for a device. They are obtained by

$$LR_w(x_m) = \frac{\sigma_w^2(x_m)_{NoControl} - \sigma_w^2(x_m)_{Control}}{\sigma_w^2(x_m)_{NoControl}} \times 100\%, \tag{5-3}$$

$$LR_\theta(x_m) = \frac{\sigma_\theta^2(x_m)_{NoControl} - \sigma_\theta^2(x_m)_{Control}}{\sigma_\theta^2(x_m)_{NoControl}} \times 100\%, \tag{5-4}$$

where $\sigma_w^2(x_m)_{Control}$ and $\sigma_w^2(x_m)_{NoControl}$ are translational mean square motions for the cases with and without control respectively; $\sigma_\theta^2(x_m)_{Control}$ and $\sigma_\theta^2(x_m)_{NoControl}$ are rotational mean square motions for the cases with and without control respectively.

5.1.3 Spatial Average Motion

Spatial average motion is used to observe the average vibration amplitude of the entire beam structure at a single frequency. It can be expressed in terms of translational and rotational motions to observe their respective average linear and angular vibration amplitudes of the entire beam structure at a single frequency. They are denoted as $\sigma_w^2(\omega_k)$ and $\sigma_\theta^2(\omega_k)$ respectively where ω_k is the interested frequency. Since the spatial average motions are used to observe the average vibration amplitudes of the entire beam structure at a certain frequency, its value should be taken on averaging the signals measured at different locations of the beam. In the simulation tests, the beam was separated into twenty equal species and twenty-one check points were established. The translational spatial average motion $\sigma_w^2(\omega_k)$ and the rotational spatial average motion $\sigma_\theta^2(\omega_k)$ were calculated from the measured signals and obtained with the following equations in discrete-time simulation tests.

$$\sigma_w^2(\omega_k) = \frac{1}{l}\int_0^l |\, w(e^{-j\omega}, x)\,|^2 dx \approx \frac{1}{M}\sum_{i=1}^{M} |\, w(e^{-j\omega}, x_i)\,|^2 , \tag{5-5}$$

$$\sigma_\theta^2(\omega_k) = \frac{1}{l}\int_0^l |\, \theta(e^{-j\omega}, x)\,|^2 dx \approx \frac{1}{M}\sum_{i=1}^{M} |\, \theta(e^{-j\omega}, x_i)\,|^2 , \tag{5-6}$$

where $|\, w(e^{-j\omega}, x)\,|^2$ and $|\, \theta(e^{-j\omega}, x)\,|^2$ are the respective PSDs of $\theta(t,x)$ and $w(t,x)$; $|\, w(e^{-j\omega}, x_i)\,|^2$ and $|\, \theta(e^{-j\omega}, x_i)\,|^2$ are the respective PSDs of $\theta(t,x)$ and $w(t,x)$ at the ith check point and M is the number of check points. Spatial average motions were used for plotting of the frequency spectrums in the sections of 5.3 and 5.4 to demonstrate the simulation results. Actually, it is similar to the power spectrum density but considering the average vibration magnitude of entire beam instead of a single point.

5.1.4 Spatial Average Mean Square Motion

Spatial average mean square motion is similar to the spatial average motion but used to observe the average vibration amplitude of the entire beam structure within a frequency band. It can be expressed in terms of translational and rotational motions to observe their respective average linear and angular vibration amplitudes of the entire beam structure within a frequency band. They are denoted as $\sigma_w^2(Global)$ and $\sigma_\theta^2(Global)$ respectively. The translational spatial average mean square motion $\sigma_w^2(Global)$ and the rotational spatial average mean square motion $\sigma_\theta^2(Global)$ are obtained by integrating their spatial average motions over a frequency band.

$$\sigma_w^2(Global) = \frac{1}{2\pi}\int_{-\pi}^{\pi}\sigma_w^2(\omega_k)d\omega \approx \frac{1}{2\pi}\sum_{j=1}^{N}\sigma_w^2(\omega_j)\Delta\omega, \tag{5-7}$$

$$\sigma_\theta^2(Global) = \frac{1}{2\pi}\int_{-\pi}^{\pi}\sigma_\theta^2(\omega_k)d\omega \approx \frac{1}{2\pi}\sum_{j=1}^{N}\sigma_\theta^2(\omega_j)\Delta\omega, \tag{5-8}$$

where $\sigma_w^2(\omega_j)$ and $\sigma_\theta^2(\omega_j)$ are the translational and rotational spatial average motions respectively at the *j*th discrete frequency; *N* is the number of discrete frequency and $\Delta\omega$ is the frequency interval.

5.1.5 Percentage of Reduction on Vibration Motion of Entire Beam

Respective percentage of reduction on the translational spatial average mean square motion $\sigma_w^2(Global)$ and the rotational spatial average mean square motion $\sigma_\theta^2(Global)$ is used as reference to evaluate the suppression performance of average translational and rotational vibration motions of the entire beam within a frequency band for a device. They are obtained by

$$GR_w = \frac{\sigma_w^2(Global)_{NoControl} - \sigma_w^2(Global)_{Control}}{\sigma_w^2(Global)_{NoControl}} \times 100\%, \quad (5\text{-}9)$$

$$GR_\theta = \frac{\sigma_\theta^2(Global)_{NoControl} - \sigma_\theta^2(Global)_{Control}}{\sigma_\theta^2(Global)_{NoControl}} \times 100\%, \quad (5\text{-}10)$$

where $\sigma_w^2(Global)_{Control}$ and $\sigma_w^2(Global)_{NoControl}$ are translational spatial average mean square motions for the cases with and without control respectively; $\sigma_\theta^2(Global)_{Control}$ and $\sigma_\theta^2(Global)_{NoControl}$ are rotational spatial average mean square motions for the cases with and without control respectively.

5.2 State-Space Model

State-space models were constructed according to the previous derived mathematical models for different coupled systems. The general form of a state-space model is shown below.

$$\dot{x} = Ax + B_1 d + B_2 u \quad (5\text{-}11)$$

$$y = Cx + Du \quad (5\text{-}12)$$

where A is the state matrix; B_1 and B_2 are the input matrices for the respective disturbance and control signals; C is the output matrix and D is equal to zero;
x is the state vector; d and u are the input vectors which represent the disturbance and control signals; y is the output vector.

THVA-beam coupled system is used as an example to demonstrate on how to use the state-space model for simulation test. Referring to equation (3-9), the modal coordinate of the system is $\ddot{q}_i = -\omega_i^2 q_i + \varphi_i(x_d)d + \varphi_i(x_a)F_a$. In general, a slight damping is introduced into the model to avoid infinite resonance and simulation error. The modal coordinate is, therefore, expressed as

$$\ddot{q}_i = -\omega_i^2 q_i - 2\xi_i\omega_i + \varphi_i(x_d)d + \varphi_i(x_a)F_a \quad (5\text{-}13)$$

where ξ_i is the modal damping ratio of the ith mode and its state-space model is expressed as

$$\begin{bmatrix} \dot{q}_1 \\ \dot{q}_2 \\ \vdots \\ \dot{q}_m \\ \ddot{q}_1 \\ \ddot{q}_2 \\ \vdots \\ \ddot{q}_m \end{bmatrix} = \begin{bmatrix} 0 & 0 & \cdots & 0 & 1 & 0 & \cdots & 0 \\ 0 & 0 & \cdots & 0 & 0 & 1 & \cdots & 0 \\ \vdots & \vdots & \vdots & \vdots & \vdots & \vdots & \vdots & \vdots \\ 0 & 0 & \cdots & 0 & 0 & 0 & 0 & 1 \\ -\omega_1^{\,2} & 0 & 0 & 0 & -2\zeta_1\omega_1 & 0 & 0 & 0 \\ 0 & -\omega_2^{\,2} & 0 & 0 & 0 & -2\zeta_2\omega_2 & 0 & 0 \\ \vdots & \vdots & \vdots & \vdots & \vdots & \vdots & \vdots & \vdots \\ 0 & 0 & 0 & -\omega_m^{\,2} & 0 & 0 & 0 & -2\zeta_m\omega_m \end{bmatrix} \begin{bmatrix} q_1 \\ q_2 \\ \vdots \\ q_m \\ \dot{q}_1 \\ \dot{q}_2 \\ \vdots \\ \dot{q}_m \end{bmatrix}$$

$$+ \begin{bmatrix} 0 & 0 \\ 0 & 0 \\ \vdots & \vdots \\ 0 & 0 \\ \varphi_1(x_d) & \varphi_1(x_a) \\ \varphi_2(x_d) & \varphi_2(x_a) \\ \vdots & \vdots \\ \varphi_m(x_d) & \varphi_m(x_a) \end{bmatrix} \begin{bmatrix} d \\ F_a \end{bmatrix} \tag{5-14}$$

$$\begin{bmatrix} \theta(t,x_a) \\ \dot{\theta}(t,x_a) \\ w(t,x_a) \\ \dot{w}(t,x_a) \\ \theta(t,x_m) \\ \dot{\theta}(t,x_m) \\ w(t,x_m) \\ \dot{w}(t,x_m) \end{bmatrix} = \begin{bmatrix} \varphi_1'(x_a) & \varphi_2'(x_a) & \cdots & \varphi_m'(x_a) & 0 & 0 & \cdots & 0 \\ 0 & 0 & \cdots & 0 & \varphi_1'(x_a) & \varphi_2'(x_a) & \cdots & \varphi_m'(x_a) \\ \varphi_1(x_a) & \varphi_2(x_a) & \cdots & \varphi_m(x_a) & 0 & 0 & \cdots & 0 \\ 0 & 0 & \cdots & 0 & \varphi_1(x_a) & \varphi_2(x_a) & \cdots & \varphi_m(x_a) \\ \varphi_1'(x_m) & \varphi_2'(x_m) & \cdots & \varphi_m'(x_m) & 0 & 0 & \cdots & 0 \\ 0 & 0 & \cdots & 0 & \varphi_1'(x_m) & \varphi_2'(x_m) & \cdots & \varphi_m'(x_m) \\ \varphi_1(x_m) & \varphi_2(x_m) & \cdots & \varphi_m(x_m) & 0 & 0 & \cdots & 0 \\ 0 & 0 & \cdots & 0 & \varphi_1(x_m) & \varphi_2(x_m) & \cdots & \varphi_m(x_m) \end{bmatrix} \begin{bmatrix} q_1 \\ q_2 \\ \vdots \\ q_m \\ \dot{q}_1 \\ \dot{q}_2 \\ \vdots \\ \dot{q}_m \end{bmatrix}$$

(5-15)

where $\dot{x} = \begin{bmatrix} \dot{q}_1 & \dot{q}_2 & \cdots & \dot{q}_m & \ddot{q}_1 & \ddot{q}_2 & \cdots & \ddot{q}_m \end{bmatrix}^T$;

$x = \begin{bmatrix} q_1 & q_2 & \cdots & q_m & \dot{q}_1 & \dot{q}_2 & \cdots & \dot{q}_m \end{bmatrix}^T$;

$$A=\begin{bmatrix} 0 & 0 & \cdots & 0 & 1 & 0 & \cdots & 0 \\ 0 & 0 & \cdots & 0 & 0 & 1 & \cdots & 0 \\ \vdots & \vdots & \vdots & \vdots & \vdots & \vdots & \vdots & \vdots \\ 0 & 0 & \cdots & 0 & 0 & 0 & 0 & 1 \\ -\omega_1{}^2 & 0 & 0 & 0 & -2\zeta_1\omega_1 & 0 & 0 & 0 \\ 0 & -\omega_2{}^2 & 0 & 0 & 0 & -2\zeta_2\omega_2 & 0 & 0 \\ \vdots & \vdots & \vdots & \vdots & \vdots & \vdots & \vdots & \vdots \\ 0 & 0 & 0 & -\omega_m{}^2 & 0 & 0 & 0 & -2\zeta_m\omega_m \end{bmatrix};$$

$$\begin{bmatrix} B_1 & B_2 \end{bmatrix}=\begin{bmatrix} 0 & 0 \\ 0 & 0 \\ \vdots & \vdots \\ 0 & 0 \\ \varphi_1(x_d) & \varphi_1(x_a) \\ \varphi_2(x_d) & \varphi_2(x_a) \\ \vdots & \vdots \\ \varphi_m(x_d) & \varphi_m(x_a) \end{bmatrix};$$

$$y=\begin{bmatrix} \theta(t,x_a) & \dot{\theta}(t,x_a) & w(t,x_a) & \dot{w}(t,x_a) & \theta(t,x_m) & \dot{\theta}(t,x_m) & w(t,x_m) & \dot{w}(t,x_m) \end{bmatrix}^T;$$

$$C=\begin{bmatrix} \varphi_1'(x_a) & \varphi_2'(x_a) & \cdots & \varphi_m'(x_a) & 0 & 0 & \cdots & 0 \\ 0 & 0 & \cdots & 0 & \varphi_1'(x_a) & \varphi_2'(x_a) & \cdots & \varphi_m'(x_a) \\ \varphi_1(x_a) & \varphi_2(x_a) & \cdots & \varphi_m(x_a) & 0 & 0 & \cdots & 0 \\ 0 & 0 & \cdots & 0 & \varphi_1(x_a) & \varphi_2(x_a) & \cdots & \varphi_m(x_a) \\ \varphi_1'(x_m) & \varphi_2'(x_m) & \cdots & \varphi_m'(x_m) & 0 & 0 & \cdots & 0 \\ 0 & 0 & \cdots & 0 & \varphi_1'(x_m) & \varphi_2'(x_m) & \cdots & \varphi_m'(x_m) \\ \varphi_1(x_m) & \varphi_2(x_m) & \cdots & \varphi_m(x_m) & 0 & 0 & \cdots & 0 \\ 0 & 0 & \cdots & 0 & \varphi_1(x_m) & \varphi_2(x_m) & \cdots & \varphi_m(x_m) \end{bmatrix};$$

x_d, x_a and x_m are the respective disturbance, feedback sensor and monitor sensor locations; d and F_a are the respective disturbance and control signals; m is the truncated number of modes.

5.3 Comparison of RHVA and THVA on Local and Global Vibration Suppression

Simulation tests were conducted to test control performance of the RHVA and THVA. Angular and linear vibration amplitudes at the HVA coupling position and the twenty-one check points were measured in the simulation tests. Mean square motions, spatial average motions and spatial average mean square motions were calculated in terms of translational and rotational motions for the cases with and without HVA control on the basis of the simulation results. Percentages of reduction on mean square motions at the HVA coupling point were calculated to evaluate and compare the vibration suppression performance of the RHVA and THVA at the local coupling point. Percentages of reduction on the spatial average mean square motions were calculated to evaluate and compare the global vibration suppression performance of the RHVA and THVA on the entire beam structure. Spatial average motions were calculated and used for plotting of its PSDs.

5.3.1 Simulation Details on RHVA-THVA Comparison Tests

In the numerical tests, a cantilever beam was used as a tested structure. White noise was used as a disturbance and separately applied to a single point and a portion of the beam span. The point disturbance was acted at a point $x_d = 0.2l$ and the distributed disturbance was applied on a portion of the beam span from its mounting position to point $x_d = 0.2l$. Figures 5-1 and 5-2 show the schematics of a point disturbance on a cantilever beam which is coupled with a RHVA and a THVA respectively. Figures 5-3 and 5-4 show the schematics of a distributed disturbance on a cantilever beam which is coupled with a RHVA and a THVA respectively.

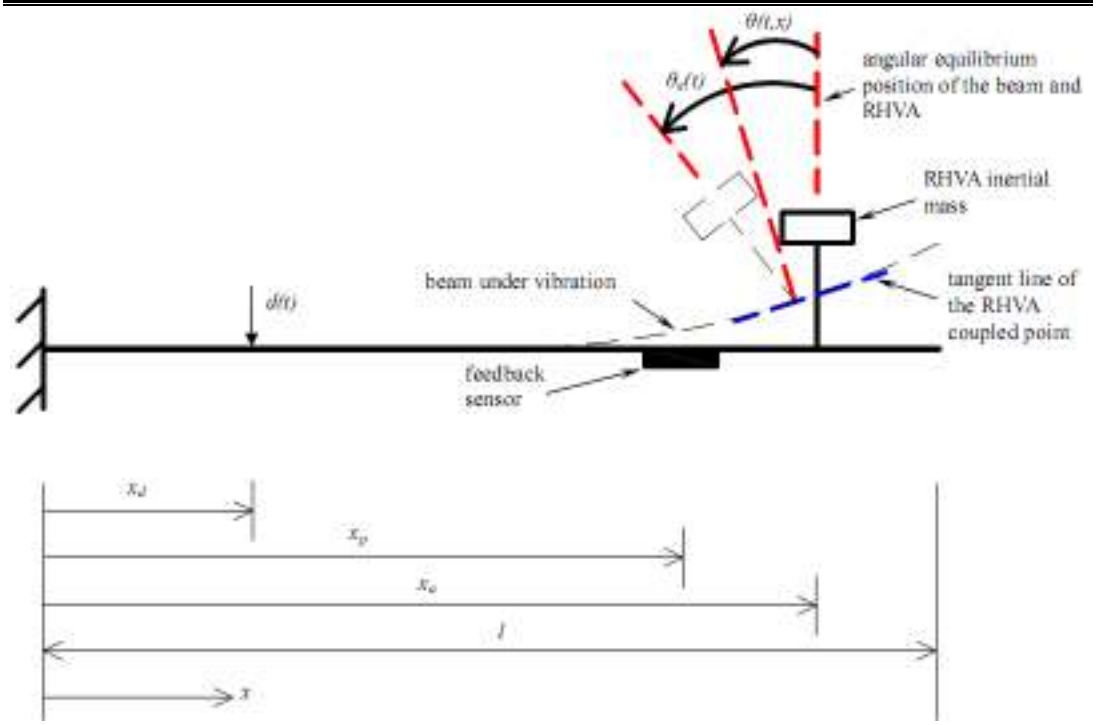

Figure 5-1 Point disturbance on a cantilever beam-RHVA system

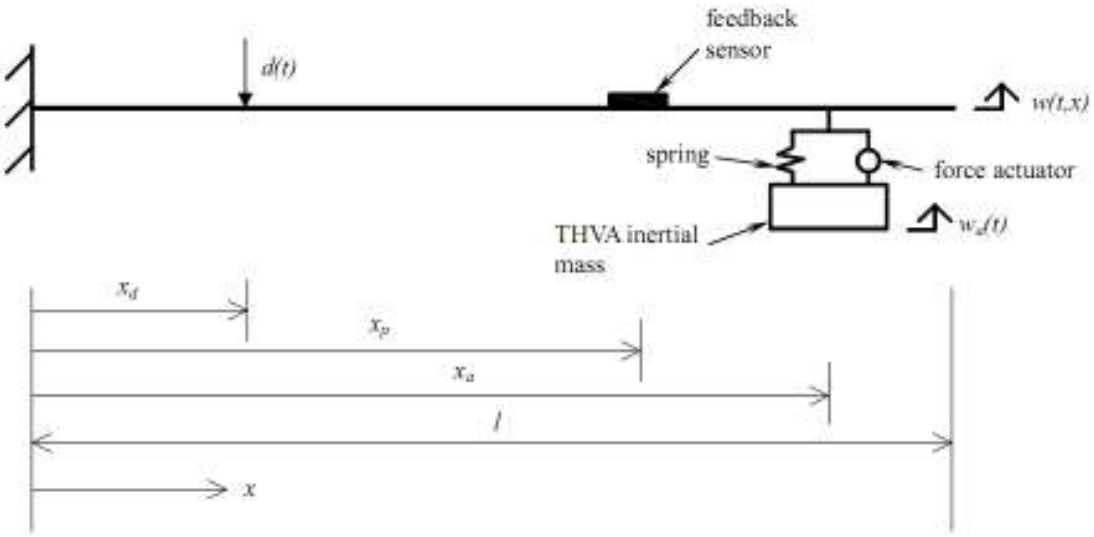

Figure 5-2 Point disturbance on a cantilever beam-THVA system

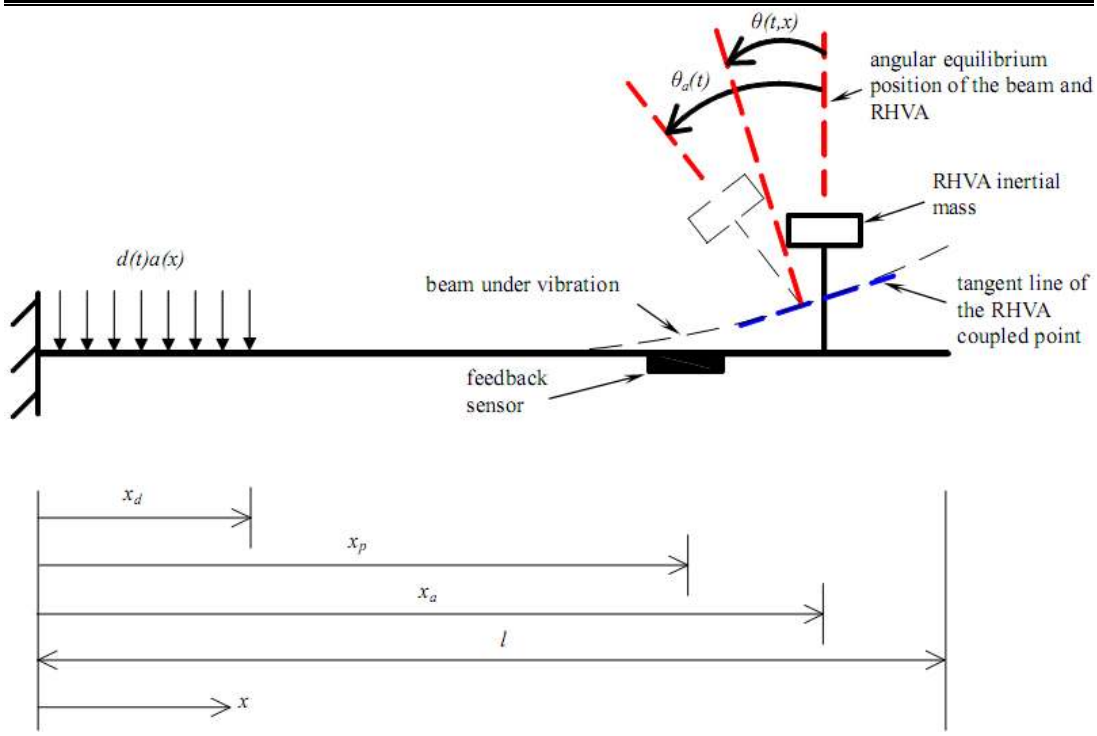

Figure 5-3 Distributed disturbance on a cantilever beam-RHVA system

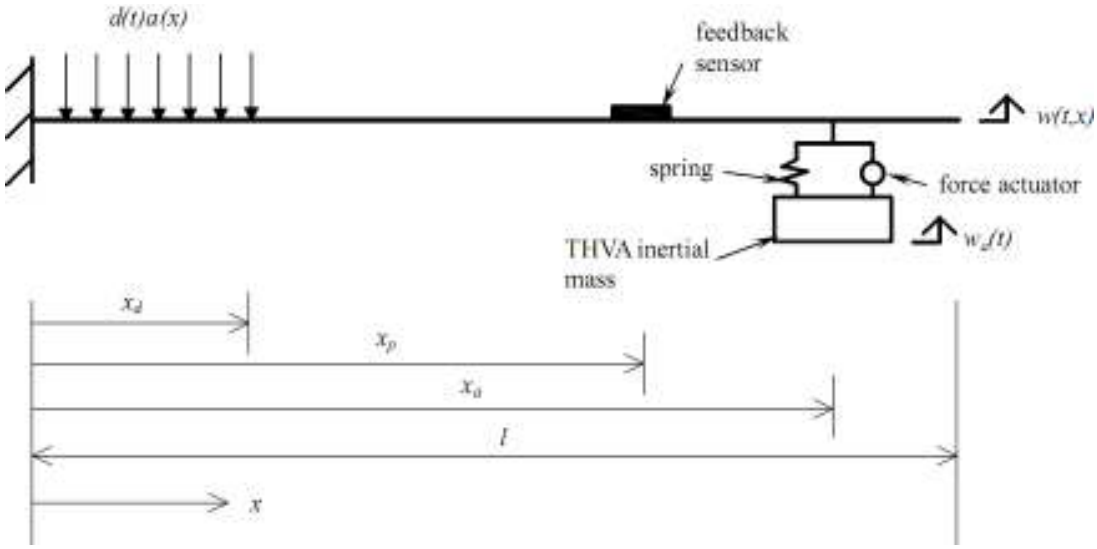

Figure 5-4 Distributed disturbance on a cantilever beam-THVA system

In the figures, $\theta(t,x)$ and $\theta_a(t)$ denotes the angular displacements of the beam and the RHVA; $w(t,x)$ and $w_a(t)$ denotes the linear displacements of the beam and the THVA; $d(t)$ denotes a point disturbance and $d(t)a(x)$ denotes a

distributed disturbance in which $d(t)$ is a temporal function and $a(x)$ is a spatial function bounded everywhere except at a finite number of points (a possible example is $a(x)=\begin{cases}1 & 0<x<x_d\\ 0 & x_d<x<l\end{cases}$). The simulation details of the cantilever beam and the HVA(s) are shown in the following table.

	THVA-Beam Coupled System	RHVA-Beam Coupled System
Beam length l	3 meter	
Beam width w	0.05 meter	
Beam thickness t	0.003 meter	
Beam density per length ρ	0.405 kg/m	
Young's modulus of Beam E	65×10^{9} N/m^2	
Moment of inertia of cross section of beam I	1.125×10^{-4} m^4	
Beam mass	1.215 kg	
Modal damping of each mode ξ_i	0.005	
Truncated number of modes m	5	
HVA coupling position x_a	l	
Feedback sensor location x_p	l	
Inertial mass of HVA m_a	0.1215 kg	
Second moment of inertia of the inertial mass J	-	0.0109 kgm^2
Effective stiffness of the HVA spring k	0.3348 N/m	0.0301 Nm/rad
Passive absorption frequency	$\sqrt{\frac{k}{m_a}}$ =1.66 rad/s	$\sqrt{\frac{k}{J}}$ =1.66 rad/s

Table 5-1 Simulation details on RHVA-THVA comparison

In the simulation tests, the models were truncated to the first five modes and this is a reasonable approximation of the models. The eigen-function of the cantilever beam, which was used to construct the eigen-function-based state-space model, is shown below:

$$\varphi_i(x) = \left[\cos(\lambda_i x) - \cosh(\lambda_i x)\right] - \mu_i\left[\sin(\lambda_i x) - \sinh(\lambda_i x)\right], \tag{5-16}$$

where x is a position variable of the cantilever beam; $\varphi_i(x)$ is the *i*th mode of the eigen-function of the cantilever beam at position *x*; $\mu_i = \dfrac{\cos(\lambda_i l) + \cosh(\lambda_i l)}{\sin(\lambda_i l) + \sinh(\lambda_i l)}$ is a constant and $\lambda_i l$ is the eigen-value of the *i*th mode;

The eigen-values of the first five modes are 1.875, 4.694, 7.854, 10.995 and 14.137. The natural frequencies can be expressed by $\omega_i = (\lambda_i l)^2 \sqrt{\dfrac{EI}{\rho l^4}}$. The beam characteristic parameters were on the basis of aluminum 6061 material and shown in the above table. The natural frequencies are 1.6600, 10.4032, 29.1292, 57.0816 and 94.3600 rad/s. The sampling frequency at the simulation test is 220 rad/s.

Referring to equations (3-2) and (3-31), the respective dynamic equation of the cantilever beam-THVA and cantilever beam-RHVA coupled systems when applying a point disturbance to the cantilever beam at the point x_d=0.2l are shown below:

$$\rho\ddot{w}(t,x0 + EIw''''(t,x) = d(t)\delta(x - 0.2l) + F_a\delta(x - l), \qquad 0 < x < l, \tag{5-17}$$

$$\rho\ddot{w}(t,x) + EIw''''(t,x) = d(t)\delta(x - 0.2l) + \frac{\partial[M_a\delta(x - l)]}{\partial x}, \quad 0 < x < l, \tag{5-18}$$

Referring to equations (3-22) and (3-48), dynamic equations of the cantilever beam-THVA and cantilever beam-RHVA coupled systems, when applying a distributed disturbance to the cantilever beam from its mounting position to the point x_d=0.2l, are shown below:

$$\rho\ddot{w}(t,x) + EIw''''(t,x) = d(t)a(x) + F_a\delta(x - l), \tag{5-19}$$

$$\rho\ddot{w}(t,x) + EIw''''(t,x) = d(t)a(x) + \frac{\partial[M_a\delta(x - l)]}{\partial x}, \tag{5-20}$$

where $0 < x < l$, $\qquad a(x) = \begin{cases} 1 & 0 < x < 0.2l \\ 0 & 0.2l < x < l \end{cases}$

The feedback sensor was collocated with the HVA at the tip position of the cantilever beam. This is because the end position of a cantilever beam is an antinode for all of its modes. Same inertial mass value was used for the RHVA and THVA. This is because one aim of the simulation tests is to test their control performance in case both of the HVA(s) carried with the same inertial mass. The passive absorption frequency of each HVA was tuned to the first resonant frequency 1.66 rad/s. Parameter α, which was used to damp the roots, was set as 0.96. This value was found to be the best for the HVA to introduce active damping to the cantilever beam by trial and error methods in which the percentage reduction on spatial average mean square motion was used as the reference. Theoretically, the closer α to zero, the stronger active damping is introduced to the root. However, it was found that better attenuation performance can be achieved with less active damping. Eigen-function-based state-space models were constructed on the basis of the previous derived models with the toolbox "simulink" of the commercial software MatLAB. The constructed state-space models were then transformed to discrete-time-based models with MatLAB toolbox. This is to emulate the real experimental situation since those measured experimental signals are in the discrete-time form.

5.3.2 Local Vibration Suppression Performance on a Cantilever Beam with Point Disturbance

This section is focused on the control performance of the RHVA and THVA on the vibration suppression performance of translational and rotational vibration motions at the HVA coupling point. This suppression performance is called local vibration suppression performance since it considers the motions of the local HVA coupling point. For the case of applying a point disturbance at point $x_d = 0.2l$ of a cantilever beam which was separately coupled with a RHVA and a THVA at its end position, Figures 5-5 and 5-6 show the PSDs of $w(t, x_a)$ and $\theta(t, x_a)$ for the cases with and without controls of RHVA and THVA.

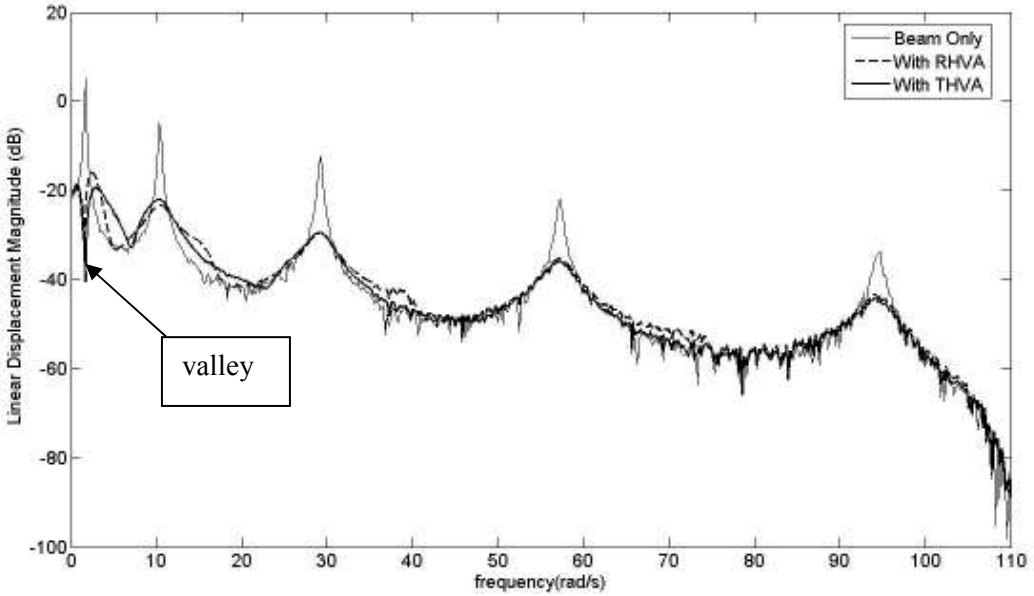

Figure 5-5 PSDs of $w(t,x_a)$ with/without RHVA and THVA (point disturbance at $x_d=0.2l$)

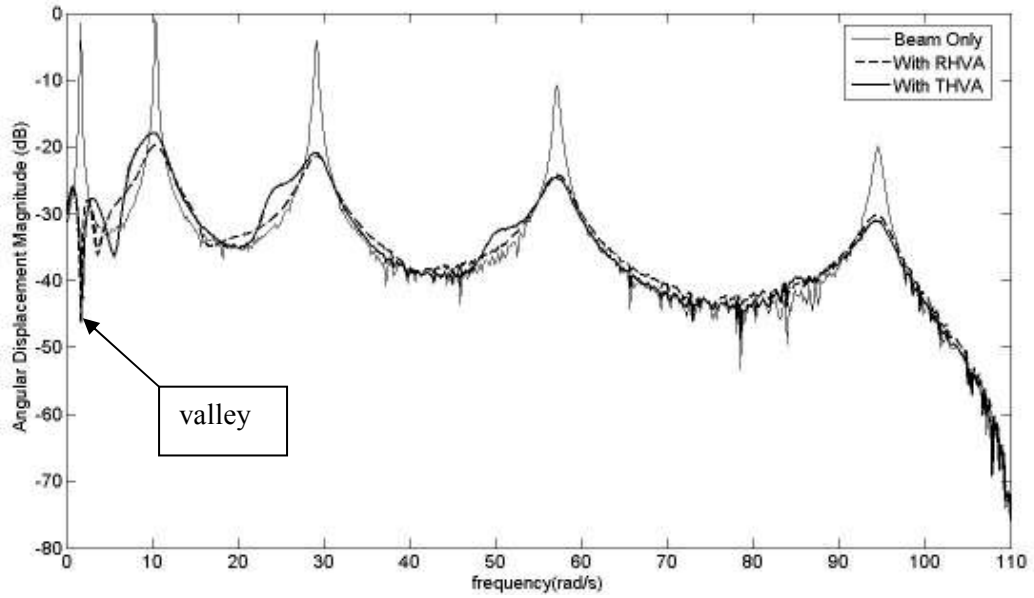

Figure 5-6 PSDs of $\theta(t,x_a)$ with/without RHVA and THVA (point disturbance at $x_d=0.2l$)

In figures 5-5 and 5-6, a valley appears at the first mode of the respective PSDs of the translational and rotational motions for RHVA and THVA. The valley indicates that both the RHVA and THVA can introduce an absorption frequency to the first mode of the cantilever beam for absorption of its translational and rotational vibration motions at the respective HVA coupling point. This absorption frequency in reality can be simply tuned with the passive parameters of the RHVA and THVA by $\sqrt{\frac{k}{m_a}}$ and $\sqrt{\frac{k}{J}}$ respectively. On the other hand, the resonant peaks of both translational and rotational motions were significantly damped down by RHVA and THVA in all modes. This clearly demonstrates that the proposed controller can successfully introduce active damping to the cantilever beam at the respective HVA coupling position.

To quantify the vibration motions of the local HVA coupling point, the translational and rotational mean square motions at the HVA coupling position, $\sigma_w^2(x_a)$ and $\sigma_\theta^2(x_a)$, were calculated on the basis of the simulation results for the RHVA and THVA separately for the cases with and without control. The respective percentage of reduction on the translational and rotational mean square motions, $LR_w(x_a)$ and $LR_\theta(x_a)$, was calculated separately for the RHVA and THVA to evaluate their vibration attenuation performance at the local coupling point. The calculated results show that RHVA can suppress 92.7% of the translational mean square motion and 87.5% of the rotational mean square motion while THVA can suppress 91.1% of translational mean square motion and 80.5% of rotational mean square motion. This shows that the RHVA has better mitigation ability than the THVA on the rotational vibration motion but similar attenuation performance on the translational vibration motion at its local coupling point. To obtain better understanding on how the disturbance location affects the control performance of the HVA, the point disturbance was acted at different location of x_d including 0.2l, 0.4l, 0.6l, 0.8l and l. The respective percentage of reduction on translation and rotational mean square motions for RHVA and THVA is shown in the following table.

Disturbance location x_d	RHVA		THVA	
	$LR_w(x_a)(\%)$	$LR_\theta(x_a)(\%)$	$LR_w(x_a)(\%)$	$LR_\theta(x_a)(\%)$
$0.2l$	92.7	87.5	91.1	80.5
$0.4l$	94.3	92.5	93.4	85.9
$0.6l$	95.3	95.7	94.9	92.9
$0.8l$	96.1	96.9	95.7	96.4
l	96.5	96.0	96.0	95.1

Table 5-2 Local percentage reductions by RHVA and THVA (point disturbance)

Table 5-2 shows that the respective percentage reduction on the local translational and rotational mean square motions, $LR_w(x_a)$ and $LR_\theta(x_a)$, for RHVA and THVA when a point disturbance was applied at different locations of a cantilever beam. The readings show that the RHVA generally has better alleviation ability than the THVA on the local rotational vibration motion but similar attenuation performance on the local translational vibration motion at its local coupling point even a point disturbance was applied in different locations.

5.3.3 Global Vibration Suppression Performance on a Cantilever Beam with Point Disturbance

This section is focused on the control performance of the RHVA and THVA on the vibration suppression performance of the average translational and rotational vibration motions of the entire cantilever beam. This suppression performance is called global vibration suppression performance since it considers the motions of entire beam instead of the local HVA coupling point. For the case of applying a point disturbance at point $x_d = 0.2l$ of a cantilever beam which was separately coupled with a RHVA and a THVA at its end position, Figures 5-7 and 5-8 show the respective PSD of translational spatial average motion $\sigma_w(\omega_k)$ and rotational spatial average motion $\sigma_\theta(\omega_k)$ within a frequency band for the cases with and without controls of RHVA and THVA.

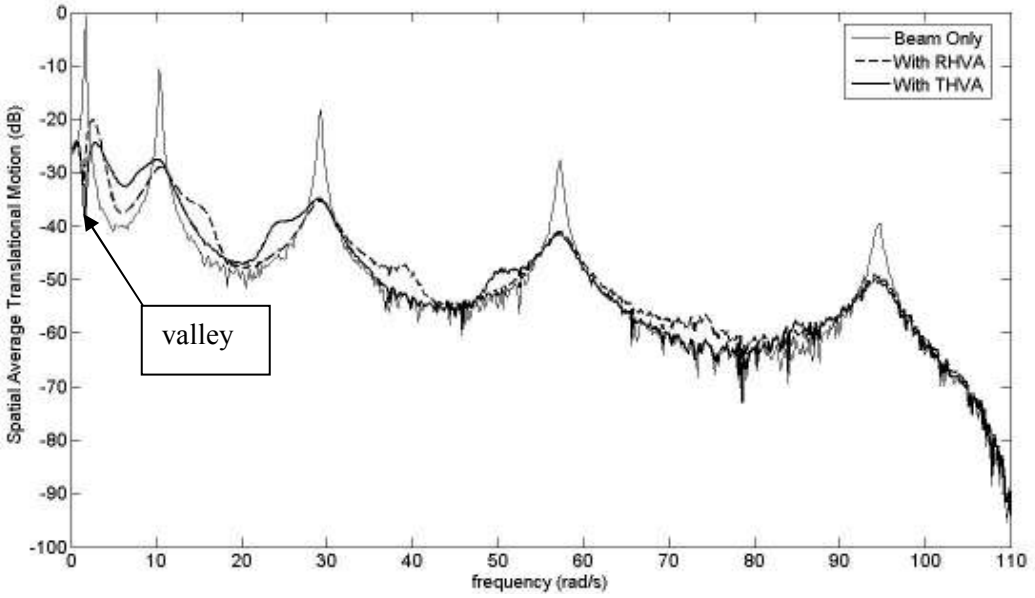

Figure 5-7 PSDs of translational spatial average motion with/without RHVA and THVA (point disturbance at x_d=0.2l)

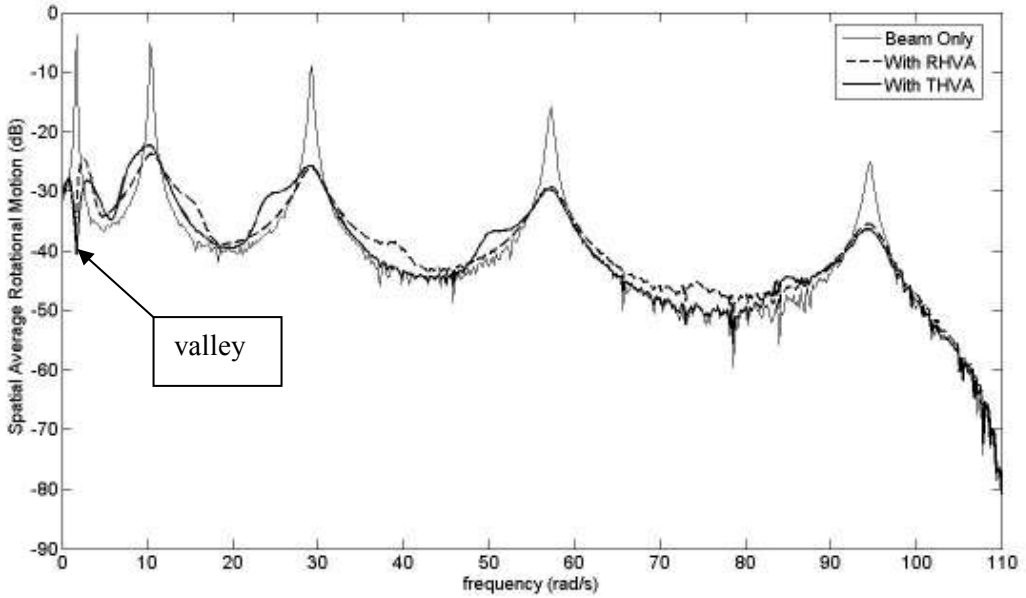

Figure 5-8 PSDs of rotational spatial average motion with/without RHVA and THVA (point disturbance at x_d=0.2l)

In figures 5-7 and 5-8, a valley appears at the first mode of the respective PSD of the translational and rotational spatial average motions for RHVA and THVA. The valley indicates that both the RHVA and THVA can introduce an absorption frequency to the first mode of the cantilever beam for suppression of its translational

and rotational vibration motions at all the measuring check points. This absorption frequency in reality can be simply tuned with the passive parameters of the RHVA and THVA by $\sqrt{\frac{k}{m_a}}$ and $\sqrt{\frac{k}{J}}$ respectively. On the other hand, the resonant peaks of both translational and rotational spatial average motions were remarkably damped down by RHVA and THVA in all modes. This clearly shows that the proposed controller can successfully introduce active damping to the cantilever beam at all the measuring check points and the goal of introducing global active damping to the entire cantilever beam for global broadband structural vibration control was achieved.

To quantify the average vibration motions of the entire cantilever beam, the translational and rotational spatial average mean square motions of the entire cantilever beam, $\sigma_w^2(Global)$ and $\sigma_\theta^2(Global)$, were calculated on the basis of the translational and rotational spatial average motions for the RHVA and THVA separately for the cases with and without control. The respective percentage of reduction on the translational and rotational spatial average mean square motions, GR_w and GR_θ, was calculated separately for the RHVA and THVA to evaluate their global vibration suppression performance on the entire cantilever beam. The calculated results show that RHVA can suppress 90.3% of the translational spatial average mean square motion and 86.9% of the rotational spatial average mean square motion while THVA can suppress 88.6% of translational spatial average mean square motion and 81.4% of rotational spatial average mean square motion. This indicates that the RHVA has better mitigation ability than the THVA on the average rotational vibration motion of the entire cantilever beam but similar attenuation performance on the average translational vibration motion of the entire cantilever beam. To obtain better understanding on how the disturbance location affects the control performance of the HVA, the point disturbance was acted at different location of x_d including 0.2l, 0.4l, 0.6l, 0.8l and l. The respective percentage of reduction on translation and rotational spatial average mean square motions for RHVA and THVA is shown in the following table.

Disturbance location x_d	RHVA		THVA	
	GR_w(%)	GR_θ(%)	GR_w(%)	GR_θ(%)
0.2l	90.3	86.9	88.6	81.4
0.4l	92.2	91.5	91.7	87.3
0.6l	93.8	94.3	93.9	93.0
0.8l	95.1	95.7	95.1	95.6
l	96.0	95.8	95.6	95.1

Table 5-3 Global percentage reductions by RHVA and THVA (point disturbance at different locations)

Table 5-3 shows that the respective percentage reduction on the translational and rotational spatial average mean square motions, GR_w and GR_θ, for RHVA and THVA when a point disturbance was applied at different locations of a cantilever beam. The readings show that the RHVA generally has better suppression ability than the THVA on the average rotational vibration motion of the entire cantilever beam but similar attenuation performance on the average translational vibration motion of the entire cantilever beam even a point disturbance was applied in different locations.

5.3.4 Local Vibration Suppression Performance on a Cantilever Beam with Distributed Disturbance

This section is focused on the control performance of the RHVA and THVA on the local vibration suppression performance, when a distributed disturbance was applied at a portion of the cantilever beam span from its mounting position to point $x_d = 0.2l$. Figures 5-9 and 5-10 show PSDs of $w(t, x_a)$ and $\theta(t, x_a)$ for the cases with and without controls of RHVA and THVA.

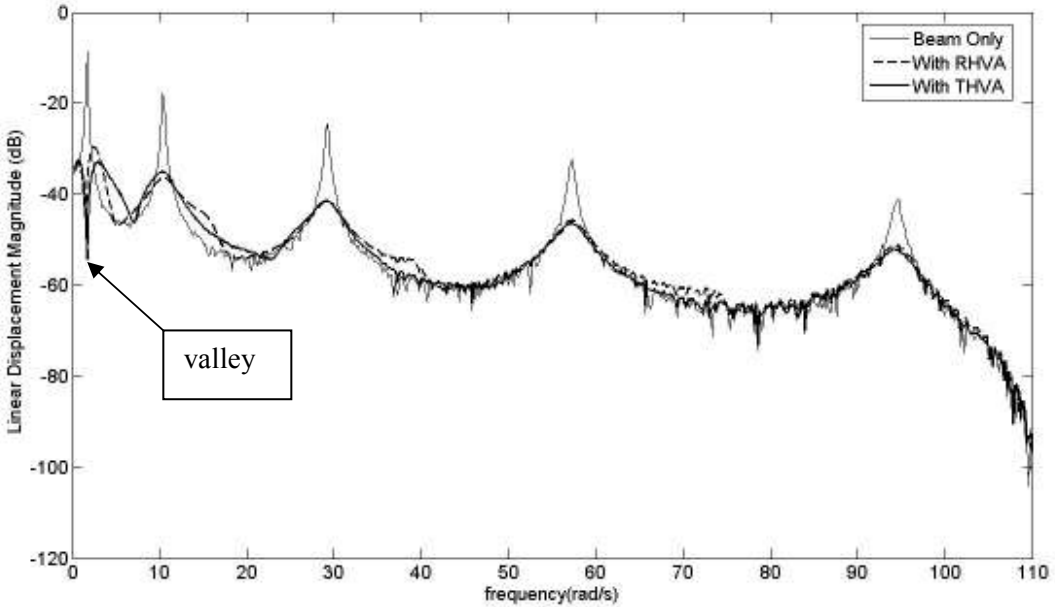

Figure 5-9 PSDs of $w(t,x_a)$ with/without RHVA and THVA (distributed disturbance from x=0 to x_a=0.2l)

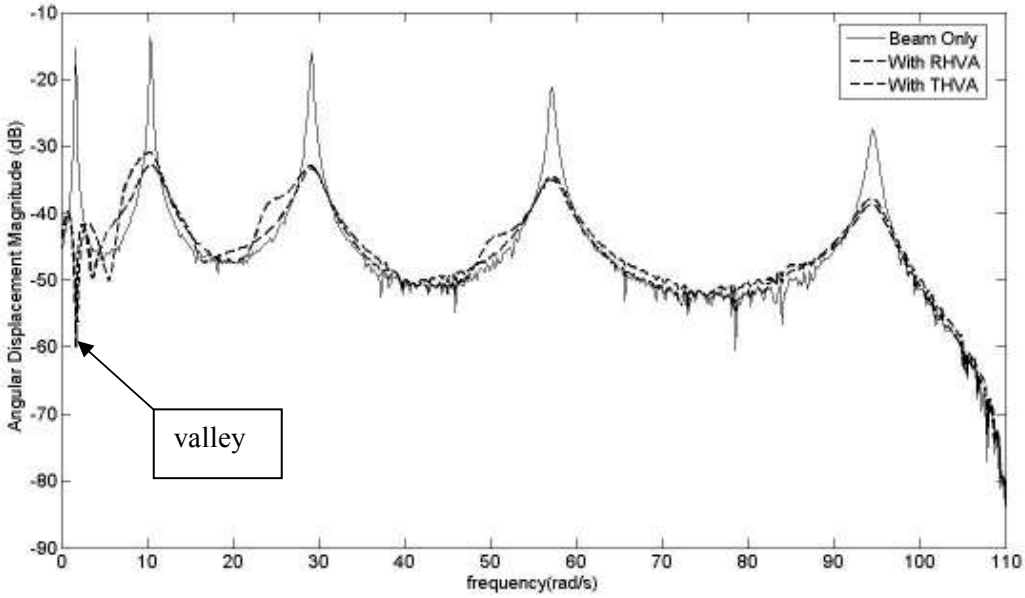

Figure 5-10 PSDs $\theta(t,x_a)$ with/without RHVA and THVA (distributed disturbance from x=0 to x_a=0.2l)

In figures 5-9 and 5-10, a valley appears at the first mode of the respective PSD of the translational and rotational motions for RHVA and THVA. Similar to the case of applying a point disturbance to the cantilever beam, the valley indicates that both the RHVA and THVA can introduce an absorption frequency to the first mode of the

cantilever beam for attenuation of its translational and rotational vibration motions at the respective HVA coupling point. On the other hand, the resonant peaks of both translational and rotational motions were notably damped down by RHVA and THVA in all modes. This indicates that the proposed controller can successfully introduce active damping to the cantilever beam at the respective HVA coupling position even distributed disturbance acting on the cantilever beam span.

The respective percentage of reduction on the translational and rotational mean square motions, $LR_w(x_a)$ and $LR_\theta(x_a)$, was calculated separately for the RHVA and THVA to evaluate their vibration alleviation performance at the local coupling point. The calculated results show that RHVA can suppress 92.2% of the translational mean square motion and 85.4% of the rotational mean square motion while THVA can suppress 90.5% of translational mean square motion and 79.6% of rotational mean square motion. This shows that the RHVA has better mitigation ability than the THVA on the rotational vibration motion but similar attenuation performance on the translational vibration motion at its local coupling point. To obtain better understanding on how the disturbance location affects the control performance of the HVA, the distributed disturbance was acted from the beam's mounting position to different location of x_d including 0.2l, 0.4l, 0.6l, 0.8l and l. The respective percentage of reduction on translation and rotational mean square motions for RHVA and THVA is shown in the following table.

Disturbance boundary from x=0 to x_d	RHVA		THVA	
	$LR_w(x_a)$(%)	$LR_\theta(x_a)$(%)	$LR_w(x_a)$(%)	$LR_\theta(x_a)$(%)
$x_d = 0.2l$	92.2	85.4	90.5	79.6
$x_d = 0.4l$	93.5	90.3	92.3	82.7
$x_d = 0.6l$	94.5	93.3	93.8	87.3
$x_d = 0.8l$	95.3	95.5	94.8	92.3
$x_d = l$	95.9	96.8	95.5	95.7

Table 5-4 Local percentage reductions by RHVA and THVA (distributed disturbance at different locations)

Table 5-4 shows that the respective percentage reduction on the local translational and rotational mean square motions, $LR_w(x_a)$ and $LR_\theta(x_a)$, for RHVA and THVA when distributed disturbance was applied at different locations of a cantilever beam. The readings show that the RHVA generally has better mitigation ability than the THVA on the local rotational vibration motion but similar suppression performance on the local translational vibration motion at its local coupling point when a distributed disturbance was applied in different locations of the cantilever beam.

5.3.5 Global Vibration Suppression Performance on a Cantilever Beam with Distributed Disturbance

This section is focused on the control performance of the RHVA and THVA on the global vibration suppression performance of the entire cantilever beam, when a distributed disturbance was applied at a portion of the cantilever beam span from its mounting position to point x_d = 0.2l. Figures 5-11 and 5-12 show the respective PSDs of translational spatial average motion $\sigma_w(\omega_k)$ and rotational spatial average motion $\sigma_\theta(\omega_k)$ within a frequency band for the cases with and without controls of RHVA and THVA.

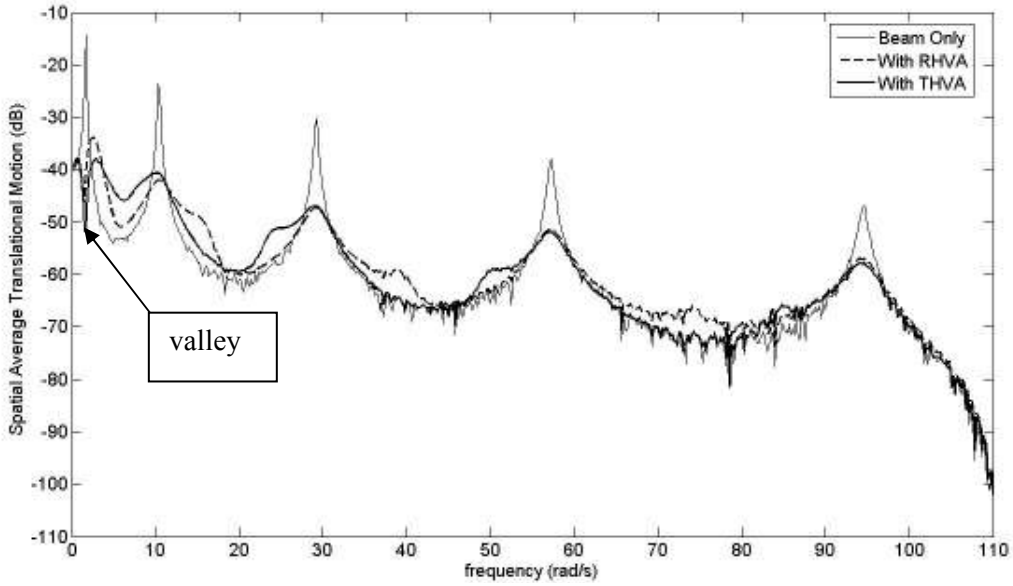

Figure 5-11 PSDs of translational spatial average motion with/without RHVA and THVA (distributed disturbance from x=0 to x_d=0.2l)

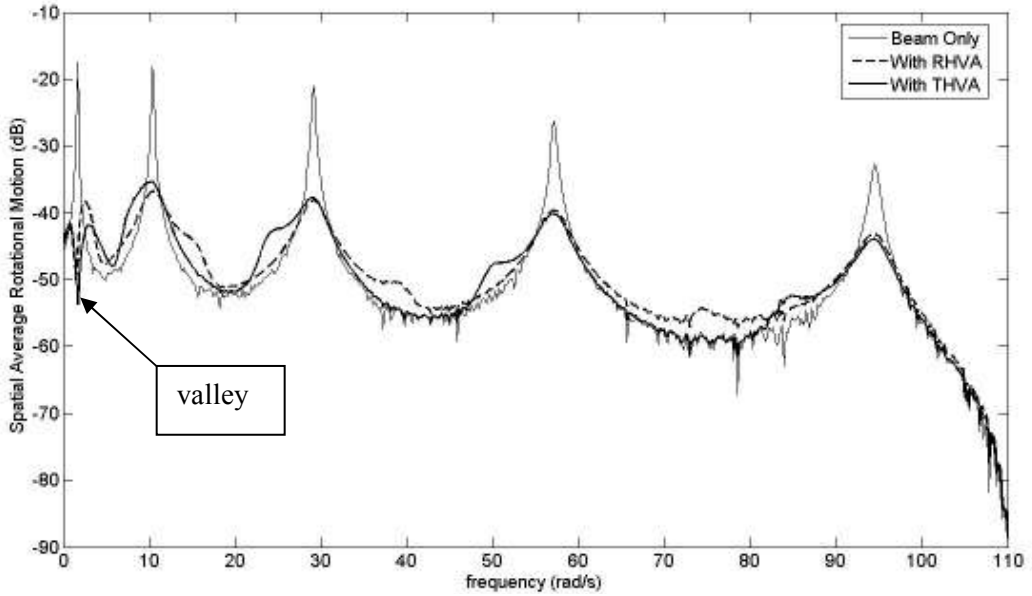

Figure 5-12 PSDs of rotational spatial average motion with/without RHVA and THVA (distributed disturbance from x=0 to x_d=0.2l)

In figures 5-11 and 5-12, a valley appears at the first mode of the respective PSD of the translational and rotational spatial average motions for RHVA and THVA. Similar to the case of applying a point disturbance at the cantilever beam, the valley indicates that both the RHVA and THVA can introduce an absorption frequency to the first mode of the cantilever beam for alleviation of its translational and rotational vibration motions at all the measuring check points. On the other hand, the resonant peaks of both translational and rotational spatial average motions were effectively damped down by both RHVA and THVA in all modes. This clearly shows that the proposed controller can successfully introduce damping effect to the cantilever beam at all the measuring check points even a distributed disturbance was applied to the cantilever beam span. This signifies the goal of introducing global active damping to the entire cantilever beam for global broadband structural vibration control was achieved.

The respective percentage of reduction on the translational and rotational spatial average mean square motions, GR_w and GR_θ, was calculated separately for the RHVA and THVA to evaluate their global vibration suppression performance on the entire cantilever beam. The calculated results show that RHVA can suppress 89.8%

of the translational spatial average mean square motion and 85.1% of the rotational spatial average mean square motion while THVA can suppress 87.7% of translational spatial average mean square motion and 80.1% of rotational spatial average mean square motion. This indicates that the RHVA has better mitigation ability than the THVA on the average rotational vibration motion of the entire cantilever beam but similar attenuation performance on the average translational vibration motion of the entire cantilever beam. To obtain better understanding on how the disturbance location affects the control performance of the HVA, the distributed disturbance was acted from the beam's mounting position to different location of x_d including $0.2l$, $0.4l$, $0.6l$, $0.8l$ and l. The respective percentage of reduction on translation and rotational spatial average mean square motions for RHVA and THVA is shown in the following table.

Disturbance boundary from x=0 to x_d	RHVA		THVA	
	GR_w(%)	GR_θ(%)	GR_w(%)	GR_θ(%)
$x_d = 0.2l$	89.8	85.1	87.7	80.1
$x_d = 0.4l$	91.2	89.5	90.2	84.0
$x_d = 0.6l$	92.6	92.2	92.2	88.6
$x_d = 0.8l$	93.8	94.1	93.7	92.5
$x_d = l$	94.8	95.4	94.7	94.9

Table 5-5 Global percentage reductions by RHVA and THVA (distributed disturbance at different locations)

Table 5-5 shows that the respective percentage reduction on the translational and rotational spatial average mean square motions, GR_w and GR_θ, for RHVA and THVA when a distributed disturbance was applied at different locations of a cantilever beam. The readings show that the RHVA generally has better suppression ability than the THVA on the average rotational vibration motion of the entire cantilever beam but similar attenuation performance on the average translational

vibration motion of the entire cantilever beam when a distributed disturbance was applied in different locations of the cantilever beam.

5.3.6 Conclusion on RHVA-THVA Comparison Tests

The above figures and tables show that implementation of the proposed controller with either RHVA or THVA can introduce a passive absorption frequency to both the local HVA coupling point and the measuring check points. Unlike the THVA, RHVA is easier to tune its passive absorption frequency in real application via varying the second moment of inertia of the HVA inertial mass. This, therefore, gives the practical advantage to the RHVA and makes the user easier to use the HVA.

From the calculated indices, RHVA can at least suppress 85% of mean square motions and 85% of spatial average mean square motions while THVA can at least suppress 79% of mean square motions and 80% of spatial average mean square motions. Those values will change when disturbance is acting at different locations of the cantilever beam with different form. In general, the RHVA has better suppression performance on the rotational vibration motions but similar attenuation performance on the translational vibration motions of a cantilever beam at a local HVA coupling point and on the entire beam structure.

For the disturbance, the readings of the discussed tables demonstrate that the disturbance form and location can affect the vibration alleviation performance of the HVA and the proposed controller. The simulation results show that disturbance variation can reduce about 8% and 15% of the global attenuation performance on the translational and rotational vibration motions for THVA respectively and reduce about 6% and 10% of the global attenuation performance on the translational and rotational vibration motions for RHVA respectively. These results can be calculated by subtracting the maximum and minimum values of percentages discussed in the tables 5-2, 5-3, 5-4 and 5-5 for the respective HVA. For example, the maximum and minimum percentages of reduction on translational spatial average mean square motion among the four tables for THVA are 95.6% and 87.7%, the percentage

reduction on its global attenuation performance due to disturbance variation is therefore equal to 8%. This signifies that the RHVA can provide more stable mitigation performance than the THVA for the structure when disturbance form and location are changed. Integrating all of the above discussed vantages, RHVA, therefore, can be considered as a better alternative HVA design than the conventional THVA.

For the proposed controller, the figures indicate that all the resonant peaks of the cantilever beam can successfully damp down for all modes at both local HVA coupling point and the measuring check points no matter a point or a distributed disturbance was applied on the beam structure. This signifies that the proposed controller can successfully introduce global active damping to the entire beam structure for global structural vibration control within a frequency band. Besides, the figures in tables 5.2 to 5.5 show that the controller has better vibration attenuation performance if the disturbance is near to the sensor and RHVA coupling location. Generally, this is because collocation between the disturbance, sensor and RHVA can improve the vibration suppression performance of the controller.

5.4 Comparison of RHVA and Groundhook Damper on Local and Global Vibration Suppression Performance

Simulation tests were conducted to test and compare control performance of the RHVA and groundhook damper. Angular and linear vibration amplitudes at the RHVA or groundhook damper coupling position and the twenty-one check points were measured in the simulation tests. Mean square motions, spatial average motions and spatial average mean square motions were calculated in terms of translational and rotational motions for the cases with and without control on the basis of the simulation results. Percentages of reduction on mean square motions at the device coupling point were calculated to evaluate and compare the vibration suppression performance of the RHVA and groundhook damper at the local coupling point. Percentages of reduction on the spatial average mean square motions were calculated to evaluate and compare the global vibration suppression

performance of the RHVA and groundhook damper on the entire beam structure. Spatial average motions were calculated and used for plotting of its frequency spectrum.

5.4.1 Simulation Details on RHVA-Groundhook Damper Comparison Tests

In the numerical tests, a cantilever beam was used as a tested structure. White noise was used as a disturbance and separately applied to a single point and a portion of the beam span. The point disturbance was acted at a point $x_d = 0.2l$ and the distributed disturbance was applied on a portion of the beam span from its mounting position to point $x_d = 0.2l$. The respective schematic of separately applying a point disturbance and a distributed disturbance to a cantilever-beam-RHVA coupled system were shown in Figures 5-1 and 5-3. Figures 5-13 and 5-14 show the respective schematic of a cantilever beam-groundhook damper coupled system when a point disturbance and a distributed disturbance were separately applied to the beam structure.

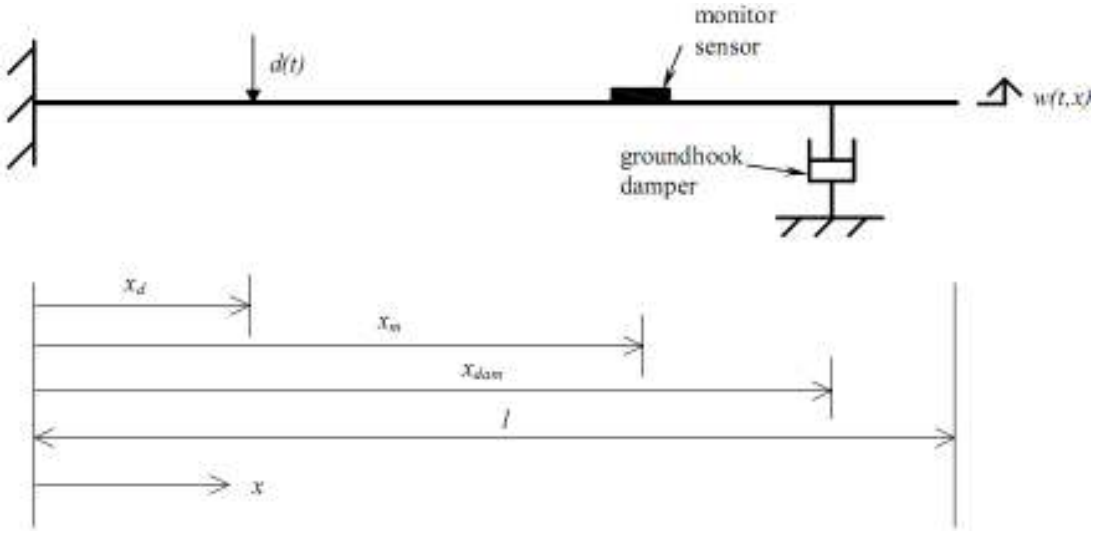

Figure 5-13 Point disturbance on a cantilever beam-groundhook damper system

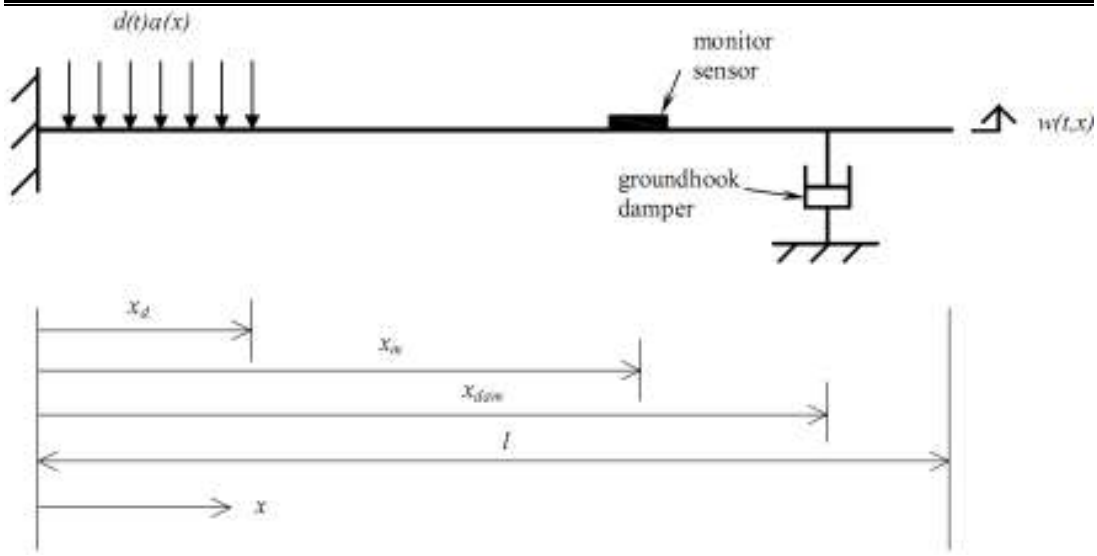

Figure 5-14 Distributed disturbance on a cantilever beam-groundhook damper system

In the figures, $\theta(t,x)$ and $\theta_a(t)$ denotes the angular displacements of the beam and the RHVA; $w(t,x)$ denotes the linear displacements of the beam; $d(t)$ denotes a point disturbance and $d(t)a(x)$ denotes a distributed disturbance in which $d(t)$ is a temporal function and $a(x)$ is a spatial function bounded everywhere except at a finite number of points (a possible example is $a(x)=\begin{cases}1 & 0<x<x_d\\ 0 & x_d<x<l\end{cases}$). The simulation details of the cantilever beam, RHVA and groundhook damper are shown in the following table.

	RHVA-Beam Coupled System	Groundhook Damper-Beam Coupled System
Beam length l	3 meter	
Beam width w	0.05 meter	
Beam thickness t	0.003 meter	
Beam density per length ρ	0.405 kg/m	
Young's modulus of Beam E	65×10^9 N/m^2	
Moment of inertia of cross section of beam I	1.125×10^{-4} m^4	

Beam mass	1.215 kg	
Modal damping of each mode ξ_i	0.005	
Truncated number of modes m	5	
Device coupling position	$x_a = l$	$x_{dam} = l$
Feedback/monitor sensor location	$x_p = l$	$x_m = l$
Inertial mass of HVA m_a	0.1215 kg	-
Second moment of inertia of the inertial mass J	0.0109 kgm^2	-
Effective stiffness of the HVA spring k	0.0301 Nm/rad	-
Passive absorption frequency	$\sqrt{\frac{k}{J}}$ =1.66 rad/s	-
Damping coefficient of the groundhook damper	-	0.4 Ns/m

Table 5-6 Simulation details on RHVA-groundhook damper comparison

In the simulation tests, the models were truncated to the first five modes and this is a reasonable approximation of the models. The eigen-function of the cantilever beam, which was used to construct the eigen-function-based state-space model, was presented in equation (5-16). The eigen-values of the first five modes are 1.875, 4.694, 7.854, 10.995 and 14.137. The beam characteristic parameters were on the basis of aluminum 6061 material and shown in the above table. The natural frequencies are 1.6600, 10.4032, 29.1292, 57.0816 and 94.3600 rad/s. The sampling frequency in the simulation test is 220 rad/s.

Referring to equation (3-56), the respective dynamic equation of the cantilever beam-groundhook damper coupled system, when applying a point disturbance to the cantilever beam at the point x_d=0.2l, is shown below:

$$\rho\ddot{w}(t,x) + EIw''''(t,x) = d(t)\delta(x-0.2l) + F_{dam}\delta(x-l), \qquad 0 < x < l, \tag{5-21}$$

Referring to equation (3-66), the respective dynamic equation of the cantilever beam-groundhook damper coupled system, when applying a distributed disturbance

to the cantilever beam from its mounting position to the point x_d=0.2l, is shown below:

$$\rho\ddot{w}(t,x) + EIw''''(t,x) = d(t)a(x) + F_{dam}\delta(x-l), \qquad 0 < x < l, \tag{5-22}$$

where $0 < x < l$, $\quad a(x) = \begin{cases} 1 & 0 < x < 0.2l \\ 0 & 0.2l < x < l \end{cases}$

For the cantilever beam-RHVA coupled system, its system dynamic equations can be referred to equations (5-18) and (5-20) for the point disturbance and distributed disturbance respectively.

The feedback sensor was collocated with the RHVA at the tip position of the cantilever beam. The passive absorption frequency of the RHVA was tuned to the first resonant frequency 1.66 rad/s. Parameter α, which was used to damp the roots, was set as 0.96. The damping coefficient of the groundhook damper was set as 0.4 Ns/m. In general, the vibration attenuation performance of a groundhook damper can be enhanced by increasing its damping coefficient. However, it is meaningless to use a very large damping coefficient to conduct the numerical tests and compare the results with the RHVA. This is because very large damping coefficient will significantly change the boundary condition of the cantilever beam from fixed-free to fixed-support condition. This study is to evaluate whether a RHVA can provide similar vibration attenuation performance as a groundhook damper. In the simulation tests, the damping coefficient of the groundhook damper was selected as 0.4 Ns/m. This value can provide similar percentage reductions on mean square motions and spatial average mean square motions as the RHVA when a point disturbance was applied at the point x_d=0.2l of the cantilever beam. It was used as the reference damping coefficient for the groundhook damper in all of the simulation tests. Eigen-function-based state-space models were constructed on the basis of the previous derived models with the toolbox “simulink” of the commercial software MatLAB. The constructed state-space models were then transformed to discrete-time-based models with MatLAB toolbox. This is to emulate the real

experimental situation since those measured experimental signals are in the discrete-time form.

5.4.2 Local Vibration Suppression Performance on a Cantilever Beam with Point Disturbance

This section is focused on the control performance of the RHVA and groundhook damper on the vibration suppression performance of translational and rotational vibration motions at the coupling point of the respective device. For the case of applying a point disturbance at point $x_d = 0.2l$ of a cantilever beam which was separately coupled with a RHVA and a groundhook damper at its end position $x=l$, Figures 5-15 and 5-16 show the respective PSD of $w(t,l)$ and $\theta(t,l)$ for the cases with and without controls of RHVA and groundhook damper.

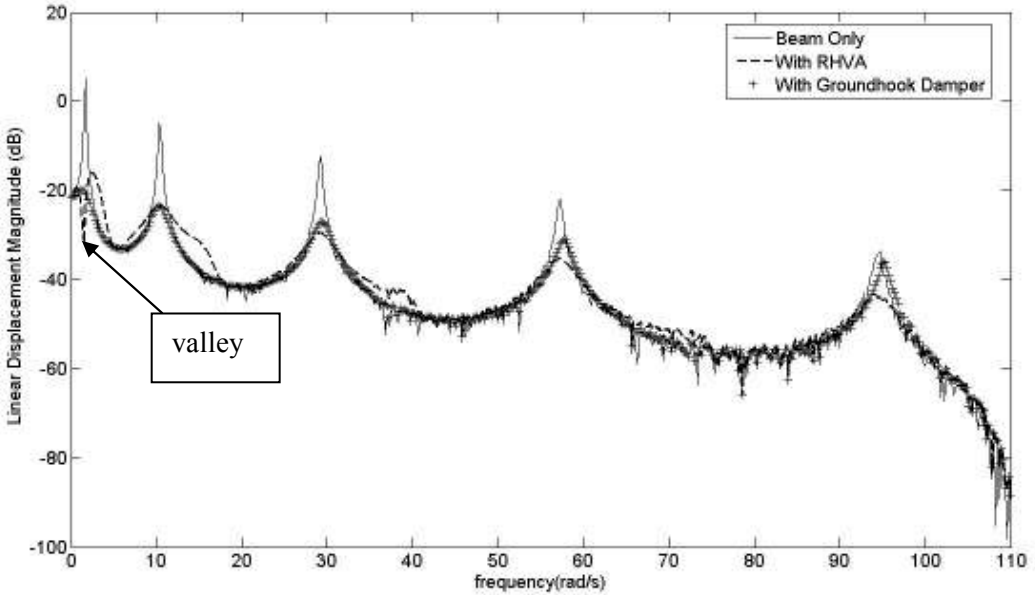

Figure 5-15 PSDs of *w(t,l)* with/without RHVA and groundhook damper (point disturbance at x_d=0.2*l*)

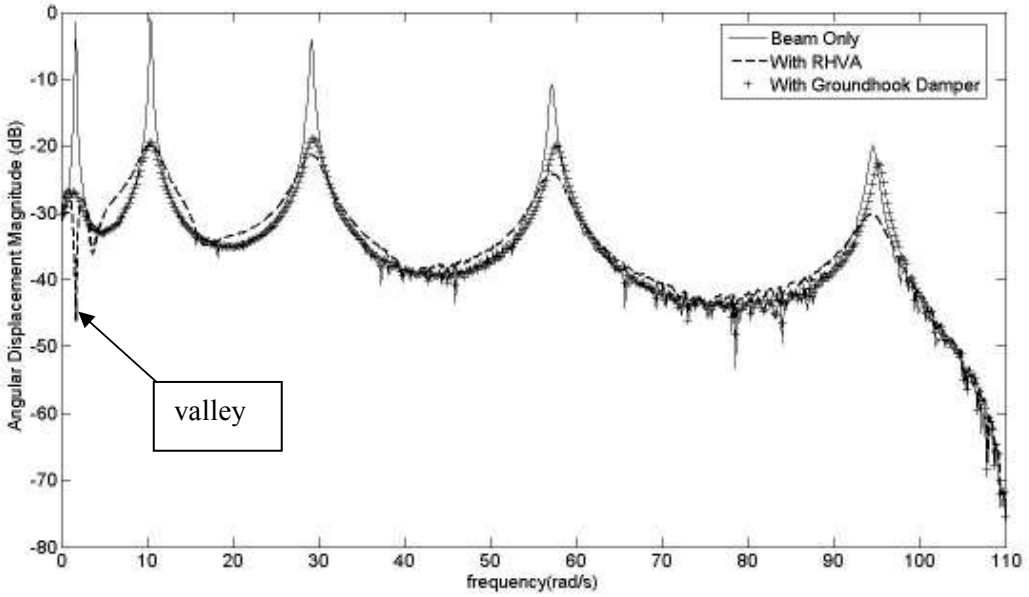

Figure 5-16 PSDs of $\theta(t,l)$ with/without RHVA and groundhook damper (point disturbance at x_d=0.2l)

In figures 5-15 and 5-16, the resonant peaks of all modes in the respective PSD of the translational and rotational motions can be damped down by the groundhook damper. This shows the groundhook damper can effectively dissipate the vibrating energy of the cantilever beam at its coupling point. For the RHVA, a valley appears at the first mode of the respective PSD of the translational and rotational motions. This valley was introduced by the RHVA when its passive absorption frequency was tuned to the first resonant frequency of the cantilever beam. The valley can remarkably reduce the translational and rotational vibration motions of the first resonant mode of the cantilever beam at the RHVA coupling point. On the other hand, the RHVA can also significantly damp down the resonant peaks of both translational and rotational motions of the cantilever beam in all modes. This is because the RHVA introduces active damping to the cantilever beam at the RHVA coupling point.

To quantify the vibration motions of the device coupling point, the translational and rotational mean square motions at the device coupling position, $\sigma_w^2(l)$ and $\sigma_\theta^2(l)$, were calculated on the basis of the simulation results for the RHVA and groundhook damper separately for the cases with and without control. The respective percentage

of reduction on the translational and rotational mean square motions, $LR_w(l)$ and $LR_\theta(l)$, was calculated separately for the RHVA and groundhook damper to evaluate their vibration attenuation performance at the local coupling point. The calculated results show that RHVA can suppress 92.7% of the translational mean square motion and 87.5% of the rotational mean square motion while groundhook damper can suppress 95.6% of translational mean square motion and 87.1% of rotational mean square motion. This shows that the RHVA has similar mitigation ability to the groundhook damper on both translational and rotational vibration motions at its local coupling point. To obtain better understanding on how the disturbance location affects the control performance of the groundhook damper and RHVA, the point disturbance was acted at different location of x_d including 0.2l, 0.4l, 0.6l, 0.8l and l. The respective percentage of reduction on translation and rotational mean square motions for groundhook damper and RHVA is shown in the following table.

Disturbance location x_d	RHVA		Groundhook Damper	
	$LR_w(l)$(%)	$LR_\theta(l)$(%)	$LR_w(l)$(%)	$LR_\theta(l)$(%)
0.2l	92.7	87.5	95.6	87.1
0.4l	94.3	92.5	96.8	93.8
0.6l	95.3	95.7	97.1	96.1
0.8l	96.1	96.9	97.1	96.9
l	96.5	96.0	97.1	96.2

Table 5-7 Local percentage reductions by RHVA and groundhook damper (point disturbance at different locations)

Table 5-7 shows that the respective percentage reduction on the local translational and rotational mean square motions, $LR_w(l)$ and $LR_\theta(l)$, for RHVA and groundhook damper when a point disturbance was applied at different locations of a cantilever beam. The readings show that the RHVA has similar alleviation ability to the groundhook damper on the local translational and rotational vibration motions

when a point disturbance was applied in different locations. The maximum performance difference between the RHVA and groundhook damper is about 3%.

5.4.3 Global Vibration Suppression Performance on a Cantilever Beam with Point Disturbance

This section is focused on the control performance of the RHVA and groundhook damper on the vibration suppression performance of the average translational and rotational vibration motions of the entire cantilever beam. This suppression performance is called global vibration suppression performance since it considers the motions of entire beam instead of the coupling point of device. For the case of applying a point disturbance at point $x_d = 0.2l$ of a cantilever beam which was separately coupled with a RHVA and a groundhook damper at its end position, Figures 5-17 and 5-18 show the respective PSD of translational spatial average motion $\sigma_w(\omega_k)$ and rotational spatial average motion $\sigma_\theta(\omega_k)$ within a frequency band for the cases with and without controls of RHVA and groundhook damper.

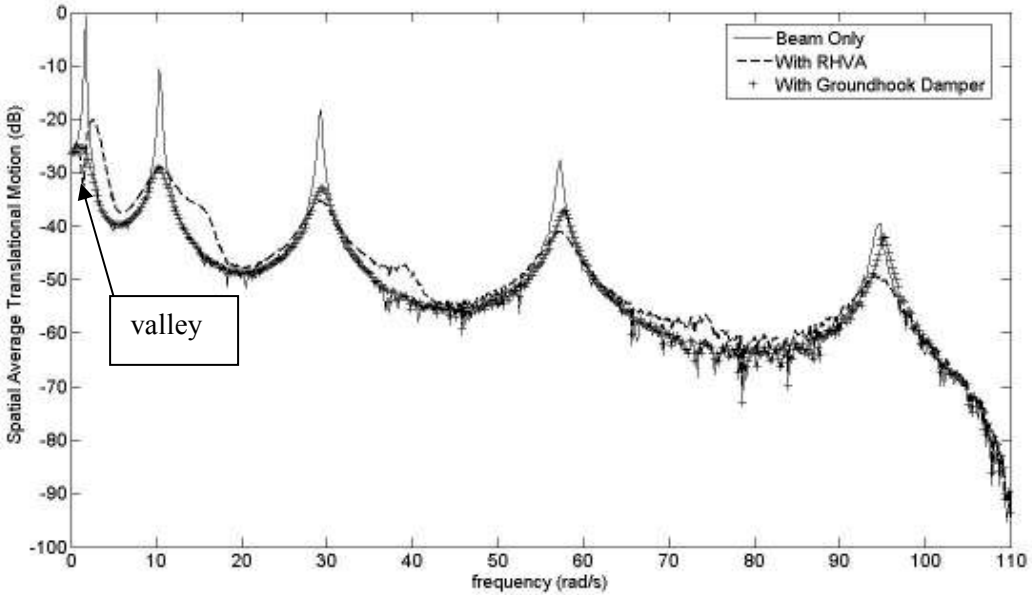

Figure 5-17 PSDs of translational spatial average motion with/without RHVA and groundhook damper (point disturbance at x_d=0.2l)

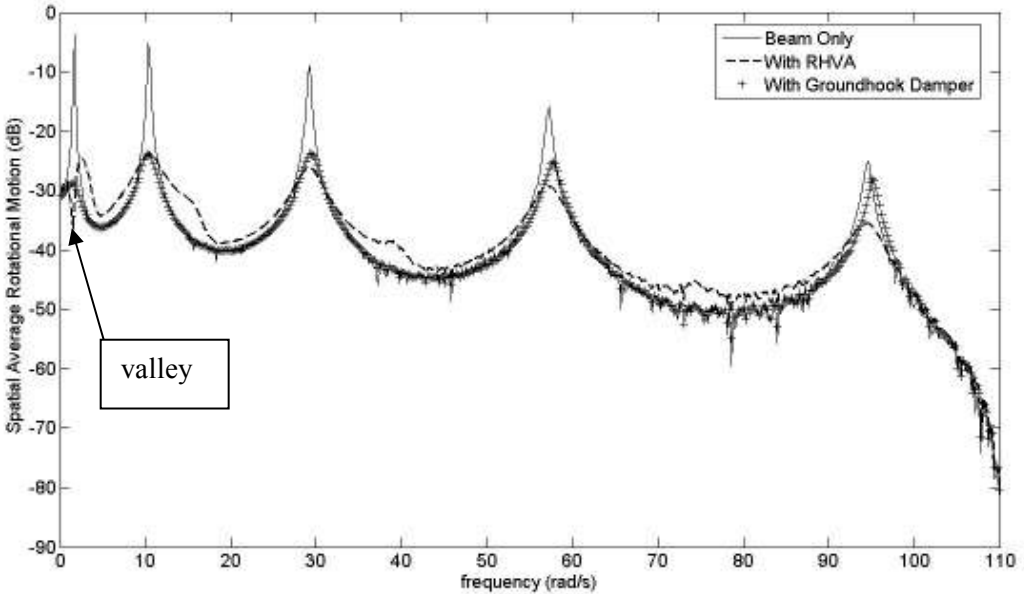

Figure 5-18 PSDs of rotational spatial average motion with/without RHVA and groundhook damper (point disturbance at x_d=0.2l)

In figures 5-17 and 5-18, the resonant peaks of all modes in the respective PSD of the translational and rotational spatial average motions can be damped down by the groundhook damper. This indicates the groundhook damper can effectively dissipate the vibrating energy of the entire cantilever beam. For the RHVA, a valley appears at the first mode of the respective frequency spectrum of the translational and rotational spatial average motions. This valley was introduced by the RHVA when its passive absorption frequency was tuned to the first resonant frequency of the cantilever beam. The valley can notably reduce the translational and rotational vibration motions of the first resonant mode of the cantilever beam at all the measuring check points. On the other hand, the RHVA can also significantly damp down the resonant peaks of both translational and rotational spatial average motions of the cantilever beam in all modes. This is because the RHVA introduces active damping to the cantilever beam at all the measuring check points.

To quantify the average vibration motions of the entire cantilever beam, the translational and rotational spatial average mean square motions of the entire cantilever beam, $\sigma_w^2(Global)$ and $\sigma_\theta^2(Global)$, were calculated on the basis of the translational and rotational spatial average motions for the RHVA and groundhook damper separately for the cases with and without control. The respective percentage

of reduction on the translational and rotational spatial average mean square motions, GR_w and GR_θ, was calculated separately for the RHVA and groundhook damper to evaluate their global vibration suppression performance on the entire cantilever beam. The calculated results show that RHVA can suppress 90.3% of the translational spatial average mean square motion and 86.9% of the rotational spatial average mean square motion while THVA can suppress 95.5% of translational spatial average mean square motion and 88.9% of rotational spatial average mean square motion. This indicates that the groundhook damper has better mitigation ability than the RHVA on the average translational vibration motion but similar suppression ability on the average rotational vibration motion of the entire cantilever beam. To obtain better understanding on how the disturbance location affects the control performance of the RHVA and groundhook damper, the point disturbance was acted at different location of x_d including $0.2l$, $0.4l$, $0.6l$, $0.8l$ and l. The respective percentage of reduction on translation and rotational spatial average mean square motions for RHVA and groundhook damper is shown in the following table.

Disturbance location x_d	RHVA		Groundhook Damper	
	GR_w(%)	GR_θ(%)	GR_w(%)	GR_θ(%)
$0.2l$	90.3	86.9	95.5	88.9
$0.4l$	92.2	91.5	96.7	94.7
$0.6l$	93.8	94.3	97.0	96.5
$0.8l$	95.1	95.7	97.1	97.0
l	96.0	95.8	97.1	96.6

Table 5-8 Global percentage reductions by RHVA and groundhook damper (point disturbance at different locations)

Table 5-8 shows that the respective percentage reduction on the translational and rotational spatial average mean square motions, GR_w and GR_θ, for RHVA and groundhook damper when a point disturbance was applied at different locations of a cantilever beam. The readings show that the groundhook damper has better suppression ability than the RHVA on the average translational vibration motion but

similar attenuation ability on the average rotational vibration motion of the entire cantilever beam when a point disturbance was applied in different locations. Although groundhook damper is superior to the RHVA on its global attenuation performance, the maximum performance difference between the RHVA and the groundhook damper is about 5%. In the simulation tests, the RHVA generally can alleviate more than 87% of the average vibration motions of the entire cantilever beam when a point disturbance was applied to the beam structure. This signifies that the RHVA can provide an excellent global suppression performance to the entire cantilever beam for global structural vibration control.

5.4.4 Local Vibration Suppression Performance on a Cantilever Beam with Distributed Disturbance

This section is focused on the control performance of the RHVA and groundhook damper on the local vibration suppression performance when a distributed disturbance was applied at a portion of the cantilever beam span from its mounting position to point $x_d = 0.2l$. Figures 5-19 and 5-20 show PSDs of $w(t,l)$ and $\theta(t,l)$ for the cases with and without controls of RHVA and groundhook damper.

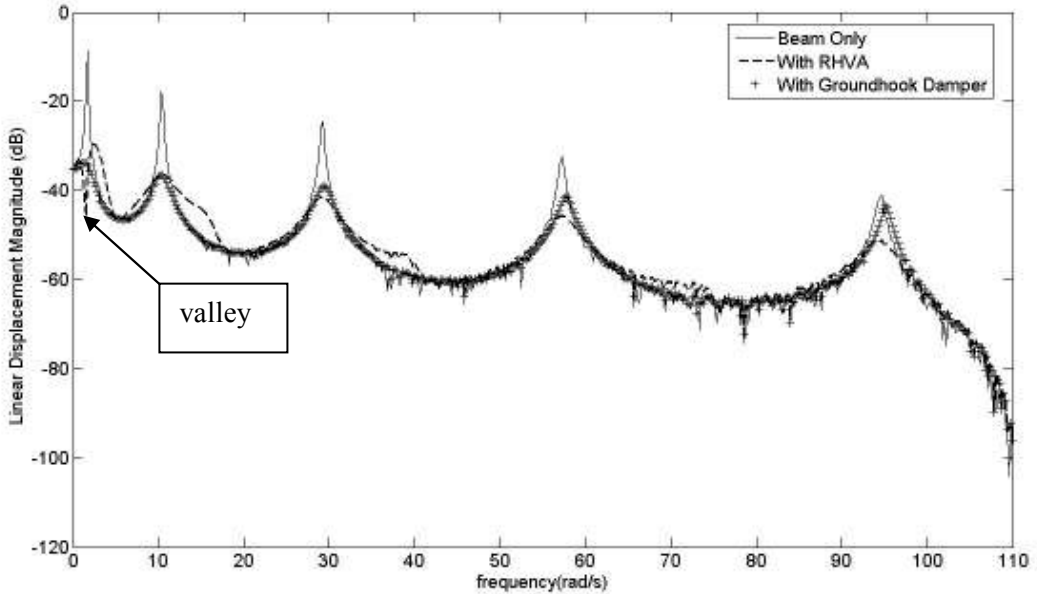

Figure 5-19 PSDs of *w(t,l)* with/without RHVA and groundhook damper (distributed disturbance from x=0 to x_d=0.2l)

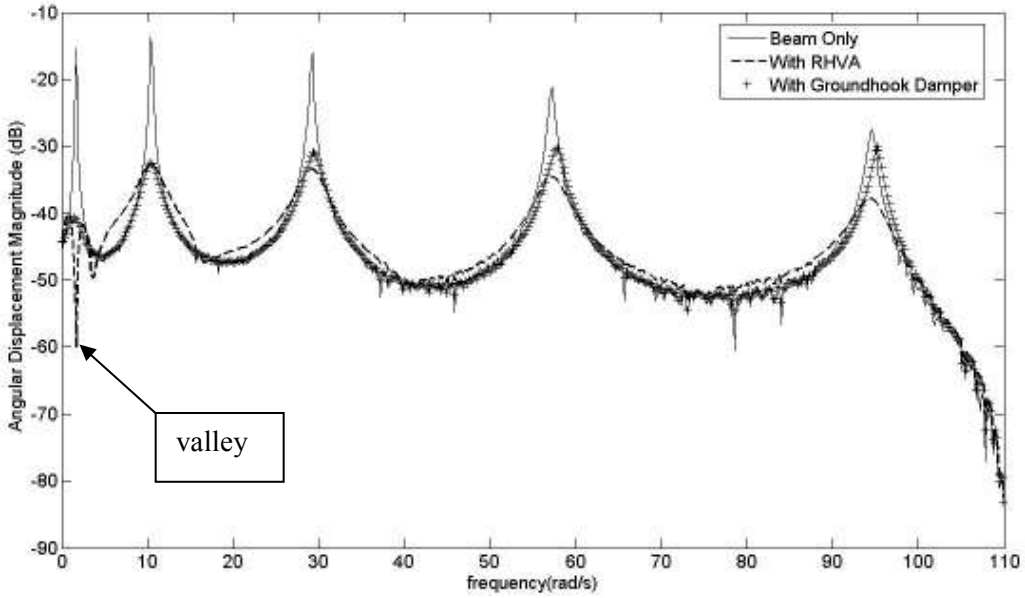

Figure 5-20 PSDs of $\theta(t,l)$ with/without RHVA and groundhook damper (distributed disturbance from x=0 to x_d=0.2l)

In figures 5-19 and 5-20, the resonant peaks of all modes in the respective PSD of the translational and rotational motions can be damped down by the groundhook damper. This shows the groundhook damper can effectively dissipate the vibrating energy of the cantilever beam at its coupling point when a distributed disturbance was applied on the beam. For the RHVA, a valley appears at the first mode of the respective PSD of the translational and rotational motions. The valley can remarkably reduce the translational and rotational vibration motions of the first resonant mode of the cantilever beam at the RHVA coupling point. On the other hand, the RHVA can significantly damp down the resonant peaks of both translational and rotational motions of the cantilever beam in all modes since active damping was introduced by the RHVA.

The respective percentage of reduction on the translational and rotational mean square motions, $LR_w(l)$ and $LR_\theta(l)$, was calculated separately for the RHVA and groundhook damper to evaluate their vibration attenuation performance at the local coupling point. The calculated results show that RHVA can suppress 92.2% of the translational mean square motion and 85.4% of the rotational mean square motion while groundhook damper can suppress 95.0% of translational mean square motion

and 83.0% of rotational mean square motion. This shows that the RHVA has similar mitigation ability to the groundhook damper on both translational and rotational vibration motions at its local coupling point. To obtain better understanding on how the disturbance location affects the control performance of the groundhook damper and RHVA, the distributed disturbance was acted from the beam's mounting position to different location of x_d including $0.2l$, $0.4l$, $0.6l$, $0.8l$ and l. The respective percentage of reduction on translation and rotational mean square motions for groundhook damper and RHVA is shown in the following table.

Disturbance boundary from x=0 to x_d	RHVA		Groundhook Damper	
	$LR_w(l)$(%)	$LR_\theta(l)$(%)	$LR_w(l)$(%)	$LR_\theta(l)$(%)
$x_d = 0.2l$	92.2	85.4	95.0	83.0
$x_d = 0.4l$	93.5	90.3	96.3	91.5
$x_d = 0.6l$	94.5	93.3	96.8	94.6
$x_d = 0.8l$	95.3	95.5	97.0	96.1
$x_d = l$	95.9	96.8	97.1	96.9

Table 5-9 Local percentage reductions by RHVA and groundhook damper (distributed disturbance at different locations)

Table 5-9 shows that the respective percentage reduction on the local translational and rotational mean square motions, $LR_w(l)$ and $LR_\theta(l)$, for RHVA and groundhook damper when a point disturbance was applied at different locations of a cantilever beam. The readings show that the RHVA has similar alleviation ability to the groundhook damper on the local translational and rotational vibration motions when a distributed disturbance was applied in different locations of the cantilever beam. The maximum performance difference between the RHVA and groundhook damper is about 3%.

5.4.5 Global Vibration Suppression Performance on a Cantilever Beam with Distributed Disturbance

This section is focused on the control performance of the RHVA and groundhook damper on the global vibration suppression performance of the entire cantilever beam when a distributed disturbance was applied at a portion of the cantilever beam span from its mounting position to point $x_d = 0.2l$. Figures 5-21 and 5-22 show PSDs of translational spatial average motion $\sigma_w(\omega_k)$ and rotational spatial average motion $\sigma_\theta(\omega_k)$ within a frequency band for the cases with and without controls of RHVA and groundhook damper.

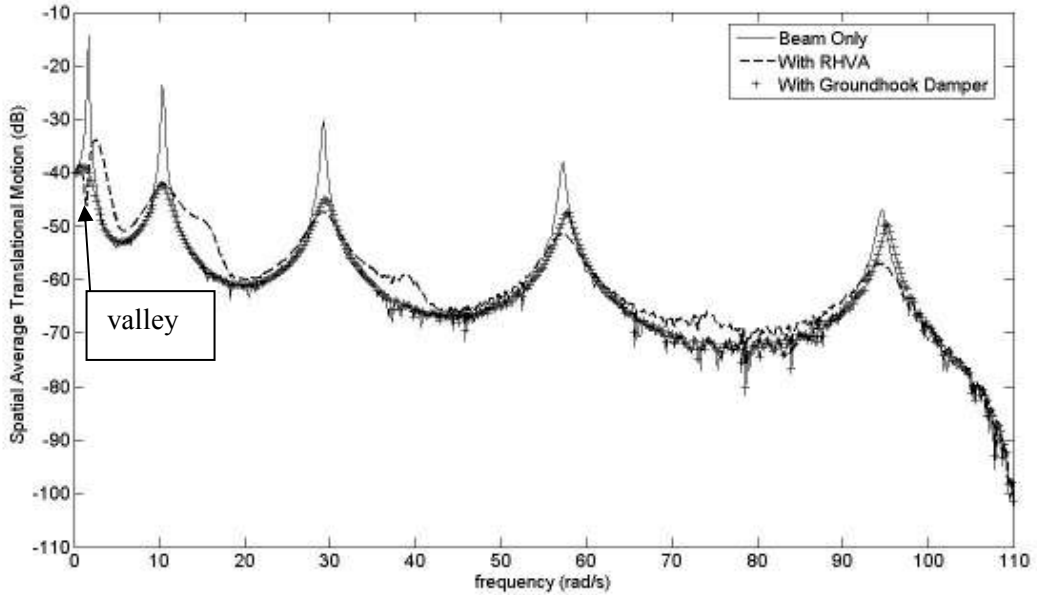

Figure 5-21 PSDs of translational spatial average motion with/without RHVA and groundhook damper (distributed disturbance from x=0 to x_d=0.2l)

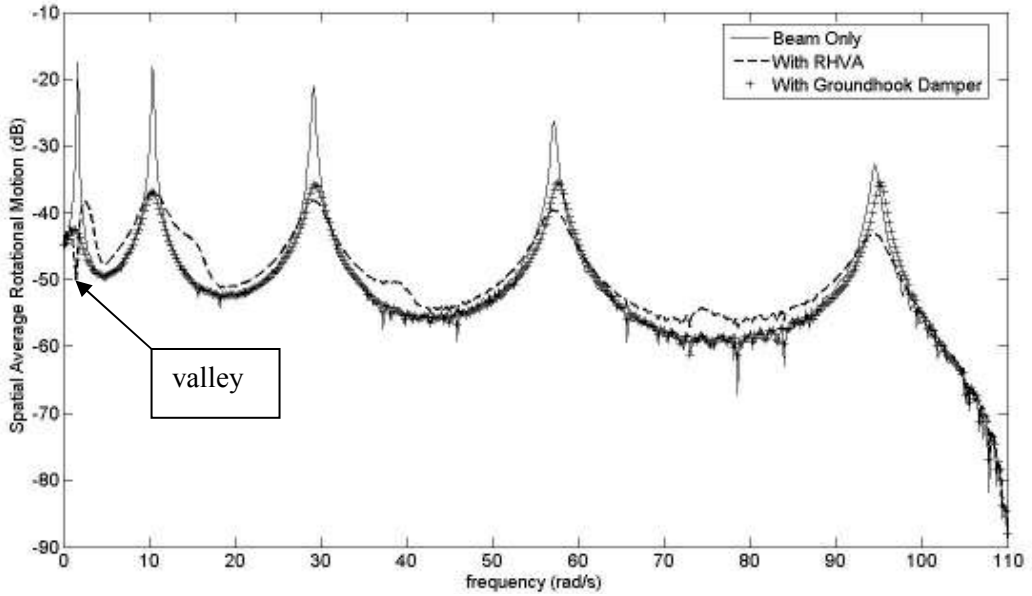

Figure 5-22 PSDs of rotational spatial average motion with/without RHVA and groundhook damper (distributed disturbance from x=0 to x_d=0.2l)

In figures 5-21 and 5-22, the resonant peaks of all modes in PSDs of the translational and rotational spatial average motions can be damped down by the groundhook damper. This indicates the groundhook damper can effectively dissipate the vibrating energy of the entire cantilever beam when a distributed disturbance was applied on the beam structure. For the RHVA, a valley appears at the first mode of the respective frequency spectrum of the translational and rotational spatial average motions. The valley can notably reduce the translational and rotational vibration motions of the first resonant mode of the cantilever beam at all the measuring check points. On the other hand, the RHVA can also effectively damp down the resonant peaks of both translational and rotational spatial average motions of the cantilever beam in all modes since active damping was introduced to the cantilever beam at all the measuring check points.

The respective percentage of reduction on the translational and rotational spatial average mean square motions, GR_w and GR_θ, was calculated separately for the RHVA and groundhook damper to evaluate their global vibration suppression performance on the entire cantilever beam. The calculated results show that RHVA can suppress 89.8% of the translational spatial average mean square motion and

85.1% of the rotational spatial average mean square motion while damper can suppress 94.9% of translational spatial average mean square motion and 85.2% of rotational spatial average mean square motion. This indicates that the groundhook damper has better mitigation ability than the RHVA on the average translational vibration motion but similar suppression ability on the average rotational vibration motion of the entire cantilever beam. To obtain better understanding on how the disturbance location affects the control performance of the RHVA and groundhook damper, the distributed disturbance was acted from the beam's mounting position to different location of x_d including $0.2l$, $0.4l$, $0.6l$, $0.8l$ and l. The respective percentage of reduction on translation and rotational spatial average mean square motions for RHVA and groundhook damper is shown in the following table.

Disturbance boundary from x=0 to x_d	RHVA		Groundhook Damper	
	GR_w(%)	GR_θ(%)	GR_w(%)	GR_θ(%)
$x_d = 0.2l$	89.8	85.1	94.9	85.2
$x_d = 0.4l$	91.2	89.5	96.2	92.7
$x_d = 0.6l$	92.6	92.2	96.8	95.3
$x_d = 0.8l$	93.8	94.1	97.0	96.5
$x_d = l$	94.8	95.4	97.1	97.0

Table 5-10 Global percentage reductions by RHVA and groundhook damper (distributed disturbance at different locations)

Table 5-10 shows that the respective percentage reduction on the translational and rotational spatial average mean square motions, GR_w and GR_θ, for RHVA and groundhook damper when a distributed disturbance was applied at different locations of a cantilever beam. The readings show that the groundhook damper has better suppression ability than the RHVA on the average translational vibration motion but similar attenuation ability on the average rotational vibration motion of the entire cantilever beam when a distributed disturbance was applied in different locations. Although groundhook damper is superior to the RHVA on its global attenuation performance the maximum performance difference between the RHVA

and the groundhook damper is about 5%. In the simulation tests, the RHVA generally can suppress more than 85% of the average vibration motions of the entire cantilever beam when a distributed disturbance was applied to the beam structure. This indicates that the RHVA can provide an excellent global suppression performance to the entire cantilever beam for global structural vibration control.

5.4.6 Conclusion on RHVA-Groundhook Damper Comparison Tests

The above figures and tables show that groundhook damper is an effective device to suppress structural vibration control at the local coupling point and the entire beam structure. It can dissipate the vibrating energy of the vibrating cantilever beam at the local coupling point and the measuring check points.

For the RHVA, a valley, which is introduced by its passive absorption frequency, can be applied to reduce vibration of the entire cantilever beam at a pre-tuned resonant mode. Unlike the groundhook damper, RHVA can provide flexibility to the user to reduce the vibration of certain dominant resonant frequency. RHVA can also introduce active damping to the entire cantilever beam to damp down the resonant peaks of the remaining modes.

From the calculated indices, the groundhook damper can suppress at least 83% of the mean square motions and 85% of the spatial average mean square motions while the RHVA can at least suppress 85% of mean square motions and 85% of spatial average mean square motions. Those values will change when disturbance is acting at different locations of the cantilever beam with different form. In general, groundhook damper has similar local attenuation performance but better global suppression performance than the RHVA. Although groundhook damper is superior to the RHVA, the maximum performance difference between them is about 5%. This signifies that RHVA still can provide an excellent alleviation performance to the vibrating cantilever beam for global structural vibration control. Comparing with the groundhook damper, RHVA does not need a mounting base for installation and can be directly mounted on a structure for vibration control. RHVA, therefore, provides

a better alternative choice for engineer to choose in case base mounting is not available for the groundhook damper.

5.5 Summary

In this chapter, indices of mean square motion, spatial average motion and spatial average mean square motion are introduced and used to quantify the local and global vibration motions of a cantilever beam. Percentage reductions on mean square motion and spatial average mean square motion are discussed and used to evaluate the local and global vibration suppression performance of the RHVA, THVA and groundhook damper. Simulation tests are conducted for cantilever beam-RHVA, cantilever beam-THVA and cantilever beam-groundhook damper, subject to a point and a distributed disturbance. Numerical results of the above systems are presented. The local and global vibration attenuation performance between RHVA and THVA and also between RHVA and groundhook damper are compared. Conclusions are drawn for each of the devices. The RHVA is found to be a better alternative to THVA and groundhook damper.

6 EXPERIMENTAL ARRANGEMENT AND RESULTS

In this chapter, the apparatus used in the experiment, are described in the section of experimental configuration. The experimental methodology discusses on how to do the experiment. In the section of results and discussion, experimental results are presented. Simulation test was conducted with real experimental parameters and its results are presented. Indices, including mean square motion, spatial average motion and spatial average mean square motion, are calculated separately with the experimental and simulation results. The calculated indices are finally used to verify the analytical model of the RHVA and the global structural vibration controller.

6.1 Experimental Configuration

A number of apparatus were used in the experiment and their application detail in the experiment will be discussed in this section.

6.1.1 Piezoelectric Sensor and Accelerometer

Piezoelectric sensor shown in Figure 6-1 and accelerometer shown in Figure 6-2 were used in the experiment to measure the angular and linear displacements of a cantilever beam. In the experiment, two piezoelectric film sensors were used and adhered to a cantilever beam. One of the piezoelectric sensors was used as the feedback sensor and collocated with the RHVA. It provided the angular displacement of the beam at the RHVA coupling point. This feedback signal was sent back to the control system for generation of control signals. Another piezoelectric sensor was used as a monitor sensor to measure the corresponding angular displacement of the cantilever beam at different measuring check points. An accelerometer was also used as a monitor sensor to measure the corresponding linear displacement of the cantilever beam at different measuring check points.

Figure 6-1 Piezoelectric film sensor

Figure 6-2 Accelerometer

6.1.2 Piezoelectric Actuator

Piezoelectric actuator was used to generate the active moment for the RHVA and apply random disturbance to the cantilever beam. In the experiment, a pair of piezoelectric actuators in plate shape was adhered to both sides of the connecting beam of the RHVA at its root position. Four pairs of piezoelectric actuators, shown in Figure 6-3, were adhered to both sides of the cantilever beam at its root position. The piezoelectric actuators were connected in opposite phase. When one piezoelectric plate extends, the other one contracts simultaneously. This combination makes the piezoelectric actuators generate active moment to the RHVA and random disturbance to the cantilever beam. The contraction and extension depend on the respective control signals.

Figure 6-3 Piezoelectric actuator pair

6.1.3 Sensor Amplifier

Charge amplifiers shown in Figure 6-4 were used to amplify the measuring signals for the piezoelectric film sensors and the accelerometer. In the experiment, piezoelectric sensor provided direct angular displacement measurement, so charge amplifier was used to amplify the measured signal. Unlike the piezoelectric sensor, accelerometer provided linear acceleration of the cantilever beam as the measuring signal, so charge amplifier was used to integrate the acceleration signal back to the linear displacement and amplified this converted signal.

Figure 6-4 Charge amplifier for sensor

6.1.4 Piezoelectric Actuator Amplifier

A voltage amplifier shown in Figure 6-5 was used to amplify the disturbance signals and control signals. The amplified signals were used to drive the pairs of piezoelectric actuator.

Figure 6-5 Charge amplifier for piezoelectric actuator

6.1.5 dSPACE Control System

A dSPACE controller board with model DS1104 was used as the control system. It was a PCI card and plugged into the motherboard of the computer. MatLAB code can be directly converted to C code and loaded to the memory of the DS1104 controller with the commercial software ControlDesk provided by dSPACE. This controller card equips with the analogue to digital (A/D) converter and digital to analogue (D/A) converter. Sensor signals were sampled by the card with a pre-tuned sampling frequency and converted to digital form by the A/D converter. The sampled signals were further processed and control signals were generated according to the written control algorithm. Control signals were then converted from digital form to analogue signal by the D/A converter. This analogue signals were finally amplified by the charge amplifier and used to control the piezoelectric actuator.

Figure 6-6 dSPACE controller card

6.1.6 Low-Pass Filter

An Alligator AAF-3PCI low-pass filter shown in 6-7 was used to filter high frequency signal to avoid aliasing and instability arising from the frequency signal of the higher residue modes. It was a PCI card and plugged in the motherboard of the computer. The low-pass filter equips with 8 channels and the sampling frequency of each channel can be tuned by a program provided by the Alligator company.

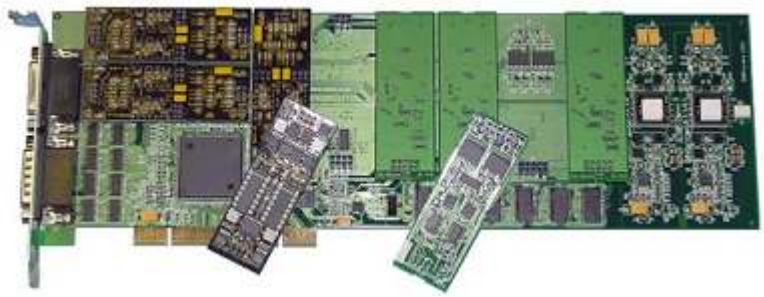

Figure 6-7 Low-pass filter

6.1.7 Rotational Hybrid Vibration Absorber

The rotational hybrid vibration absorber (RHVA) shown in Figure 6-8 was composed of a pair of acyclic plates and a stainless steel strip of dimension 0.02 m x 0.1 m x 0.003 m. The total mass of the RHVA is about 48.5 grams and was considered as a lumped mass. Its structure is the same as the one described in Figure 3-4. A pair of inertial mass was clamped onto the stainless steel strip by bolts and nuts and can be slid along the strip vertically for tuning of the passive absorption frequency. A pair of piezoelectric actuators was adhered to both sides of the strip at its root position. The piezoelectric actuators were connected in opposite phase. They can generate active moment to the RHVA via self contraction and extension. One end of the RHVA was fixed on the tested cantilever beam by bolts and nuts.

Figure 6-8 Rotational hybrid vibration absorber

6.1.8 Cantilever Beam

A 0.3 m x 0.05 m x 0.003 m cantilever beam, shown in Figure 6-9, was fabricated with stainless steel 304 for structural vibration control. Its angular and linear displacements were measured by the piezoelectric sensor and accelerometer. It was mounted on a pneumatic isolation table to isolate external vibration.

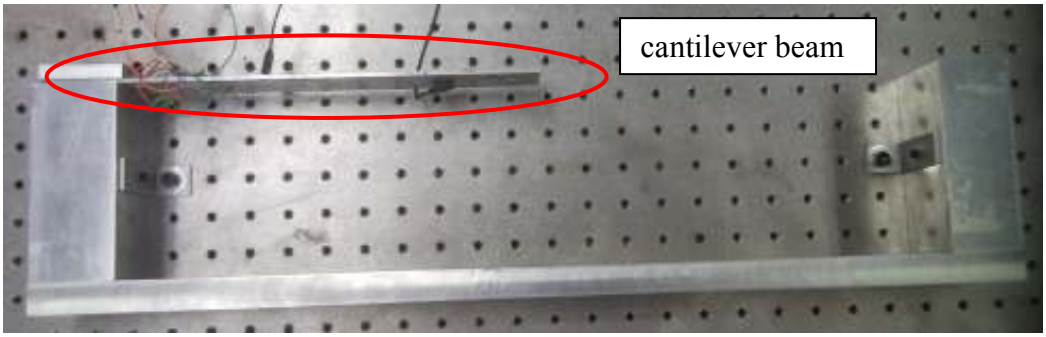

Figure 6-9 Cantilever Beam

6.2 Experimental Methodology

This section will discuss on the experimental details including the whole set-up of the test rig, tuning method of the RHVA, procedure of processing off-line system identification, controller calculation, and vibration measurement of the cantilever beam and analysis of the experimental data.

6.2.1 Test Rig

Figure 6-10 shows the schematic of the experimental setup for testing the control performance of the RHVA. Figure 6-11(a) shows the real experimental setup. Figure 6-11(b) shows the illustration of the experimental setup. In the experiment, a cantilever beam was mounted on an isolation table. White noise was used to generate random disturbance at a point of the cantilever beam by piezoelectric actuator pairs. The piezoelectric actuator pairs were adhered to the sides of the beam at the position of 0.05 meter from its mounting position. RHVA was coupled at the tip position of the cantilever beam. A pair of piezoelectric actuators was adhered to the sides of the stainless steel strip of the RHVA to provide active moment. Feedback piezoelectric sensor was adhered to the cantilever beam and collocated with the RHVA. Accelerometer and another piezoelectric sensor were used as the monitor sensors to measure the respective linear and angular vibration amplitudes of the cantilever beam at five points. These five points were separated by equal interval. The captured data were stored in the MAT file and further analyzed by the MatLAB software. Other apparatus including charge amplifiers, low-pass filter and the dSPACE controller were connected according to the illustration of the experimental set-up.

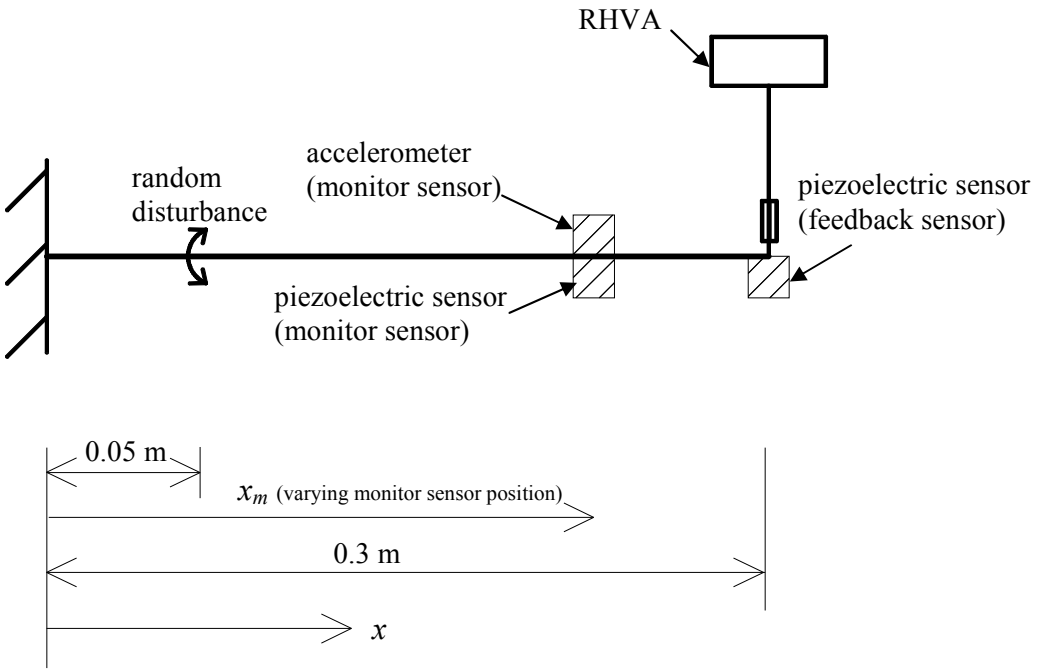

Figure 6-10 Experimental setup for testing the RHVA

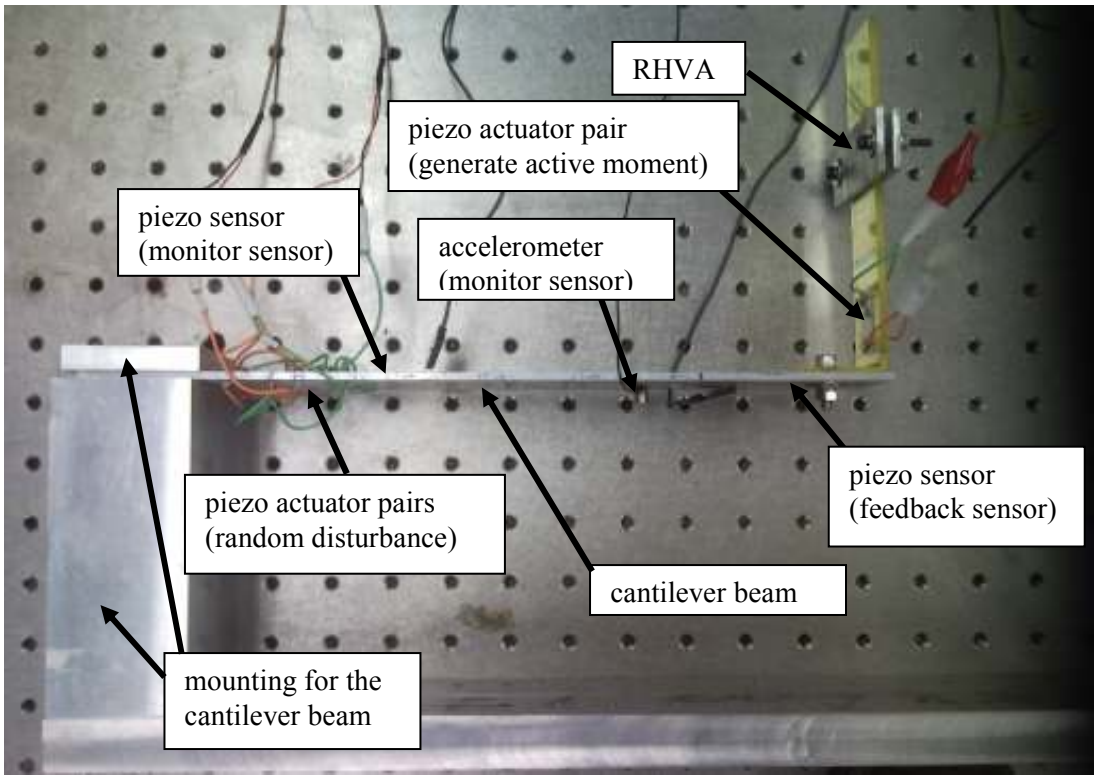

Figure 6-11(a) Real experimental setup

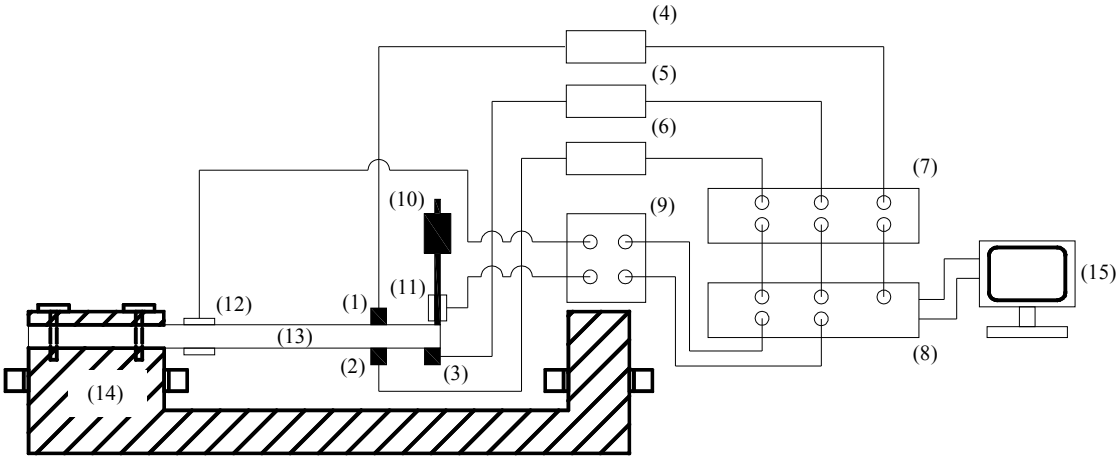

(1) Brüel & Kjær charge accelerometer Type 4374 used as monitor sensor for linear displacement measurement

(2) Shielded piezo film sensor SDT1-028K used as monitor sensor for angular displacement measurement

(3) Shielded piezo film sensor SDT1-028K used as feedback sensor for angular displacement measurement

(4) Brüel & Kjær charge amplifier Type 2635

(5) Brüel & Kjær charge amplifier Type 2635

(6) Brüel & Kjær charge amplifier Type 2635

(7) Alligator AAF-3PCI low-pass filter

(8) dSPACE PCI controller card Model DS1104 plugged into a computer

(9) Cedrat charge amplifier Model LC/LA75A

(10) Rotational hybrid vibration absorber (RHVA)

(11) Piezoelectric actuator pair used to generate active moment for the RHVA

(12) Piezoelectric actuator pairs used to generate random disturbance for the cantilever beam

(13) 0.3 m x 0.05 m x 0.003 m stainless steel 304 cantilever beam

(14) Mounting for the cantilever beam

(15) Monitor

Figure 6-11(b) Illustration of the experimental setup

6.2.2 Filtering of Higher Frequency Signals

In the experiment, only the first three resonant modes of the cantilever beam were focused. This is because the first three modes typically are the dominant modes of a cantilever beam and truncation can minimize the demand on the processing speed of the controller. The three resonant frequencies of the tested cantilever beam are 164 rad/s (26Hz), 1002 rad/s (159Hz) and 2100rad/s (334Hz). To achieve the truncation in real practice, higher frequency signals were filtered by the low-pass filter. According to the sampling theorem, the sampling frequency should be twice the highest frequency of interest. In the experiment, the highest frequency of interest was set as 3770 rad/s (600Hz), therefore, the sampling frequency was set as 7540 rad/s (1200 Hz) and frequency signals higher than the highest frequency of interest were filtered out by the low-pass filter. Apart from the truncation, the low-pass filter can enhance the system stability from higher residue modes. In general, feedback signal used for control contains signals from the truncated number of modes and the higher residue modes, but the controller only makes effects to the truncated number of modes and neglects the residue number of modes. The instability of the closed-loop control system, therefore, arises from the un-processed residue signals. With the help of the low-pass filter, signals with the higher residue modes can be filtered out and avoid entering the closed-loop control system. Instability problem of the closed-loop control system, therefore, can be prevented.

6.2.3 Tuning of RHVA

As described in the section 4.1, passive parameters of the RHVA can introduce an absorption frequency to the closed-loop control system. Therefore, passive absorption frequency of the RHVA was tuned to the first resonant mode of the cantilever beam before operating the control process of the experiment. The tuning method was very convenient by moving the inertial mass of the RHVA along the stainless steel strip vertically. Once finishing the tuning process, the passive absorption frequency of the RHVA was checked with the following steps. A random

disturbance was applied to the piezoelectric actuator pair, which was adhered to the sides of the stainless steel strip of the RHVA at its root position, from the DS1104 controller card by the software ControlDesk. The vibrating signals of the RHVA were measured by an accelerometer. The measured signals were sent back to the controller card and stored as MAT file by the ControlDesk. The collected signals were further analyzed by Fast Fourier Transformation (FFT) technique with MatLAB and the tuned passive absorption frequency of the RHVA can be checked.

6.2.4 Processing of Off-Line System Identification

After tuning of the passive absorption frequency of the RHVA, open-loop transfer function between the RHVA and the feedback sensor was identified with the off-line system identification for further controller design. The identification detail was discussed in the section 4.2. In the experiment, the tuned RHVA was coupled with the tested cantilever beam at its end position. A piezoelectric sensor was adhered to the beam's surface and collocated with the RHVA. This sensor was used as a feedback sensor to measure the angular displacement of the cantilever beam at the RHVA coupling position. A random disturbance was applied to the piezoelectric actuator pair, which was adhered to the roots of the RHVA, from the DS1104 controller card with the software ControlDesk, angular vibration signal measured by the feedback sensor was sent back to the controller card again. The disturbance and the feedback signals were collected in MAT file by ControlDesk. The collected signals were then used to identified the open-loop transfer function between the RHVA and the feedback sensor with a self-written MatLAB program on the basis of the equations (4-9) and (4-11). Feasibility function J was used to roughly evaluate the system order n. Figure 6-12 is a plot of feasibility function J against system order n of the real experimental data. Referring to Figure 6-12, the system order n was set as 20 in the experiment.

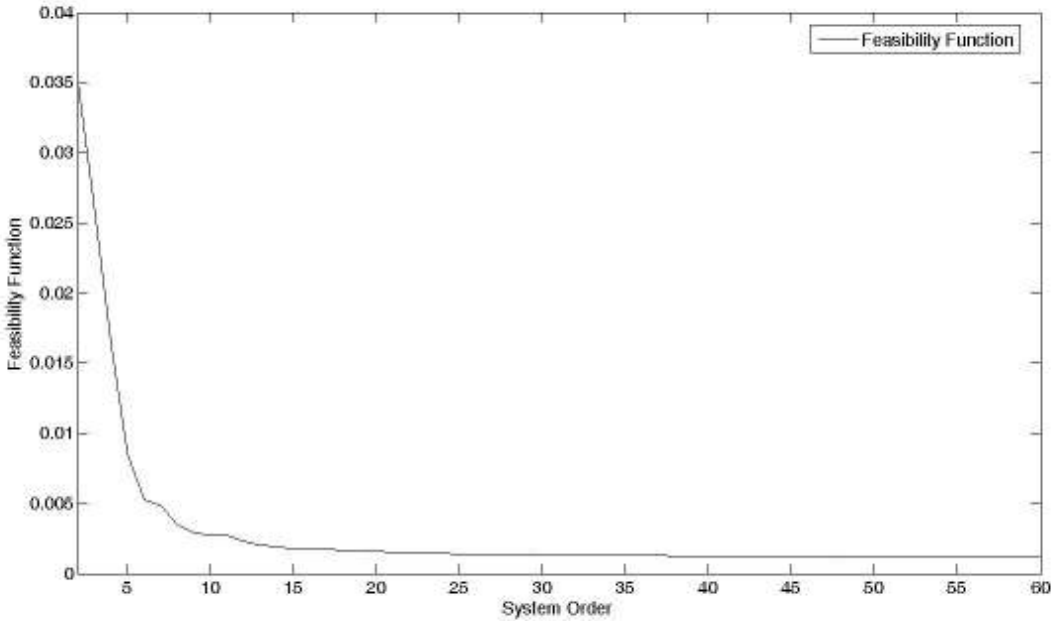

Figure 6-12 Feasibility function *J* against system order *n*

6.2.5 Set-Up of Global Structural Vibration Controller

After identifying the open-loop transfer function between the RHVA and the feedback sensor, the global structural vibration controller was then calculated by a self-written MatLAB program on the basis of the equation (4-6). In the experiment, the active damping factor α described in equations (4-4a) and (4-4b) was set as 0.96 and the prototype polynomial *T(z)* was established with the damped roots of the identified transfer function.

6.2.6 Vibration Measurements on the Cantilever Beam

In the experiment, a piezoelectric sensor, which was collocated with the RHVA, was used as a feedback sensor to measure the angular displacement of the cantilever beam at the RHVA coupling position. The feedback signals were sent back to the controller and used to generate the control signals. An accelerometer and a piezoelectric sensor were used as monitor sensors and measured the respective linear and angular displacements of the cantilever beam at five check-points separately.

6.2.7 Analysis of Experimental Data

The signals measured by the monitor sensors were stored in MAT files by the ControlDesk. The data was further analyzed by the FFT technique with the MatLAB. Mean square motions, spatial average motions and spatial average mean square motions were calculated from the analyzed data. The respective percentage of reduction on the local vibration motions and the average vibration motions of the entire cantilever beam were also calculated on the basis of the mean square motions and the spatial average mean square motions. Local and global vibration suppression performances of the RHVA were finally evaluated from the calculated percentages.

6.3 Results and Discussion

In this section, the experimental results will be presented. Simulation was conducted with the real experimental parameters including beam characteristics and RHVA properties to compare with the experimental results. Indices, including mean square motions, spatial average motions and spatial average mean square motions, were calculated separately with the experimental and simulation results. They will be used to evaluate the local and global vibration suppression performances of the RHVA. Comparison between the experimental and simulation results will also be discussed.

6.3.1 Local Vibration Suppression Performance

Local vibration suppression performance of the RHVA focuses on the attenuation of the vibration motions at the RHVA coupling point of the tested cantilever beam.
Figures 6-13 and 6-14 show power spectral densities (PSDs) of $w(t,l)$ and $\theta(t,l)$, for the cases with and without control of RHVA in the experimental test.

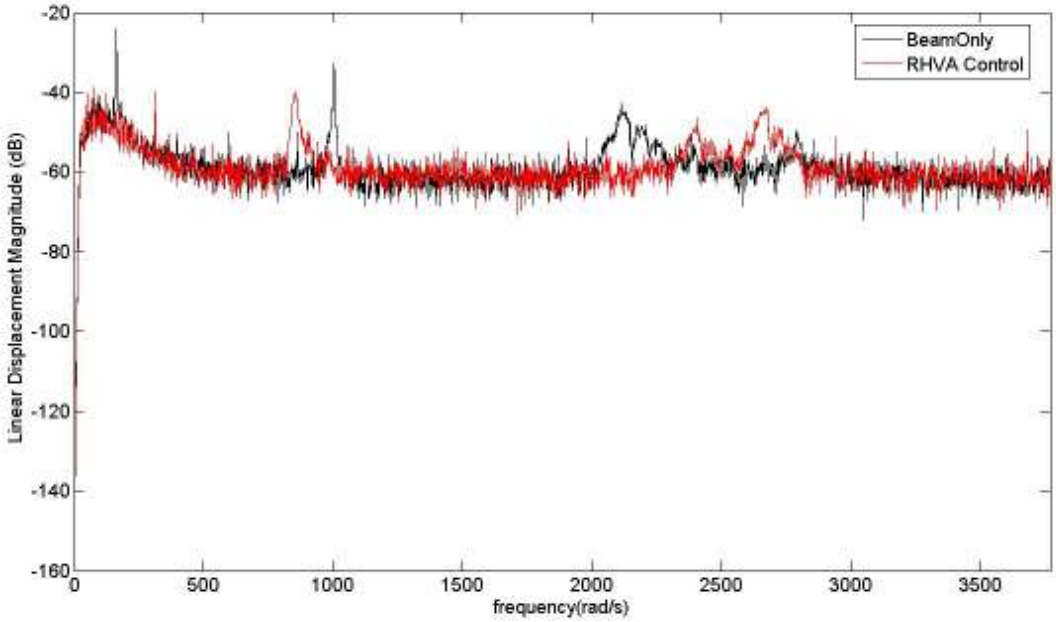

Figure 6-13 PSDs of *w(t,l)* with/without RHVA (experiment)

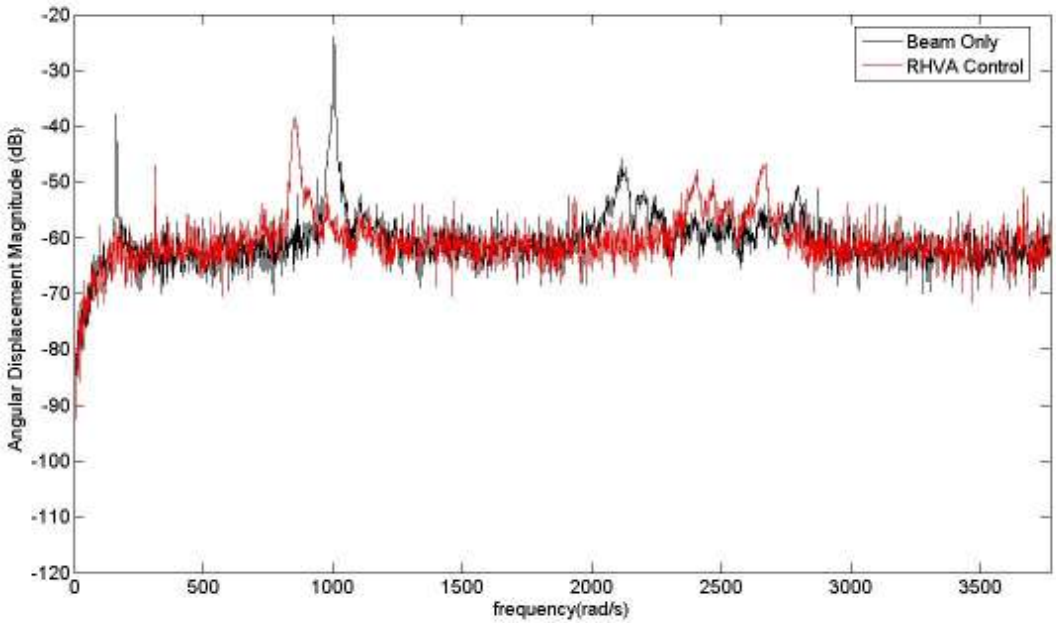

Figure 6-14 PSDs of *θ(t,l)* with/without RHVA (experiment)

Simulation was conducted with the experimental parameters and compare with the experimental results. The following table shows the beam characteristics and the RHVA detail.

	RHVA-Beam Coupled System
Beam length l	0.3 meter
Beam width w	0.05 meter
Beam thickness t	0.003 meter
Beam density per length ρ	1.17 kg/m
Young's modulus of Beam E	200×10^{9} N/m^2
Moment of inertia of cross section of beam I	1.125×10^{-4} m^4
Beam mass	0.35 kg
Modal damping of each mode ξ_i	0.002 (Calculated by half-power method)
Truncated number of modes m	3
Disturbance location	0.05 meter
RHVA coupling position x_a	0.3 meter
Feedback sensor location x_p	0.3 meter
Inertial mass of RHVA m_a	0.0485 kg
Second moment of inertia of the inertial mass J	0.000485 kgm^2
Effective stiffness of the RHVA spring	12.75 Nm/rad
Passive absorption frequency	$\sqrt{\frac{k}{J}}$ =162 rad/s

Table 6-1 Beam characteristics and RHVA details

Figures 6-15 and 6-16 show PSDs of $w(t,l)$ and $\theta(t,l)$ of the tested cantilever beam for the cases with and without control of RHVA in the simulation test.

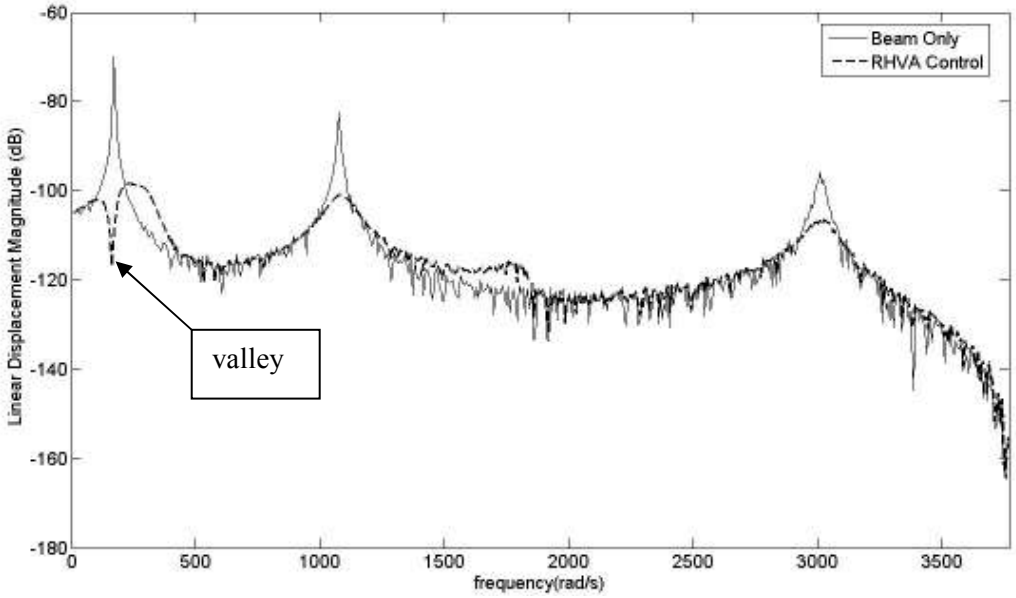

Figure 6-15 PSDs of *w(t,l)* with/without RHVA (simulation)

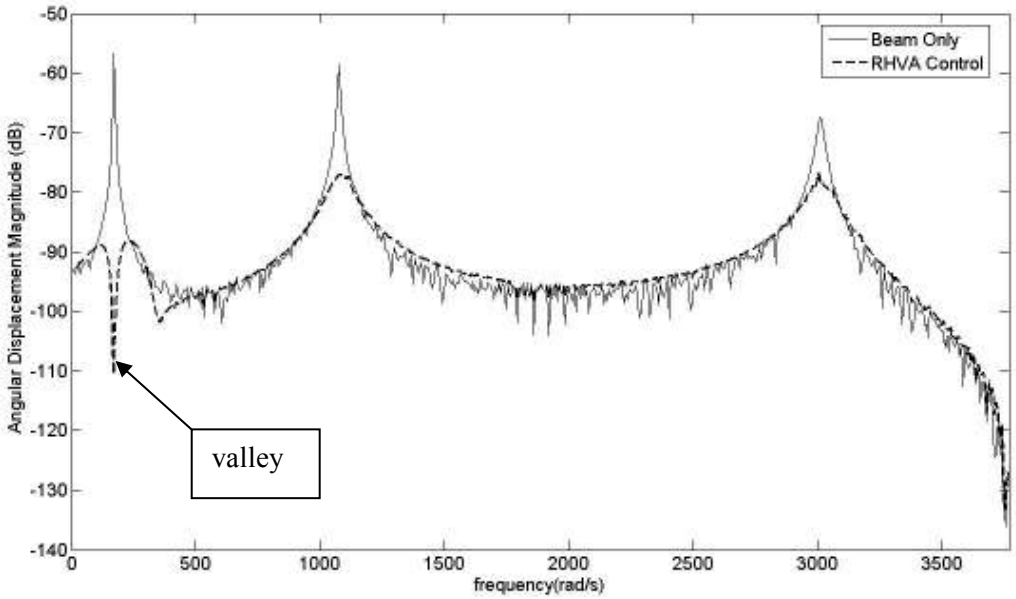

Figure 6-16 PSDs of *θ(t,l)* with/without RHVA (simulation)

From figures 6-13 to 6-16, the natural frequencies of the PSDs are different between the experimental and simulation results. This may cause by the material characteristics since the real beam characteristics are different from the theoretical values. In the figures, the resonant peaks of all the PSDs were effectively damped down in all modes. This indicates that the proposed controller can successfully introduce active damping to the cantilever beam at the RHVA coupling position. Now focusing on the first mode of the cantilever beam, PSDs shown in figure 6-15

and 6-16 have a valley at their respective first resonant mode but PSDs shown in Figures 6-13 and 6-14 do not have. In fact, this valley was introduced by the passive absorption frequency of the RHVA. The passive absorption frequency gives the RHVA flexibility to further suppress the vibration motions of the cantilever beam at certain resonant mode. The absence of the valleys indicates that the passive absorption frequency of the RHVA can effectively suppress the local vibration motions of the cantilever beam at the first resonant mode in the simulation but not effective in the experiment. Actually this may cause by the damping of the RHVA. In general, the depth of the valley decreases when damping of the RHVA increases. In the experiment, the RHVA was coupled with the cantilever beam by bolts and nuts and damping may exist in the fasteners of the RHVA. Although the valleys do not exist in Figures 6-13 and 6-14, the attenuation of the translational and rotational vibration motions in their respective first resonant mode still larger than the second and the third modes. This signifies that the passive absorption frequency of the RHVA was able to further alleviate the vibration motions of the first mode of the cantilever beam.

The respective percentage of reduction on the translational and rotational mean square motions, $LR_w(l)$ and $LR_\theta(l)$, was separately calculated for the experimental and simulation results. They are used to evaluate the vibration alleviation performance of the RHVA at the local coupling point. The results are shown in the following table.

	$LR_w(l)(\%)$	$LR_\theta(l)(\%)$
Experimental Results	64.6	67.3
Simulation Results	82.2	78.1

Table 6-2 Local control performance of RHVA (experiment and simulation)

Table 6-2 clearly demonstrates that the local vibration suppression performance of the RHVA is reasonably closed between the experiments and the simulation tests. The maximum performance difference between the experimental and simulation results is about 18%.

6.3.2 Global Vibration Suppression Performance

Global vibration suppression performance of the RHVA focuses on the attenuation of the average vibration motions of the entire cantilever beam. Figures 6-17 and 6-18 show PSDs of translational spatial average motion $\sigma_w(\omega_k)$ and rotational spatial average motion $\sigma_\theta(\omega_k)$ of the tested cantilever beam for the cases with and without control of RHVA in the experimental test.

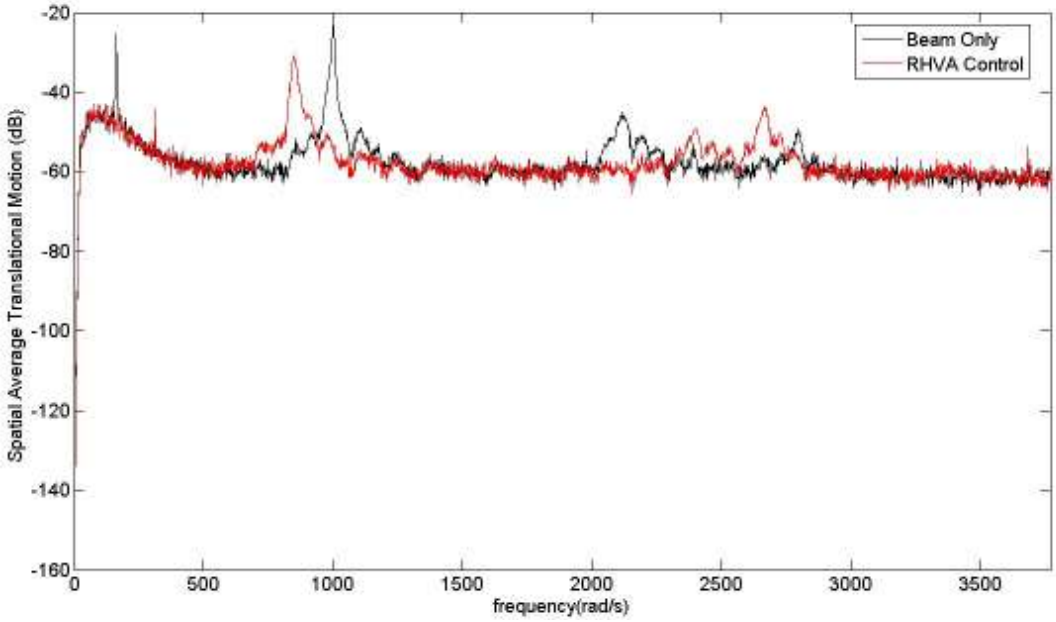

Figure 6-17 PSDs of translational spatial average motion with/without RHVA (experiment)

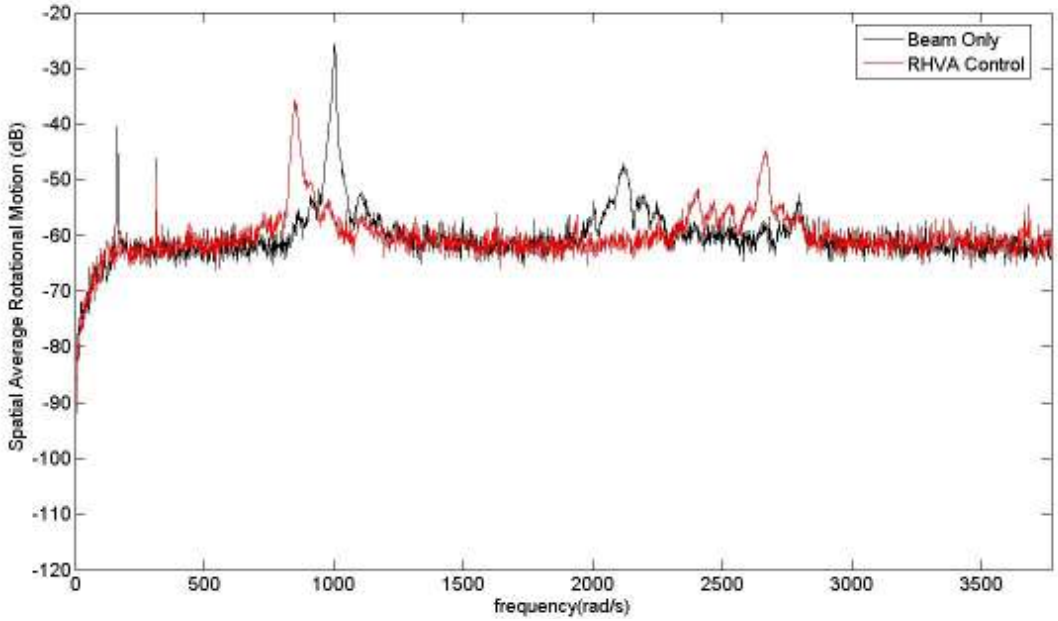

Figure 6-18 PSDs of rotational spatial average motion with/without RHVA (experiment)

Figures 6-19 and 6-20 show the respective PSDs of translational spatial average motion $\sigma_w(\omega_k)$ and rotational spatial average motion $\sigma_\theta(\omega_k)$ of the tested cantilever beam for the cases with and without control of RHVA in the simulation test.

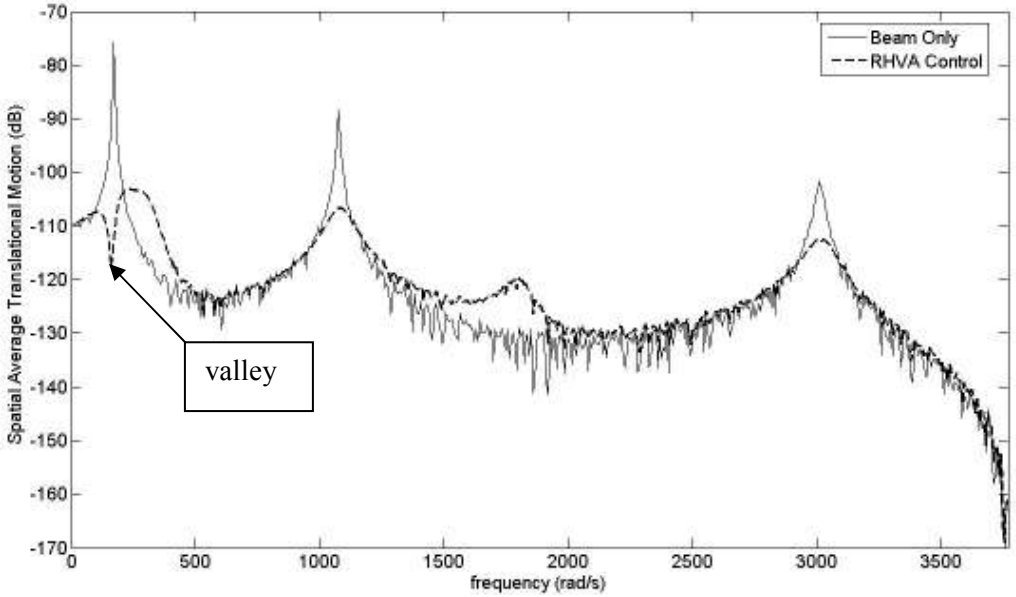

Figure 6-19 PSDs of translational spatial average motion with/without RHVA (simulation)

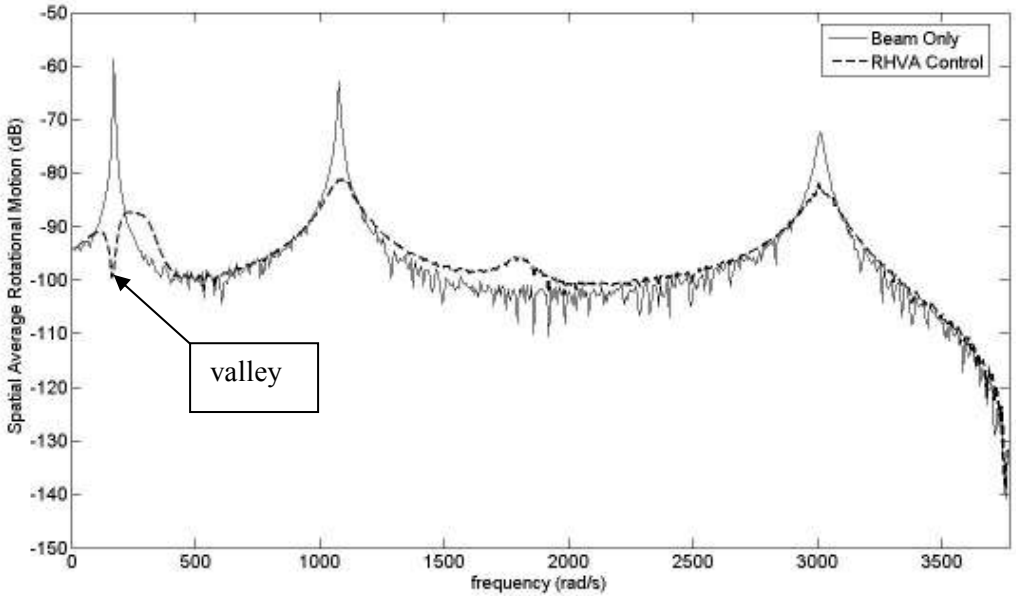

Figure 6-20 PSDs of rotational spatial average motion with/without RHVA (simulation)

From figures 6-17 to 6-20, the resonant peaks of all PSDs were remarkably damped down in all modes. This reflects that the controller introduced active damping to the entire cantilever beam. Now focusing on the first mode of the cantilever beam, frequency spectrums shown in Figures 6-19 and 6-20 have a valley at their respective first resonant mode but PSDs shown in Figures 6-17 and 6-18 do not have. The reason of the absence of the valley is similar to the one discussed in the previous section. It is because of the existing of the damping induced by the fasteners of the RHVA. Although the valleys do not exist in Figures 6-17 and 6-18, the attenuation of the translational and rotational spatial average motions in their respective first resonant mode is still larger than the second and the third modes. This signifies that the passive absorption frequency of the RHVA was able to further alleviate the average vibration motions of the first mode of the entire cantilever beam.

The respective percentage of reduction on the translational and rotational spatial average mean square motions, GR_w and GR_θ, was separately calculated for the experimental and simulation results. They are used to evaluate the global vibration suppression performance of the RHVA. The results are shown in the following table.

	$GR_w(\%)$	$GR_\theta(\%)$
Experimental Results	63.7	65.2
Simulation Results	80.1	76.4

Table 6-3 Global control performance of RHVA (experiment and simulation)

Table 6-3 demonstrates clearly that the global vibration suppression performance of the RHVA is acceptable in the experiments and the simulation tests. The maximum performance difference between the experimental and simulation results is about 17%. This indicates that the experimental results are reasonably close to the simulation results. Therefore, the proposed global structural vibration controller and the analytical model of the RHVA can be validated by both the experimental and simulation results.

6.4 Summary

In this chapter, apparatus used in the experiment and the experimental methodology are discussed. Experimental and simulation results of testing the RHVA performance are presented. Indices used to evaluate the local and global vibration suppression performance of the RHVA are calculated separately with the experimental and simulation results. The indices are finally used to verify the analytical model of the RHVA and the global structural vibration controller.

7 CONCLUSIONS AND SUGGESTIONS FOR FUTURE WORK

7.1 Conclusions

This project aimed to design a new type of rotational hybrid vibration absorber (RHVA) and a global vibration controller which is applicable to either rotational HVA or translational HVA (THVA). The proposed RHVA was compared with the THVA and groundhook damper on their local and global vibration suppression performance, and checked on the feasibility of implementing it as a better alternative device to THVA and skyhook/groundhook damper. The whole project was successfully performed via the following tasks.

1) An analytical model on the basis of Euler-Bernoulli beam equation was derived for the proposed RHVA.
2) A global structural vibration controller, which is applicable to either THVA or RHVA, was developed on the basis of pole placement method and Bezout equation. This controller is able to introduce active damping and an absorption frequency to entire beam structure for global structural vibration control.
3) Analytical models of three types of coupled systems including cantilever beam-RHVA coupled system, cantilever beam-THVA coupled system and cantilever beam-groundhook damper coupled system were written as MatLAB codes and used for further simulation tests.
4) Indices including mean square motions, spatial average motions and spatial average mean square motions were calculated from the numerical results for each of the three coupled system.
5) The RHVA and THVA were compared on their local and global vibration suppression performance with the calculated indices.
6) The RHVA and groundhook damper were compared on their local and global vibration suppression performance with the calculated indices.

7) A test rig consisted of a beam and a rotational type HVA was fabricated and used for experimental test.
8) Simulation test with real experimental parameters was conducted.
9) Indices were calculated separately with the experimental and simulation results. The analytical model of the RHVA and the global structural vibration controller were validated by the calculated indices.

After performing the investigations on the above nine tasks, the following conclusions were obtained:

1) An analytical model was derived for the proposed RHVA, which is coupled with a flexible structure.
2) A novel global structural vibration controller was developed on the basis of pole placement method. This controller is applicable to either THVA or RHVA. It can introduce active damping and an absorption frequency to the entire flexible structure.
3) RHVA can be a better alternative design of HVA. Its mitigation performance can be prior to the THVA on the rotational vibration motion but similar to the THVA on the translational vibration motion. Comparing with the THVA, RHVA can be easier to tune its passive absorption frequency.
4) RHVA can be a better alternative to replace a skyhook/groundhook damper. Its suppression performance can be similar to a skyhook/groundhook damper in case the damping coefficient of the damper was fixed to certain value. Comparing with the skyhook/groundhook damper, RHVA can be mounted directly on a vibrating structure and do not require mounting base. It can also provide a tunable passive absorption frequency to further alleviate the vibration motions of a vibrating structure at certain dominant frequency.
5) The analytical model of the proposed RHVA and the global structural vibration controller were validated by both the experimental and simulation results.

7.2 Suggestions for Future Work

After performing this study, some tasks are suggested for future work:

1) Optimum value of the active damping factor α is not considered in this study. Basically, the attenuation performance of the RHVA depends on the value of the active damping factor α. In general, the smaller value of the active damping factor α, the stronger active damping can introduce to the system. However, too small or too large value of active damping factor α may significantly affect the attenuation performance of the RHVA. Up to now, it was found that slight active damping can provide better local and global vibration suppression performance to the RHVA. Therefore, finding the optimum value of the active damping factor α can be useful to improve the attenuation performance of the RHVA. One of the simple methods to find the optimum value of the active damping factor α is used the spatial average mean square motion of the beam structure as an objective function. Optimum value of the active damping factor α can be the one provided with the minimum spatial average mean square motion. This process can be achieved by numerical simulations with different values of active damping factor α.
2) The optimum coupling location of the RHVA is not considered in this project. Generally, it was found that coupling the RHVA at the nodal position of certain resonant mode of a vibrating structure may remarkably affect the alleviation performance of the RHVA. In this study, the RHVA was coupled to the end of a cantilever beam to avoid this problem since the tip position of the cantilever beam was the anti-node of all modes. However, studying the optimum coupling location of the RHVA can be a significant research task. One way to find the optimum coupling location of the RHVA is used the spatial average mean square motion of the beam structure as an objective function. A number of check points can be initially established on the beam structure in which the beam is separated by very small and equal intervals. By coupling the RHVA at different locations of the beam structure in the simulation tests, the optimum

coupling location of the RHVA can be the one accompanied with the minimum spatial average mean square motion.

3) In this project, RHVA was designed to control vibration of a beam structure. In general, a beam can be considered as one-dimensional case. However, the case of implementing the proposed design of RHVA into two-dimensional structure such as plate or multi-dimensional structure for vibration control is not considered. One way to solve this problem may increase the degree of freedom. However, coupling effect may exist between different degrees of freedom. Therefore, more advanced analytical model and its experimental validation may be necessary for advanced design of RHVA which is capable to control vibration for multi-dimensional structures.

References

Adachi, K., Awakura, Y., and Iwatsubo, T. (**2004**). "Active control effort of hybrid piezoelectric absorber for structural control," Applied Acoustics **65**, 277-292.

Anusonti-Inthra, P., and Gandhi, F. (**2004**). "Cyclic modulation of semi-active controllable dampers for tonal vibration isolation," Journal of Sound and Vibration **275**, 107-126.

Bai, Y., and Grigoriadis, K. M. (**2009**). "Damping parameter design optimization in structural systems using an explicit H[infinity] norm bound," Journal of Sound and Vibration **319**, 795-806.

Balas, M. J. (**1978**). "Active control of flexible systems," Journal of Optimization Theory and Applications **25**, 415-436.

Benassi, L., and Elliott, S. J. (**2004**). "Active vibration isolation using an inertial actuator with local displacement feedback control," Journal of Sound and Vibration **278**, 705-724.

Bhatta, P., and Sinha, A. (**2003**). "A discrete-time, optimal, active vibration absorber," Journal of Sound and Vibration **268**, 201-208.

Bruner, A. M., Belvin, W. K., Horta, L. G., and Juang, J. N. (**1992**). "Active vibration absorber for the CSI evolutionary model - Design and experimental results," Journal of Guidance, Control, and Dynamics **15**, 1253-1257.

Buhr, C., Franchek, M. A., and Bernhard, R. J. (**1997**). "Non-collocated adaptive-passive vibration control," Journal of Sound and Vibration **206**, 371-398.

Burdisso, R. A., and Heilmann, J. D. (**1998**). "A new dual-reaction mass dynamic vibration absorber actuator for active vibration control," Journal of Sound and Vibration **214**, 817-831.

Cartmell, M., and Lawson, J. (**1994**). "Performance enhancement of an autoparametric vibration absorber by means of computer control," Journal of Sound and Vibration **177**, 173-195.

Cha, P. D., and Zhou, X. (**2006**). "Imposing points of zero displacements and zero slopes along any linear structure during harmonic excitations," Journal of Sound and Vibration **297**, 55-71.

Chang, J. C. H., and Soong, T. T. (**1980**). "Structural control using active tuned mass dampers," Journal of the Engineering Mechanics Division, ASCE **106**, 1091-1098.

Chen, Y. D., Fuh , C. C., and Tung, P. C. (**2005**). "Application of voice coil motors in active dynamic vibration absorbers," Magnetics, IEEE Transactions on **41**, 1149-1154.

Cheung, Y. L., and Wong, W. O. (**2008**). "Isolation of bending vibration in a beam structure with a translational vibration absorber and a rotational vibration absorber," Journal of Vibration and Control **14**, 1231-1246.

Cheung, Y. L., and Wong, W. O. (**2009**). "H_∞ and H_2 optimizations of a dynamic vibration absorber for suppressing vibrations in plates," Journal of Sound and Vibration **320**, 29-42.

Chiba, M., and Sugimoto, T. (**2003**). "Vibration characteristics of a cantilever plate with attached spring-mass system," Journal of Sound and Vibration **260**, 237-263.

Chung, L. L., Lin, R. C., Soong, T. T., and Reinhorn, A. M. (**1989**). "Experimental study of active control for MDOF seismic structures," Journal of Engineering Mechanics **115**, 1609-1627.

Cicek, I., and Ertas, A. (**2002**). "Experimental investigation of beam-tip mass and pendulum system under random excitation," Mechanical Systems and Signal Processing **16**, 1059-1072.

Cuvalci, O., Ertas, A., Ekwaro-Osire, S., and Cicek, I. (**2002**). "Non-linear vibration absorber for a system under sinusoidal and random excitation: experiments," Journal of Sound and Vibration **249**, 701-718.

Davis, C. L., and Lesieutre, G. A. (**2000**). "An actively tuned solid-state vibration absorber using capacitive shunting of piezoelectric stiffness," Journal of Sound and Vibration **232**, 601-617.

Dayou, J. (**2006**). "Fixed-points theory for global vibration control using vibration neutralizer," Journal of Sound and Vibration **292**, 765-776.

Dayou, J., and Brennan, M. J. (**2003**). "Experimental verification of the optimal tuning of a tunable vibration neutralizer for global vibration control," Applied Acoustics **64**, 311-323.

Den Hartog, J. P. (**1956**). "Mechanical vibrations," McGraw Hill, New York.

Deng, H. X., Gong, X. L., and Wang, L. H. (**2006**). "Development of an adaptive tuned vibration absorber with magnetorheological elastomer," Smart Materials and Structures **15**, N111-N116-N111-N116.

Du, Y., Burdisso, R. A., and Nikolaidis, E. (**2005**). "Control of internal resonances in vibration isolators using passive and hybrid dynamic vibration absorbers," Journal of Sound and Vibration **286**, 697-727.

Elmali, H., Renzulli, M., and Olgac, N. (**2000**). "Experimental comparison of delayed resonator and PD controlled vibration absorbers using electromagnetic actuators," Journal of Dynamic Systems, Measurement, and Control **122**, 514-520.

Engelen, K., Ramon, H., Saeys, W., Franssens, W., and Anthonis, J. (**2007**). "Positioning and tuning of viscous damper on flexible structure," Journal of Sound and Vibration **304**, 845-862.

Ertas, A., Cuvalci, O., and Ekwaro-Osire, S. (**2000**). "Performance of pendulum absorber for a non-linear system of varying orientation," Journal of Sound and Vibration **229**, 913-933.

Filipovic, D., and Schröder, D. (**1998**). "Bandpass vibration absorber," Journal of Sound and Vibration **214**, 553-566.

Filipovic, D., and Schröder, D. (**1999**). "Vibration absorption with linear active resonators: continuous and discrete time design and analysis," Journal of Vibration and Control **5**, 685-708.

Franchek, M. A., Ryan, M. W., and Bernhard, R. J. (**1996**). "Adaptive passive vibration control," Journal of Sound and Vibration **189**, 565-585.

Fujino, Y., Warnitchai, P., and Pacheco, B. M. (**1993**). "Active stiffness control of cable vibration," Journal of Applied Mechanics **60**, 948-953.

Gupta, N. K. (**1980**). "Frequency-shaped cost functions-extension of linear-quadratic-gaussian design methods," Journal of Guidance, Control, and Dynamics, AIAA, 529-535.

Hagood, N. W., and von Flotow, A. (**1991**). "Damping of structural vibrations with piezoelectric materials and passive electrical networks," Journal of Sound and Vibration **146**, 243-268.

Haxton, R. S., and Barr, A. D. S. (**1972**). "The autoparametric vibration absorber," Journal of Engineering for Industry **94**, 119-124.

Hermann, F. (**1909**). "Device for damping vibrations of bridges," German Patent 525455.

Hirata, T., Koizumi, S., and Takahashi, R. (**1995**). "H_∞ control of railroad vehicle active suspension," Automatica **31**, 13-24.

Hrovat, D., Barak, P., and Rabins, M. (**1983**). "Semi-active versus passive or active tuned mass dampers for structural control," Journal of Engineering Mechanics **109**, 691-705.

http://mathworld.wolfram.com/DeltaFunction.html.

Huang, S. J., and Lin, W. C. (**2003**). "Adaptive fuzzy controller with sliding surface for vehicle suspension control," Fuzzy Systems, IEEE Transactions on **11**, 550-559.

Hunt, J. B. (**1979**). "Dynamic vibration absorbers," Mechanical Engineering Publications Ltd.

Igusa, T., and Xu, K. (**1994**). "Vibration control using multiple tuned mass dampers," Journal of Sound and Vibration **175**, 491-503.

Ikai, S., Ohsawa, K., Nagaya, K., and Kashimoto, H. (**2000**). "Electromagnetic actuator and stacked piezoelectric sensors for controlling vibrations of a motor on a flexible structure," Journal of Sound and Vibration **231**, 393-409.

Inman, D. J. (**1994**). "Engineering vibrations," Prentice-Hill, NJ.

Jacquot, R. G. (**2000**). "Random vibration of damped modified beam systems," Journal of Sound and Vibration **234**, 441-454.

Jacquot, R. G. (**2003**). "The spatial average mean square motion as an objective function for optimizing damping in damped modified systems," Journal of Sound and Vibration **259**, 955-965.

Jalili, N. (**2000**). "A new perspective for semi-automated structural vibration control," Journal of Sound and Vibration **238**, 481-494.

Jang, S. J., and Choi, Y. J. (**2007**). "Geometrical design method of multi-degree-of-freedom dynamic vibration absorbers," Journal of Sound and Vibration **303**, 343-356.

Kaplow, C. E., and Velman, J. R. (**1978**). "Active local vibration isolation applied to a flexible space telescope," AIAA Guidance and Control Conference **78-1283R**.

Kidner, M. R. F., and Brennan, M. J. (**2002**). "Varying the stiffness of a beam-like neutralizer under fuzzy logic control," Journal of Vibration and Acoustics **124**, 90-99.

Kim, H. S., and Roschke, P. N. (**2006**). "Design of fuzzy logic controller for smart base isolation system using genetic algorithm," Engineering Structures **28**, 84-96.

Korenev, B. G., and Reznikov, L. M. (**1993**). "Dynamic vibration absorbers, theory and technical applications," Wiley, New York.

Kwanami, K., and Seto, K. (**1984**). "Optimum design of dual tuned mass dampers and their effectiveness," Proceedings of the JSME (C) **50**, 44-52 (in Japanese).

Lai, J. S., and Wang, K. W. (**1996**). "Parametric control of structural vibrations via adaptable stiffness dynamic absorbers," Journal of Vibration and Acoustics **118**, 41-47.

Lee, C. L., Chen, Y. T., Chung, L. L., and Wang, Y. P. (**2006**). "Optimal design theories and applications of tuned mass dampers," Engineering Structures **28**, 43-53.

Lee Glauser, G., Juang, J. N., and Sulla, J. L. (**1995**). "Optimal active vibration absorber: design and experimental results," Journal of Vibration and Acoustics **117**, 165-171.

Lee Glauser, G. J., Ahmadi, G., and Horta, L. G. (**1997**). "Integrated passive/active vibration absorber for multistory buildings," Journal of Structural Engineering **123**, 499-504.

Li, C., and Zhu, B. (**2006**). "Estimating double tuned mass dampers for structures under ground acceleration using a novel optimum criterion," Journal of Sound and Vibration **298**, 280-297.

Lin, J. (**2007**). "An active-passive absorber by using hierarchical fuzzy methodology for vibration control," Journal of Sound and Vibration **304**, 752-768.

Lin, J., Huang, Z. Z., and Huang, P. H. (**2007**). "An active damping control of robot manipulators with oscillatory bases by singular perturbation approach," Journal of Sound and Vibration **304**, 345-360.

Lindquist, A., and Yakubovich, V. A. (**1997**). "Optimal damping of forced oscillations in discrete-time systems," Automatic Control, IEEE Transactions on **42**, 786-802.

Ma, R. P., and Sinha, A. (**1996**). "A neural network based active vibration absorber with state feedback control," Journal of Sound and Vibration **190**, 121-128.

Main, J. A., and Krenk, S. (**2005**). "Efficiency and tuning of viscous dampers on discrete systems," Journal of Sound and Vibration **286**, 97-122.

Mansoori, M. R., and Moghadam, A. S. (**2009**). "Using viscous damper distribution to reduce multiple seismic responses of asymmetric structures," Journal of Constructional Steel Research **65**, 2176-2185.

Morgan, R. A., and Wang, K. W. (**2002**). "An active passive piezoelectric absorber for structural vibration control under harmonic excitations with time varying frequency Part 1 algorithm development and analysis," Journal of Vibration and Acoustics **124**, 77-83.

Mustafa, G., and Ertas, A. (**1995**). "Dynamics and bifurcations of a coupled column-pendulum oscillator," Journal of Sound and Vibration **182**, 393-413.

Nagarajaiah, S., and Varadarajan, N. (**2005**). "Short time Fourier transform algorithm for wind response control of buildings with variable stiffness TMD," Engineering Structures **27**, 431-441.

Nagem, R. J., Madanshetty, S. I., and Medhi, G. (**1997**). "An electromechanical vibration absorber," Journal of Sound and Vibration **200**, 551-556.

Niederberger, D., Fleming, A., Moheimani, S. O. R., and Morari, M. (**2004**). "Adaptive multi-mode resonant piezoelectric shunt damping," Smart Materials and Structures **13**, 1025-1035.

Nonami, K., Nishimura, H., and Cui, W. (**1994**). "Disturbance cancellation control for vibration of multi-degree-of-freedom systems : case of using active vibration absorber and active dynamic vibration absorber," JSME international journal. Ser. C, Dynamics, control, robotics, design and manufacturing **37**, 86-93.

Nonami, K., Nishimura, H., and Tian, H. (**1996**). "H_∞ / μ control-based frequency-shaped sliding mode control for flexible structures," JSME international journal. Ser. C, Dynamics, control, robotics, design and manufacturing **39**, 493-501.

Occhiuzzi, A. (**2009**). "Additional viscous dampers for civil structures: Analysis of design methods based on effective evaluation of modal damping ratios," Engineering Structures **31**, 1093-1101.

Olgac, N., and Holm Hansen, B. T. (**1994**). "A novel active vibration absorption technique: delayed resonator," Journal of Sound and Vibration **176**, 93-104.

Patten, W. N., Sack, R. L., and He, Q. (**1996**). "Controlled semiactive hydraulic vibration absorber for bridges," Journal of Structural Engineering **122**, 187-192.

Pourzeynali, S., Lavasani, H. H., and Modarayi, A. H. (**2007**). "Active control of high rise building structures using fuzzy logic and genetic algorithms," Engineering Structures **29**, 346-357.

Rockwell, T. H. (**1965**). "Investigation of structure-borne active vibration dampers," Journal of Acoustical Society of America **12.3i**, 623-628.

Rustighi, E., Brennan, M. J., and Mace, B. R. (**2005**). "Real-time control of a shape memory alloy adaptive tuned vibration absorber," Smart Materials and Structures **14**, 1184-1195.

Ryan, M. W., Franchek, M. A., and Bernhard, R. (**1994**). "Adaptive-passive vibration control of single frequency excitations applied to noise control," Noise Conference 94.

Sievers, L. A., and Von Flotow, A. H. (**1989**). "Comparison of two LQG-based methods for disturbance rejection," Proceedings of the 26th IEEE Conference on Decision and Control, Tampa, FL.

Snowdon, J. C. (**1968**). "Vibration and shock in damped mechanical systems," John Wiley & Sons, New York.

Sun, H. L., Zhang, P. Q., Chen, H. B., Zhang, K., and Gong, X. L. (**2008**). "Application of dynamic vibration absorbers in structural vibration control under multi-frequency harmonic excitations," Applied Acoustics **69**, 1361-1367.

Sun, H. L., Zhang, P. Q., Gong, X. L., and Chen, H. B. (**2007**). "A novel kind of active resonator absorber and the simulation on its control effort," Journal of Sound and Vibration **300**, 117-125.

Sun, J. Q., Jolly, M. R., and Norris, M. A. (**1995**). "Passive, adaptive and active tuned vibration absorbers---a survey," Journal of Mechanical Design **117**, 234-242.

Tang, J., and Wang, K. W. (**2001**). "Active-passive hybrid piezoelectric networks for vibration control: comparisons and improvement," Smart Materials and Structures **10**, 794-806.

Tang, S. L. (**2004**). "Suppression of structural vibration with a new type of vibration absorber," in *Dept. of Mechanical Engineering* (The Hong Kong Polytechnic University, Hong Kong).

Taniguchi, T., Der Kiureghian, A., and Melkumyan, M. (**2008**). "Effect of tuned mass damper on displacement demand of base-isolated structures," Engineering Structures **30**, 3478-3488.

von Flotow, A. H., Beard, A., and Bailey, D. (**1994**). "Adaptive tuned vibration absorbers: tuning laws, tracking agility, sizing, and physical implementations," Proccceings of Noise-Conference 94.

Vyas, A., and Bajaj, A. K. (**2001**). "Dynamics of autoparametric vibration absorbers using multiple pendulums," Journal of Sound and Vibration **246**, 115-135.

Warburton, G. B. (**1982**). "Optimum absorber parameters for various combinations of response and excitation parameters," Earthquake Engineering & Structural Dynamics **10**, 381-401.

Warminski, J., and Kecik, K. (**2009**). "Instabilities in the main parametric resonance area of a mechanical system with a pendulum," Journal of Sound and Vibration **322**, 612-628.

Webster, A. L., and Semke, W. H. (**2005**). "Broad-band viscoelastic rotational vibration control for remote sensing applications," Journal of Vibration and Control **11**, 1339-1356.

Wie, B., and Gonzalez, M. (**1990**). "Active control synthesis for flexible space structures excited by persistent disturbances," AIAA Guidance, Navigation and Control Conference, Portland OR.

Williams, K., Chiu, G., and Bernhard, R. (**2002**). "Adaptive-passive absorbers using shape-memory alloys," Journal of Sound and Vibration **249**, 835-848.

Williams, K. A., Chiu, G. T. C., and Bernhard, R. J. (**2005**). "Dynamic modelling of a shape memory alloy adaptive tuned vibration absorber," Journal of Sound and Vibration **280**, 211-234.

Wong, W. O., and Cheung, Y. L. (**2008**). "Optimal design of a damped dynamic vibration absorber for vibration control of structure excited by ground motion," Engineering Structures **30**, 282-286.

Wong, W. O., Tang, S. L., Cheung, Y. L., and Cheng, L. (**2007**). "Design of a dynamic vibration absorber for vibration isolation of beams under point or distributed loading," Journal of Sound and Vibration **301**, 898-908.

Wu, J. D., and Chen, R. J. (**2004**). "Application of an active controller for reducing small-amplitude vertical vibration in a vehicle seat," Journal of Sound and Vibration **274**, 939-951.

Wu, S. T., Chiu, Y. Y., and Yeh, Y. C. (**2007**). "Hybrid vibration absorber with virtual passive devices," Journal of Sound and Vibration **299**, 247-260.

Wu, S. T., and Shao, Y. J. (**2007**). "Adaptive vibration control using a virtual-vibration-absorber controller," Journal of Sound and Vibration **305**, 891-903.

Wu, S. Y. (**1998**). "Method for multiple mode shunt damping of structural vibration using a single PZT transducer," Proceedings of the SPIE Smart Structures and Materials, Smart Structures and Intelligent Systems **3327**, 159-168.

Xu, J. (**1993**). "Disturbance isolation and robust active vibration control," Ph.D thesis, University of Cincinnati, Ohio, USA.

Yasuda, M., Gu, R., Nishihara, O., Matsuhisa, H., Ukai, K., and Kondo, M. (**1996**). "Development of antiresonance enforced active vibration absorber system," JSME international journal. Ser. C, Dynamics, control, robotics, design and manufacturing **39**, 464-469.

Yuan, J. (**2000**). "Hybrid vibration absorption by zero/pole-assignment," Journal of Vibration and Acoustics **122**, 466-469.

Yuan, J. (**2001**). "Multi-point hybrid vibration absorption in flexible structures," Journal of Sound and Vibration **241**, 797-807.

Zhang, Y., and Alleyne, A. (**2003**). "A simple novel approach to active vibration isolation with electrohydraulic actuation," Journal of Dynamic Systems, Measurement, and Control **125**, 125-128.